"TEORIA VARIACIONAL DE L'ESTAT DE TRANSICIÓ: NOUS DESENVOLUPAMENTS METODOLÒGICS I LA SEVA APLICACIÓ A SISTEMES D'INTERÈS QUÍMIC"

Jordi Villà i Freixa

Departament de Química

Universitat Autònoma de Barcelona

Article 3

"Variational transition state theory and tunneling calculations with reorientation of the generalized transition states for methyl cation transfer"

Angels González-Lafont, Jordi Villà, José M. Lluch, Juan Bertrán, Rozeanne Steckler, Donald G. Truhlar

The Journal of Physical Chemistry, enviat.

Variational Transition State Theory and Tunneling Calculations with Reorientation of the Generalized Transition States for Methyl Cation Transfer

Angels González-Lafont, Jordi Villà, José M. Lluch* and Juan Bertrán
Department de Química, Universitat Autònoma de Barcelona, 08193 Bellaterra (Barcelona), Spain

Rozeanne Steckler
Sand Diego Supercomputer Center, P. O. Box 85608, San Diego CA 92186-9784, USA

and Donald G. Truhlar*
Department of Chemistry and Supercomputer Institute, University of Minnesota, Minneapolis, Minnesota 55455-0431 USA

Abstract. The new RODS algorithm based on optimizing the orientation of the dividing suface at each point along the reaction path in order to maximize the free energy of the generalized transition state containing that point, has been used to carry out variational transition state calculations and tunneling calculations for two reactions with high-frequency vibrations strongly coupled to the reaction coordinate

$$(Cl^-)(CH_3NH_3^+) \rightarrow \begin{bmatrix} ClCH_3(NH_3) \\ ClCH_3 + NH_3 \end{bmatrix}$$

and

$$CH_3Cl(H_2O) + NH_3(H_2O) \rightarrow (CH_3NH_3^+)(Cl^-)(H_2O)_2$$

These reactions, both of which involve the transfer of a methyl cation between Cl^- and NH_3, show much larger variational-transition-state and tunneling effects than were observed in previous studies of the transfer of methyl cations between anionic centers. However, they are hard to study because the adiabatic potential energy curves of both reactions and, as a consequence, the corresponding free energy of activation profiles show big dips when the minimum energy path (MEP) is followed using standard methods, even when very small step sizes are taken to compute the steepest-descent path. The application of RODS methodology eliminates those dips giving rise to smooth free energy of activation profiles and vibrationally adiabatic potential curves. Calculation of variational rate constants and tunneling effects are significantly improved.

1. INTRODUCTION

The fundamental hypothesis of conventional transition state theory (TST) is that, in terms of classical mechanics, no trajectories in an equilibrium ensemble recross a transition-state dividing surface (a hypersurface dividing reactants from products) centered at the saddle point on a potential energy hypersurface.[1] Because of this assumption, TST in a classical world overestimates the thermal rate constants of chemical reactions.[1,2] Variational transition state theory (VTST) minimizes this error by locating the transition state dividing surface such that it yields the smallest possible calculated rate constant. It can be shown that this maximizes the free energy of activation.[3,4] In practice, one adds quantum mechanical effects on modes transverse to the reaction coordinate by computing the free energy of activation from quantum mechanical sums over states rather than classical phase space integrals.[5,6] This must be justified by the existence of locally conserved vibrational action variables that are seen to be clearly quantized in accurate quantum mechanical calculations; these are the locally adiabatic invariants of the motion.[7]

Prior to calculating the VTST rate constants one must compute generalized frequencies along the path in order to get the free energy of activation profile. VTST calculations based on search along the minimum-energy path MEP for the best location of the transition state have the drawback that it can be very expensive to calculate the MEP, because small step sizes are required to accurately compute an MEP.[8] Furthermore, if the MEP is not accurate, the generalized normal mode frequencies corresponding to the usual dividing surface normal to the path may be unphysical and differ greatly from the true locally adiabatic invariants. In a previous paper[9] a new practical method for carrying out VTST calculations without evaluating the MEP has been presented. In this method, for each point along a reaction path (which is not necessarily the minimum-energy path), the orientation of the dividing surface is optimized in order to maximize the free energy of the generalized transition state at that point. Another use of the proposed algorithm is that it can be employed to extract a stable and meaningful free energy of activation from an MEP-based calculation carried out with large steps, where the usual procedure of orienting the dividing surface normal to the gradient of the potential is inaccurate.

During the past two decades, VTST has been applied to a variety of chemical systems.[10] A wide variety of reactions of neutral species have been studied, with variational effects of various magnitudes.[10] Among ionic reactions, much attention has been devoted to bimolecular ion-neutral reactions of the S_N2 and E2 type. In particular, considerable attention

has been dedicated to ion-molecule S_N2 reactions such as[11-15]

$$^{*}Cl^{-}(H_2O)_n + CH_3Cl \rightarrow {}^{*}ClCH_3 + Cl^{-}(H_2O)_n \qquad \text{(R1)}$$

with n = 0, 1, or 2. It has been found for all ion-molecule S_N2 reactions studied so far that variational effects (by which we mean deviations of VTST predictions from TST ones) are very small both for the transition state location and for the determination of the corresponding rate constant.[11-18] For instance, calculations based on a semiempirical, analytical potential energy hypersurface indicate that the VTST rate constant for reaction R1 is within 1% of the TST result at 300 K for $n = 0$ and 1.[15] These results may be attributed to the facts that (i) as the system leaves the saddle point along the reaction path the energy tends to drop rapidly to negative values associated with ion-dipole complexes, and (ii) the vibrational frequencies change only slowly along the reaction path in the vicinity of the saddle point. One E2 reaction has been studied, namely

$$ClO^{-} + C_2H_5Cl \rightarrow HOCl + C_2H_4 + Cl^{-} \qquad \text{(R2)}$$

Variational effects on the reaction rate in the central barrier were found to be only about 4%.[18]

However, variational effects on reaction rates for S_N2 reactions need not always be small. In this paper we present the study of two reactions that show significant variational effects. These systems are dificult to study because the vibrationally adiabatic potential energy curves and the corresponding free energy of activation curves present important dips when the MEP is followed using standard methods. We will show that the application of the above mentioned new algorithm based on the reorientation of the dividing surface (which will be called RODS), eliminates the dips, giving rise to smooth free energy of activation curves. In the original paper on the RODS algorithm, three examples were used to validate the new methodology. The present paper applies the RODS algorithm for complete VTST calculations of more difficult cases involving strong coupling of high-frequency modes to the reaction coordinate. In particular, we study

$$(Cl^{-})(CH_3NH_3^{+}) \rightarrow \begin{bmatrix} ClCH_3(NH_3) \\ ClCH_3 + NH_3 \end{bmatrix} \qquad \text{(R3)}$$

and

$$CH_3Cl(H_2O) + NH_3(H_2O) \rightarrow (CH_3NH_3^{+})(Cl^{-})(H_2O)_2 \qquad \text{(R4)}$$

The presence of microsolvating water molecules in R4 makes the calculation of free energy of activation curves even less stable than for the base case. Note that the unimolecular reaction

(R3) can produce either a van der Waals complex or a pair of separated neutral products; the exoergicities of these two paths are 30.5 and 28.9 kcal/mol, respectively. Note, however, that both paths go through the same transition state so transition state theory can only predict the sum of the two rates. Reaction (R4) is a bimolecular reaction that produces a dihydrated ion pair; the exoergicity of this reaction is 20.7 kcal/mol. For both R3 and R4 we consider the gas-phase high-pressure plateau. Thus we consider that collisions are frequent enough to maintain an equilibrium distribution of reactant energies for R3 and to stabilize all products of both R3 and R4. We assume, however, that the pressure is not so extraordinarily high that collisions of bath molecules with the transition states would not be considered.

Reaction (R4) is closely related to the Menshutkin reaction, which has been widely studied.[19] The Menshutkin analog of R4 is

$$CH_3Cl(H_2O) + NH_3(H_2O) \rightarrow \begin{cases} CH_3NH_3^+ + Cl^-(H_2O)_2 \\ CH_3NH_3^+(H_2O) + Cl^-(H_2O) \end{cases} \qquad \text{(R5)}$$

which is about 85 kcal/mol endoergic. Whereas the dynamical bottleneck for R5 occurs during the dissociation of the product-like ion pair, the rates of reactions R3 and R4 are both determined by central transition states corresponding to transfer of CH_3^+. However, as compared to ion-molecule S_N2 reaction studied previously, the CH_3^+ transfer steps in R3 and R4 are between a charged and a neutral fragment rather than between two charged fragments.

In order to calculate reaction rates by variational transition state theory, potential energy information is required at the stationary points and along the reaction path. For the present studies this information is obtained directly from electronic structure calculations without the intermediacy of an analytic fit, i.e., we carry out "direct dynamics VTST".[13-17,20-23] By design, the application of RODS methodology does not imply any additional electronic structure calculation.

Section 2 presents the details of the electronic structure calculations and dynamical calculations. Section 3 presents the results, and Section 4 is the discussion. Section 5 summarizes the principal conclusions.

2. COMPUTATIONAL METHODS

2.1. Electronic structure

As our main purposes of this work are to explore qualitative features of new reaction

types and to illustrate new methodology it is not essential to include electron correlation energy. *Ab initio* restricted Hartree-Fock calculations[24] were carried out using the split valence 6-31+G(d) basis set,[25] which includes *d* polarization and diffuse functions on the heavy atoms. Full geometry optimization was carried out. Stationary points were characterized as minima or saddle points by diagonalizing their Hessian (force constant) matrices and confirming that there are zero or one negative eigenvalues, respectively.

The minimum-energy path (MEP) was calculated in mass-scaled Cartesian coordinates[26,27] with a reduced mass μ of 1 amu by using the fourth order Runge-Kutta method[20] with a variable step size. For R3 a maximum value of 0.0026 Å was employed within the interval (-0.1 Å, 0.1 Å) of the MEP. Beyond this interval, the maximum was 0.0079 Å. For R4, the corresponding values were 0.0052 Å and 0.013 Å respectively, for the same intervals. Analytic Hessians were calculated at selected points along the MEP, with the convergence criterion explained in the following section. After diagonalizing the projected Hessian[30] at each point on the MEP, we obtain the m (where m=1,2,...,3N-7, and N is the number of atoms) generalized-normal mode frequencies corresponding to the modes orthogonal to the MEP (which are ordered in decreasing order), which allow us to calculate the vibrationally adiabatic ground-state potential curve $V_a^G(s)$. This is defined by

$$V_a^G(s) = V_{MEP}(s)+ZPE(s) \quad (1)$$

where s denotes distance along the MEP in the mass-scaled system.[27] The eigenvectors $\mathbf{L}_m$ obtained from the diagonalization, along with the gradient $\mathbf{v}$ at the points on the MEP are used to compute $B_{mF}(s)$, the reaction-path curvature at each mode m, in the usual way:[27,30]

$$B_{mF}(s) = -[sign(s)]\sum_{i=1}^{3N} \frac{dv_i(s)}{ds} L_{i,m}^{GT}(s) \quad (2)$$

Partial charges on the atoms and groups (q_X and q_{XHn}, respectively, where X and H denotes atoms) were calculated for interpretive purposes (they are not required for gas-phase dynamics calculations) by the method of Mulliken population analysis.[28] For the final results, all electronic structure calculations were done using the GAMESS93 electronic structure code.[29]

2.2. Dynamics

2.2.1. Theory. Rate constants are calculated by canonical variational theory (CVT).[27]

This theory yields hybrid rate constants corresponding to classical reaction path motion with other degrees of freedom quantized. However, since the rotational energy levels are generally closely spaced, we approximate the quantal rotational partition functions by the classical ones. For vibrations, the partition functions were calculated quantum mechanically within the harmonic approximation in rectilinear coordinates.[3,27,30]

To include quantal tunneling effects for motion along the reaction coordinate, CVT rate constants were multiplied by a ground-state transmission coefficient.[4,6,14,27,31,32] In particular we employ zero-curvature tunneling[5,6,26] (ZCT) and the centrifugal-dominant small-curvature semiclassical adiabatic ground-state[31,32] (small-curvature tunneling or SCT) approximations. The ZCT method corresponds to tunneling along the MEP, and the SCT method allows corner cutting in the tunneling probabilities.

2.2.2. Grids. The potential energy information (energies, gradients and Hessians), calculated at selected points along the MEP, was used in the POLYRATE computer code, version 7.0,[31,33] in order to carry out direct dynamics studies of processes R3 and R4. To assure convergence of the calculated rate constants, preliminary rate calculations with coarse Hessian grids were used to locate the regions of the reaction path containing the temperature-dependent variational transition states and the minima of the SCT reduced mass, where the "corner cutting" aspect of the tunneling process would be greatest. Finer grids were then calculated for these critical regions to improve the accuracy of the calculated canonical rate constants and small-curvature tunneling probabilities. This strategy is sometimes called focussing.[23] A total of 79 and 67 Hessian grid points were finally used for reactions R3 and R4, respectively.

The potential energy and generalized-normal-mode vibrational frequencies were then interpolated to intervals of 0.0026 Å by 5-point Lagrangian interpolation. Both diabatic[34] and adiabatic correlation of frequencies along the MEP were carried out (for the diabatic correlation a new methodology implemented in one of our programs[35] was used). The reaction-path curvature components at each step were evaluated by POLYRATE from the corresponding generalized-normal-mode eigenvectors and the derivatives of the gradient vectors.[27]

2.2.3. Reorientation of the dividing surface (RODS). In the RODS algorithm we assume that a Taylor series of the potential, valid through quadratic terms, is available for each of a series of K points along a generic reaction path, which is not necessarily the MEP. We specify these points as $k = 1, 2, ..., K$ and let $\mathbf{x}$ denote our mass-scaled Cartesian[36] coordinate

system. Let $\mathbf{x}^L(k)$ denote the K points where the data is available. Generally, the dividing surfaces, that are hyperplanes in $\mathbf{x}$ passing through the different $\mathbf{x}^L(k)$, are obtained by projecting the gradient and the overall translations and rotations out of the Hessian matrix.[30] In RODS approach, we will consider trial dividing surfaces that are orthogonal to the overall rotations and translations and that pass through one of the points $\mathbf{x}^L(k)$. However, instead of projecting out the gradient, for each k we optimize the orientation of the dividing surface to maximize the generalized free energy of activation of the generalized transition state at k. In this way we obtain more physical dividing surfaces especially when the calculations are unstable. Details of the algorithm are given elsewhere,[9] but we note that s is still calculated by the Euler algorithm even though the RODS algorithm slightly displaces the points on the reaction path.

3. RESULTS AND DISCUSSION

3.1. Stationary points

Tables I and II give the energy, relative to reactants, at stationary points along the MEP for reactions R3 and R4; this quantity is labeled V_{MEP}. Tables I and II also give geometrical parameters and partial charges characterizing the stationary points. Both reactions can be visualized as the transfer of a CH_3^+ group between Cl^- and NH_3, accompanied by the umbrella inversion at CH_3^+.

For reaction R3, the Cl, C, and N atoms are collinear along the entire minimum-energy reaction path. The saddle point is depicted in Figure 1, along with the imaginary frequency eigenvector. One can observe that the main components of the transition vector (whose eigenvalue gives an imaginary frequency of 559i cm^{-1}) correspond to the nitrogen atom separating from the carbon atom. Therefore, the reaction coordinate is fundamentally an asymmetric stretch at the conventional transition state. The neutralization of the chloride charge progresses monotonically along the reaction path.

For the dihydrated reaction R4, the general effect of solvent is to stabilize the supermolecule as the reaction progresses, which is why this reaction would probably be studied experimentally in the ion production direction, as written, rather than in neutralization direction, as R3 is written. The dipole-dipole complex is 5.1 kcal/mol below the reactants, and the energy barrier referred to this complex is 25.6 kcal/mol. The product ion-pair complex is stabilized by the hydrating water molecules in such a way that it appears 15.6 kcal/mol below the dipole-dipole complex.

Some aspects of the geometrical structures merit discussion. At the reactants, one water molecule, called W(N), is hydrogen bonded to one of the ammonia hydrogens, while the second water molecule, called W(Cl), solvates the chlorine atom. As the reaction proceeds, an interesting motion of the different fragments takes place to stabilize the nascent charges. Initially the reactants approach with non-linear Cl-C-N arrangement to give the dipole-dipole complex shown in Figure 2, in such a way that the two water molecules are able to form a hydrogen bond between them. In addition, the W(Cl) water molecule continues to solvate the chlorine atom, and the W(N) water molecule continues to solvate the ammonia. At the saddle point, shown in Figure 3, the nitrogen, carbon and chlorine atoms are aligned. The N-C distance is short enough that both water molecules still remain hydrogen bonded to each other. We note that the transition vector is very similar to the one associated with the unhydrated reaction, such that no significant component of motion of water molecules appears. Thus, the imaginary frequency (551i cm^{-1}) has an only slightly lower value than for the R3 reaction. At the ion-pair product, shown in Figure 4, W(N) maintains the same interaction as at the saddle point, that is, it solvates ammonia and is hydrogen-bonded to W(Cl), whereas W(Cl) solvates the chloride anion; the methyl group appears completely unsolvated. This structure is reasonable in a dihydrated cluster where the chloride anion prefers to be bonded to the most positive fragment of the supermolecule. This combination of stabilizing interactions causes the ion-pair product to lie in a deep well.

3.2. VTST calculations based on the standard algorithm

3.2.1. Runge-Kutta calculations. The position of the variational transition state corresponds to the maximum of the free energy of activation profile at each temperature. At 0 K that profile equals the vibrationally adiabatic ground-state potential energy curve defined by equation 1. Solid lines in Figures 5a and 5b show the adiabatic ground state potential energy curves for reactions R3 and R4, respectively. To show the effect of temperature, the solid lines in Figures 6a and 6b present the free energy of activation profiles at $T = 300$ K for these reactions. The shapes of the profiles at the other temperatures considered are similar to their shapes at 300 K. We note in figures 5a and 5b important dips appearing in the region near the saddle point, which is the region that apparently governs the variational effects. In order to analyze the regions of these dips, we next examine the vibrational frequencies in these regions.

Figures 7 and 8 present the generalized-normal-mode vibrational frequencies of the high-frequency generalized normal modes versus the arc length along the reaction coordinate for reactions R3 and R4, respectively. Note that the mode of $(Cl^-)(CH_3NH_3^+)$ correlating with

the imaginary normal mode at the saddle point is not included because it is the reaction coordinate. The generalized normal modes shown in these two figures exhibit strong couplings at various points along the reaction path. For that reason, we have preferred to make a diabatic correlation in Figures 7 and 8. For the sake of simplicity, only the generalized normal modes associated with reactant frequencies above 1500 cm^{-1} are displayed.

In the unhydrated reaction R3, only one frequency changes significantly in the vicinity of the saddle point. This generalized normal mode frequency takes values of around 3800 cm^{-1} along the incoming part of reaction path and decreases abruptly just before the saddle point, where it reaches a local maximum of 3813 cm^{-1}. Another dip occurs on the product side of the MEP. The analysis of the associated generalized-normal-mode eigenvector along the reaction path shows that this mode corresponds to a vibrational motion of the ammonia hydrogen atoms in the 3800 cm^{-1} region. The two dips of this frequency just before and after the saddle point are explained by a strong mode coupling that changes the components of the generalized-normal-mode eigenvector which in those two zones correspond to the motion of the ammonia hydrogen atoms plus the motion of the nitrogen atom separating from the carbon atom. As a consequence of the variation of this frequency, the total zero point energy goes down rapidly just before and after the saddle point, as it can be seen in Figure 5a.

For the dihydrated reaction R4, there are two frequencies, labeled A and B in Figure 8, that change significantly in the vicinity of the saddle point. For the frequency A three zones can be distinguished. Coming from reactants, frequency A takes values above 4000 cm^{-1}. Just before the saddle point it drops abruptly below 1500 cm^{-1}. Finally, just after the saddle point, where it has a value of 3659 cm^{-1}, up to products it remains nearly constant. In the first zone, the associated generalized-normal-mode eigenvector involves primarily the movement of the water hydrogen atoms. In the second zone, when the frequency goes down, the normal mode consists of the motion of the ammonia and W(N) water hydrogen atoms plus the N-C stretching (the incorporation of these two heavy atoms causes the dip of the frequency). In the third zone, this generalized-normal-mode eigenvector becomes mainly a motion of the ammonia hydrogen atoms.

Frequency B in Figure 8 takes values close to 4000 cm^{-1} from reactants up to the saddle point. Just at the saddle point, this frequency begins to decrease to values below 1500 cm^{-1} and then it recovers rapidly to values around 4000 cm^{-1}. Its associated generalized-normal-mode eigenvector successively varies in the following way: first, it consists of the motion of the water hydrogen atoms; then, it involves the movement of the ammonia

and W(N) water hydrogen atoms plus the N-C stretching; finally, it becomes essentially the motion of the W(N) water hydrogen atoms.

In summary, the frequency dips appear to be explained by spurious mixing of high-frequency motions into the reaction coordinate and the concomitant mixing of the heavy-atom motion along the reaction coordinate into transverse modes. This flattens the potential energy surface in the direction normal to the reaction coordinate.

3.2.2. Smaller step sizes. It is very hard to eliminate the spurious frequencies by simply decreasing the step sizes. For example, using the Euler algorithm and the ACESRATE code,[37] we decreased the step size for reaction R3 to 5.29×10^{-4} Å. Although this somewhat decreases the oscillations, V_{MEP} is still not smooth, and V_a^G still shows a several kcal/mol dip. We therefore turn to the RODS algorithm, which we shall apply using the original 0.0026 Å-stepsize data set that was generated with the Runge-Kutta algorithm implemented in GAMESS93.

3.3. VTST calculations based on the RODS algorithm

3.3.1. Adiabatic potential energy curves and free energy of activation profiles. In the previous paper[9] we showed that the RODS algorithm gave significant improvement in the stability of reaction-path calculations for the OH + H_2 and H + C_2H_4 reactions. The systems studied in the present paper pose more difficult challenges because the standard algorithm yields significant dips in the generalized frequency curves and, for this reason, also in the adiabatic ground-state potential energy curves and the corresponding free energy of activation profiles. Thus these reactions are good tests for the RODS algorithm.

The dips in the generalized-normal-mode frequencies disappear when the RODS algorithm is applied, and all the frequencies exhibit smooth behaviour in the range of s considered in this paper. The frequencies obtained from the RODS algorithm do not suffer important crossings and are treated adiabatically. This translates into smooth vibrationally adiabatic ground-state potential energy curves, as shown by the dotted curves in Figures 5a and 5b for reactions R3 and R4, respectively. Analogously, dotted lines in Figures 6a and 6b show the free energy of activation profiles for R3 and R4 at 300 K. Note that the profile corresponding to reaction R4 is not very smooth, and this is attributable to the presence in this system of several low frequencies associated to the movements of water molecules. The use of a quadratic expansion of the potential on the dividing surface by RODS algorithm[9] may be quantitatively inadequate for those low frequencies and for their effect on the entropic term of

the activation free energy.[35]

3.3.2. Reaction-path curvature. Figures 9 and 10 show the absolute values of the highest reaction-path curvature components corresponding to reaction R3 and R4, respectively. These components have been calculated with eq. 2, but using the direction normal to the RODS dividing surface instead of the gradient and with the RODS generalized normal mode eigenvectors. For reaction R3 we can distinguish two different regions. The first one, the region very close to the saddle point, has sharp peaks for frequency 1 and a lower peak for frequency 5 due to the interpolation needed in this region, where no electronic structure calculations have been done, because the somewhat big initial step required in an MEP calculation. Apart from these central peaks, frequencies 5 and 6 in the R3 calculation have another peak at $s = 0.13$ Å. This other peak causes the dip on those two frequencies in this region as shown in Figure 7.

Figure 10 shows the reaction-path curvature component for reaction R4 that corresponds to frequency 2, which has been adiabatically correlated along the path. This mode yields the only significant component of the reaction-path curvature vector. This frequency includes the A and B motions discussed above, as shown in Figure 8. Again it is clear that the dips that appear in Figure 8 are caused by the strong coupling between the generalized normal mode eigenvectors associated with frequency 2 and the gradient.

We can rationalize the previous paragraphs in the following way. Let us suppose that a generalized normal mode $\mathbf{L}_m$ is strongly coupled to the gradient at a given point on the MEP. If the reaction path is not followed precisely, a numerical bobsled effect will carry the calculated path into this direction. Sharp dips in generalized normal modes analysis along the reaction path can then arise as a direct consequence of bobsledding out of the MEP, and this is, in turn, a consequence of the reaction path curvature. The RODS algorithm is useful not only for eliminating the dips but also for analyzing the causes of those dips.

3.3.3. Canonical variational theory. Notice that in both Figures 5a and 6a the maximum values of the vibrationally adiabatic potential curves and the free energy of activation profiles occur very close to where they ocurred in the conventional calculations without RODS, although one could not have had any confidence in the calculations without RODS, since the curves themselves were not globally converged. Figures 5b and 6b show more significant differences for reaction R4.

Let $s_*^{CVT}(T)$ denote the location of the variational transition state at temperature T. Table III gives s_*^{CVT} and the ratio of TST to CVT rate constants over a wide range of

temperature for reaction R3. One can see that the CVT transition state moves farther and farther towards reactants (i.e., toward negative s) as the temperature increases, and this produces a nonnegligible variational effect on the rate constant. However the quantitative effect is 15% or less over the entire temperature range in the table and is only 1.29 at 2000 K. One way to understand why the variational effect on the rate constant is small is to rescale the reaction coordinate in a more physical, system-specific way. Figure 1 shows that the transition vector is intermediate between a pure motion of carbon and a relative motion of C primarily with respect to the three hydrogen atoms bonded to nitrogen atom, which motions would have reduced masses of 12 and 2.4 amu respectively. Thus we rescaled the reaction coordinate to an intermediate value of 7 amu; this new reaction coordinate is called S. Table III shows that for this more physically scaled reaction coordinate, the deviations of the variational transition state from the saddle point are only 0.02–0.05 Å (0.11 Å at 2000 K). Furthermore, the effective potential energy including zero point contributions (i.e., the vibrationally adiabatic ground-state potential curve[6,26]) is only 0.6 kcal/mol lower at the 2000 K transition state than at the 200 K one.

Table IV lists the same variables as in Table III but corresponding now to the dihydrated reaction R4. The variational effects on the rate constants are much bigger for the dihydrated than for the unhydrated reaction, with TST overestimating the CVT result by a factor increasing from 2.08 at 200K to 2.45 at 1000K.

3.3.4. Tunneling calculations. We did not present tunneling calculations in Section 3.2 since Figure 5 shows that the adiabatic potential curves obtained without RODS are unphysical. Table V shows the ground-state transmission coefficients based on calculations in which we have implemented the RODS algorithm. For both ZCT and SCT calculations we evaluated $V_a^G(s)$ using the RODS frequencies. In addition to the shape of the effective potential energy curve, for the SCT calculations is also necessary to compute the reaction-path curvature components. As explained above, we calculated these using the direction normal to the RODS dividing surface and the RODS values of the generalized normal-mode eigenvectors.

For both reactions R3 and R4, the SCT values are significantly bigger than the ZCT ones. Since the ZCT transmission factors are based on tunneling along the MEP, while the SCT calculations account for corner cutting during tunneling, this result indicates that corner cutting of the tunneling path is important in this multidimensional reaction. A similar effect was observed in the S_N2 methyl exchange process between chloride and methyl chloride where

corner cutting of the tunneling path was attributed to the hydrogenic motions, but in that case the tunneling effect and corner cutting effect were both smaller. For example for reaction R1 at 300 K the ZCT transmission coefficients are 1.31 and 1.32 for n = 0 and 1, respectively, while the SCT transmission coefficients are 1.32 and 1.36.[15] One reason for the larger effects in the present case is that the classical barriers with respect to reactants are much higher, 7.2 kcal for R3 and 20.5 kcal for R4, as compared to 3.1 kcal[11] and 4.8 kcal[15] for R1 with n = 0 and 1, respectively. Even with these higher barriers, the values of the transmission factors obtained in this work for reactions R3 and R4 may seem surprisingly high, which is probably best interpreted by noting that Figures 1 and 3 show significant hydrogenic motions in the transition vectors. These hydrogenic motions are probably the dominant reason for the large tunneling effects. We note though that this is formally a heavy-atom tunneling effect (i.e., the dominant motion in the reaction coordinate is an atom heavier than H, D, or T), and significant tunneling of heavy atom groups has also been observed in other theoretical calculations of organic reactions.[38]

3.3.5. Rate constants. The final rate constants are given in Table VI.

4. CONCLUSIONS

We have demonstrated that the RODS algorithm allows stable VTST and tunneling calculations on a new class of reactions that had proved intractable with earlier algorithms. The difficulty occurs when there are high-frequency modes strongly coupled to the reaction coordinate in a region where the energy is varying slowly along the reaction path, such as near the saddle point.

The RODS algorithm has also proved useful for accelerating convergence on a number of other problems.[9,39] In the present case it showed its mettle on an even more intractable case. Its success in the present very difficult case is very encouraging for our ability to apply direct dynamics calculations to a wider variety of interesting applications in the future.

Finally we conclude that variational effects and tunneling effects can be significant for reactions involving methyl cation transfer when separated charge is created in the forward or reverse reaction.

5. ACKNOWLEDGMENTS

The authors are grateful to Patton Fast for helpful discussions. This work was

supported in part by the U.S. Department of Energy, Office of Basic Energy Sciences. Financial support from DGES (project No. PB95-0637) and the use of the computational facilities of the "Centre de Computació i de Comunicacions de Catalunya" are also gratefully acknowledged.

1. (a) Wigner, E. *Trans. Faraday Soc.* **1938**, *34*, 29. (b)Horiuti, J. *Bull. Chem. Soc. Jpn.* **1938**, *13*, 210.

2. Keck, J. C. *Adv. Chem. Phys.* **1967**, *13*, 85.

3. Garrett, B. C.; Truhlar, D. G. *J. Chem. Phys.* **1979**, *70*, 1593.

4. Garrett, B. C.; Truhlar, D. G. *Acc. Chem. Res.* **1980**, *13*, 440.

5. Garrett, B. C.; Truhlar, D. G. *J. Phys. Chem.* **1979**, *83*, 1079.

6. Garrett, B. C.; Truhlar D. G.; Grev, R. S.; Magnuson, A. W. *J. Phys. Chem.* **1980**, *84*, 1730.

7. (a) Chatfield, D. C.; Friedman, R. S.; Truhlar, D. G.; Garett, B. C.; Schwenke, D. W. *J. Am. Chem. Soc.* **1991**, *113*, 486. (b) Chatfield, D. C.; Friedman, R. S.; Schwenke, D. W.; Truhlar, D. G. *J. Phys. Chem.* **1992**, *96*, 2414. (c) Chatfield, D. C.; Friedman, R. S.; Mielke, S. L.; Schwenke, D. W.; Lynch, G. C.; Allison, T. C.; Truhlar, D. G. In *Dynamics of Molecules and Chemical Reactions*, edited by Wyatt, R. E. and Zhang, J. Z. H. (Marcel Dekker, New York, 1996), pp. 323-386.

8. Melissas, V. S.; Truhlar, D. G.; Garrett, B. C. *J. Chem. Phys.* **1992**, *96*, 5758.

9. Villà, J.; Truhlar, D. G. *Theor. Chem. Acct.* **1997**, *97*, 317.

10. (a) Garrett, B. C.; Truhlar, D. G.; Grev, R. S. In *Potential Energy Surfaces and Dynamics Calculations*; Truhlar, D. G., Ed.; Plenum: New York, 1981; p. 587. (b) Garrett, B. C.; Truhlar, D. G. *Annu. Rev. Phys. Chem.* **1984**, *35*, 159. (c) Truhlar, D. G.; Garrett, B. C. *J. Chem. Phys.* **1987**, *84*, 365. (d) Truhlar, D. G.; Garrett, B. C.; Klippenstein, S. J. *J. Phys. Chem.* **1996**, *100*, 12771.

11. Tucker, S. C.; Truhlar, D. G. *J. Am. Chem. Soc.* **1990**, *112*, 3347.

12. Zhao, X. G.; Tucker, S. C.; Truhlar, D. G. *J. Am. Chem. Soc.* **1991**, *113*, 826.

13. González-Lafont, A.; Truong, T. N.; Truhlar, D. G. *J. Phys. Chem.* **1991**, *95*, 4618.

14. Truhlar, D. G.; Lu, D.-h.; Tucker, S. C.; Zhao, X. G.; Gonzàlez-Lafont, A.; Truong, T. N.; Maurice, D.; Liu, Y.-P.; Lynch, G. C. *ACS Symp. Ser.*, **1992**, *502*, 16.

15. Zhao, X. G.; Lu, D.-h.; Liu, Y.-P.; Lynch, G. C.; Truhlar, D. G. *J. Chem. Phys.* **1992**, *97*, 6369.

16. Viggiano, A. A.; Paschkewitz, J.; Morris, R. A.; Paulson, J. F.; González-Lafont, A.; Truhlar, D. G. *J. Am. Chem. Soc.* **1991**, *113*, 9404.

17. (a) Hu, W.-P.; Truhlar D. G. *J. Am. Chem. Soc.* **1994**, *116*, 7797. (b) Hu, W.-P.; Truhlar, D. G. *J. Am. Chem. Soc.* **1995**, *117*, 10726.

18. Hu, W.-P.; Truhlar, D. G. *J. Am. Chem. Soc.* **1996**, *118*, 860.

19. (a) Gao, J. *J. Am. Chem. Soc.* **1991**, *113*, 7796. (b) Solà, M.; Lledós, A.; Duran, M.; Bertrán, J.; Abboud, J. L. M. *J. Am. Chem. Soc.* **1991**, *113*, 2873. (c) Gao, J. ; Xinfu, X. *J. Am. Chem. Soc.* **1993**, *115* , 9667. (d) Gao, J.; Xinfu, X. *ACS Symp. Ser.* **1994**, *568*, 212. (e) Dillet, V.; Rinaldi, D.; Bertrán, J.; Rivail, J. L. *J. Chem. Phys.* **1996**, *104*, 9437.

20. Doubleday, C., Jr.; McIver, J. W., Jr.; Page, M. *J. Phys. Chem.* **1988**, *92*, 4367.

21. Baldridge, K. K.; Gordon, M. S.; Steckler, R.; Truhlar, D. G. *J. Phys. Chem.* **1989**, *93*, 5107.

22. Truhlar, D. G. In *The Reaction Path in Chemistry*; Heidrich, D., Ed.; Kluwer: Dordrecht, 1995; p. 229.

23. Truong, T. N.; Duncan, W. T.; Bell, R. L. *ACS Symp. Ser.* **1996**, *629*, 85.

24. Szabo, A.; Ostlund, N. S. *Modern Quantum Chemistry*; MacMillan: New York, 1982.

25. Frisch, M. J.; Pople, J. A.; Binkley, J. S. *J. Chem. Phys.* **1984**, *80*, 3265.

26. Truhlar, D. G. Kupperman, A. *J. Am. Chem. Soc.* **1971**, *93*, 1840.

27. Truhlar, D. G.; Isaacson, A. D.; Garrett, B. C. In *Theory of Chemical Reaction Dynamics*; Baer, M., Ed.; CRC Press: Boca Raton, 1985; Vol. 4, p. 65.

28. Mulliken, R. S. *J. Chem. Phys.* **1955**, *23*, 1833.

29. Schmidt, M. W.; Baldridge, K. K.; Boatz, J. A.; Elbert, S. T.; Gordon, M. S.; Jensen, J. H.; Koveki, S.; Matsunaga, N.; Nguyen, K. A.; Su, S.; Windus, T. L.; Elbert, S. T. *J. Comp. Chem.* **1993**, *14*, 1347.

30. Miller, W. H.; Handy, N. C; Adams, J. E. *J. Chem. Phys.* **1980**, *72*, 99.

31. Lu, D.-h; Truong, T. N.; Melissas, V. S.; Lynch, G. C.; Liu, Y.-P.; Garrett, B. C.; Steckler, R.; Isaacson, A. D.; Rai, S. N.; Hancock, G. C.; Lauderdale, J. G.; Joseph, T.; Truhlar, D. G. *Computer Phys. Commun.* **1992**, *17*, 235.

32. Liu, Y.-P.; Lynch, G. C.; Truong, T. N.; Lu, D.-h.; Truhlar, D .G.; Garrett, B. C. *J. Am. Chem. Soc.* **1993**, *115*, 2408.

33. Steckler, R.; Chuang, Y. -Y.; Coitiño, E. L.; Hu, W.-P.; Liu, Y.-P.; Lynch,G.C.; Nguyen, K. A.; Jackels, C. F.; Gu, M. Z.; Rossi, I.; Fast, P.; Clayton, S.; Melissas, V.S.; Garrett, B.C.; Isaacson, A.D.; Truhlar, D.G. POLYRATE-version 7.0, University of Minnesota, Minneapolis, 1996 (unpublished).

34. Truhlar, D. G.; Isaacson, A. D. *J. Chem. Phys.* **1982**, *77*, 3516.

35. (a) Villà, J.; González-Lafont, A.; Lluch, J. M.; Bertrán, J. *Mol. Phys.* **1996**, *89*, 633; (b) Program CORREL can be downloaded from http://klingon.uab.es/soft/theorchemsoft.html#correl.

36. Truhlar, D. G.; Isaacson, A. D. *J. Chem. Phys.* **1991**, *94*, 357.

37. The ACESRATE program is described in Steckler, R.; Thurman, G. M.; Watts, J. D.; Bartlett, R. J. *J. Chem. Phys.* **1997**, *106*, 3926. The ACESRATE code is based on the POLYRATE dynamics code, in particular, Steckler, R.; Chuang, Y. -Y.; Coitiño, E. L.; Hu, W. -P.; Liu, Y. -P.; Lynch, G. C.; Nguyen, K. A.; Jackels, C. F.; Gu, M. Z.; Rossi, I.; Fast, P.; Clayton, S.; Melissas, V. S.; Garrett, B. C.; Isaacson, A. D.; Truhlar, D. G. POLYRATE-version 7.1, University of Minnesota, Minneapolis, February 1997 and on the ACES II electronic structure code, which is described in Stanton, J. F.; Gauss, J.; Watts, J. D.; Lauderdale, W. J.; Bartlett, R. T. *Int. J. Quantum Chem. Symp.* **1992**, *26*, 879.

38. (a) Frei, H.; Pimentel, G. C. *J. Phys. Chem.* **1981**, *85*, 3355. (b) Carpenter, B. K. *J. Am. Chem. Soc.* **1983**, *105*, 1700. (c) Dewar, M. J. S.; Merz, K. M., Jr. *J. Phys. Chem.* **1985**, *89*, 4739. (d) Dewar, M. J. S.; Merz, K. M. *THEOCHEM* **1985**, *23*, 5. (e) Dewar, M. J. S.; Merz, K. M. Jr. *J. Am. Chem. Soc.* **1986**, *108*, 5634. (f) Sponsler, M. B.; Jain, R.; Coms, F. D.; Dougherty, D. A. *J. Am. Chem. Soc.* **1989**, *111*, 2240. (g) Zerbetto, F.; Zgierski, M. Z.; Siebrand, W. *J. Am. Chem. Soc.* **1989**, *111*, 2799. (h) Zerbetto, F.; Zgierski, M. Z. *Chem. Phys.* **1989**, *130*, 4. (i) Arnold, B. R.; Radziszewski, J. G.; Campion, A.; Perry, S. S.; Michl, J. *J. Am. Chem. Soc.* **1991**, *113*, 692. (j) Orlandi, G.; Zerbetto, F. *Chem. Phys. Lett.* **1991**, *184*, 191. (k) Maier, G.; Wolf, R.; Kalinowski, H. O. *Angew. Chem., Int. Ed. Engl.*, **1992**, *31*, 738. (l) Carsky, P.; Michl, J. *Theor. Chim. Acta* **1992**, *84*, 125. (m) Bosch, E.; Moreno, M.; Lluch, J.M. *J. Am. Chem. Soc.* **1992**, *114*, 2072.

39. Fast, P. L.; Truhlar, D. G. unpublished.

Table I. Stationary-point energies, geometries, and partial charges for reaction R3

Species	V_{MEP} (kcal/mol)	R(C-N) (Å)	R(C-Cl) (Å)	θ(H-C-N) (deg)	θ(C-N-H) (deg)	q_{CH3} (a.u.)	q_{NH3} (a.u.)	q_{Cl} (a.u.)
$(Cl^-)(CH_3NH_3^+)$	0.0	1.541	2.918	107.9	111.2	0.46	0.43	-0.89
saddle point	7.2	1.900	2.474	96.1	111.1	0.49	0.21	-0.70
$ClCH_3(NH_3)$[a]	-30.5	3.533	1.793	71.5	111.1	0.12	-0.01	-0.11
$ClCH_3 + NH_3$	-28.9	∞	1.786	···	···	0.06	0.00	-0.06

[a]Dipole-dipole complex

Table II. Stationary-point energies, geometries, and partial charges for reaction R4

Species	V_{MEP} (kcal/mol)	R(C-N) (Å)	R(C-Cl) (Å)	R(N-Cl) (Å)	R(Cl-H)[a] (Å)	R(N-O)[b] (Å)	q_{CH3} (a.u.)	q_{NH3} (a.u.)	q_{Cl} (a.u.)	$q_{W(Cl)}$ (a.u.)	$q_{W(N)}$ (a.u.)
$CH_3Cl(H_2O) + NH_3(H_2O)$	0.0	∞	1.79	∞	2.84	3.04	0.11	-0.02	-0.10	0.00	0.02
$CH_3Cl(H_2O)[NH_3(H_2O)]$[c]	-5.1	3.58	1.80	4.58	2.64	3.20	0.14	-0.01	-0.12	-0.02	0.01
saddle point	20.5	2.04	2.38	4.41	2.34	2.99	0.51	0.16	-0.63	-0.04	0.01
$(CH_3NH_3^+)(Cl^-)(H_2O)_2$	-20.7	1.48	3.74	3.02	2.32	2.86	0.30	0.51	-0.78	-0.04	0.01

[a]R(Cl-H) is the distance from Cl to the closest water H atom, and $q_{W(Cl)}$ is the partial charge on the water hydrogen that is bonded to Cl.

[b]R(N-O) is the distance from N to the closest water O atom, and $q_{W(N)}$ is the partial charge on the water hydrogen that is bonded to N.

[c]Dipole-dipole complex

Table III. Variational transition state location and variational effect on the rate constant for reaction R3

T (K)	s_*^{CVT} (Å)	k^{TST}/k^{CVT}	S_*^{CVT} (Å)
200	-0.06	1.13	-0.02
300	-0.07	1.11	-0.03
400	-0.08	1.10	-0.03
600	-0.10	1.11	-0.04
800	-0.12	1.13	-0.05
1000	-0.14	1.15	-0.05

Table IV. Variational transition state location and variational effect on the rate constant for reaction R4

T (K)	s_*^{CVT} (Å)	k^{TST}/k^{CVT}	S_*^{CVT} (Å)
200	-0.06	2.08	-0.02
300	-0.06	2.20	-0.02
400	-0.07	2.28	-0.02
600	-0.07	2.37	-0.02
800	-0.07	2.42	-0.02
1000	-0.07	2.45	-0.02

Table V. Ground-state transmission coefficients to account for tunneling (RODS calculation)

T (K)	reaction R3		reaction R4	
	ZCT	SCT	ZCT	SCT
200	2.09	3.34	2.10	17.6
300	1.35	1.66	1.34	3.48
400	1.18	1.32	1.17	2.03
600	1.08	1.13	1.07	1.38
800	1.04	1.07	1.04	1.20
1000	1.03	1.05	1.03	1.12

Table VI. CVT/SCT rate constants (RODS calculations)

T(K)	R3[a]	R4[b]
200	$2.27 \cdot 10^{7}$	$1.10 \cdot 10^{-43}$
300	$1.11 \cdot 10^{9}$	$3.20 \cdot 10^{-35}$
400	$9.61 \cdot 10^{9}$	$6.14 \cdot 10^{-31}$
600	$9.96 \cdot 10^{10}$	$1.51 \cdot 10^{-26}$
800	$3.48 \cdot 10^{11}$	$2.95 \cdot 10^{-24}$
1000	$7.67 \cdot 10^{11}$	$8.04 \cdot 10^{-23}$

[a]In s^{-1}

[b]In cm^3 $molecule^{-1}$ s^{-1}

FIGURE CAPTIONS

Figure 1. Saddle point of the unhydrated reaction R3 along with components of the transition vector in mass-scaled Cartesian coordinates.

Figure 2. Dipole-dipole complex of the dihydrated reaction R4.

Figure 3. Saddle point of the dihydrated reaction R4 along with the main components of the transition vector in mass-scaled Cartesian coordinates.

Figure 4. Ion-pair product of the dihydrated reaction R4.

Figure 5. Detail of the adiabatic ground-state potential energy curves (in kcal mol^{-1}) versus the arc length along the reaction coordinate (in Å) for reactions R3 (a) and R4 (b). Solid lines correspond to the standard VTST calculation. Dotted lines correspond to RODS VTST calculation.

Figure 6. Detail of the generalized activation free energy curves at T = 300 K (in kcal mol^{-1}) versus the arc length along the reaction coordinate (in Å) for reactions R3 (a) and R4 (b). Solid lines correspond to the standard VTST calculation. Dotted lines correspond to RODS VTST calculation.

Figure 7. Diabatic generalized normal mode frequencies (in cm^{-1}) versus the arc length along the reaction coordinate (in Å) along the reaction coordinate for the unhydrated reaction R3, based on the standard algorithm. Only frequencies correlated to reactant modes above 1500 cm^{-1} are displayed.

Figure 8. Diabatic generalized normal mode frequencies (in cm^{-1}) versus the arc length along the reaction coordinate along the reaction coordinate (in Å) for the dihydrated reaction R4, based on the standard algorithm. Only frequencies correlated to reactant modes above 1500 cm^{-1} are displayed.

Figure 9. Absolute value of the reaction path curvature components B_{mF} (in $Å^{-1}$) versus the arc length along the reaction coordinate (in Å) for modes 1, 5 and 6 for reaction R3.

Figure 10. Absolute value of the reaction path curvature components B_{mF} (in $Å^{-1}$) versus the arc length along the reaction coordinate (in Å) for mode 2

for reaction R3.

1, 0.0 cm**-1
ens 0.0 km/mol
ıan int******** A**4/amu

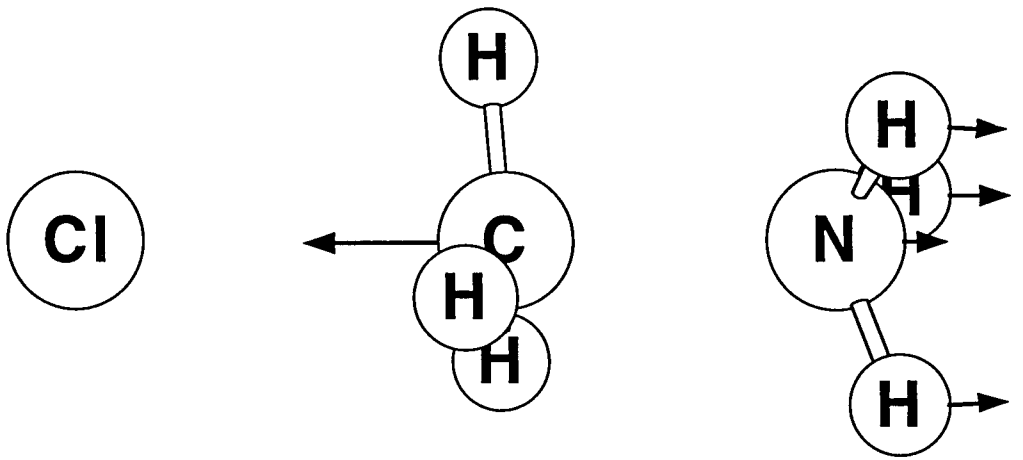

H
H

Cl
H
H
C
H

H
O
H

N
H
H
H

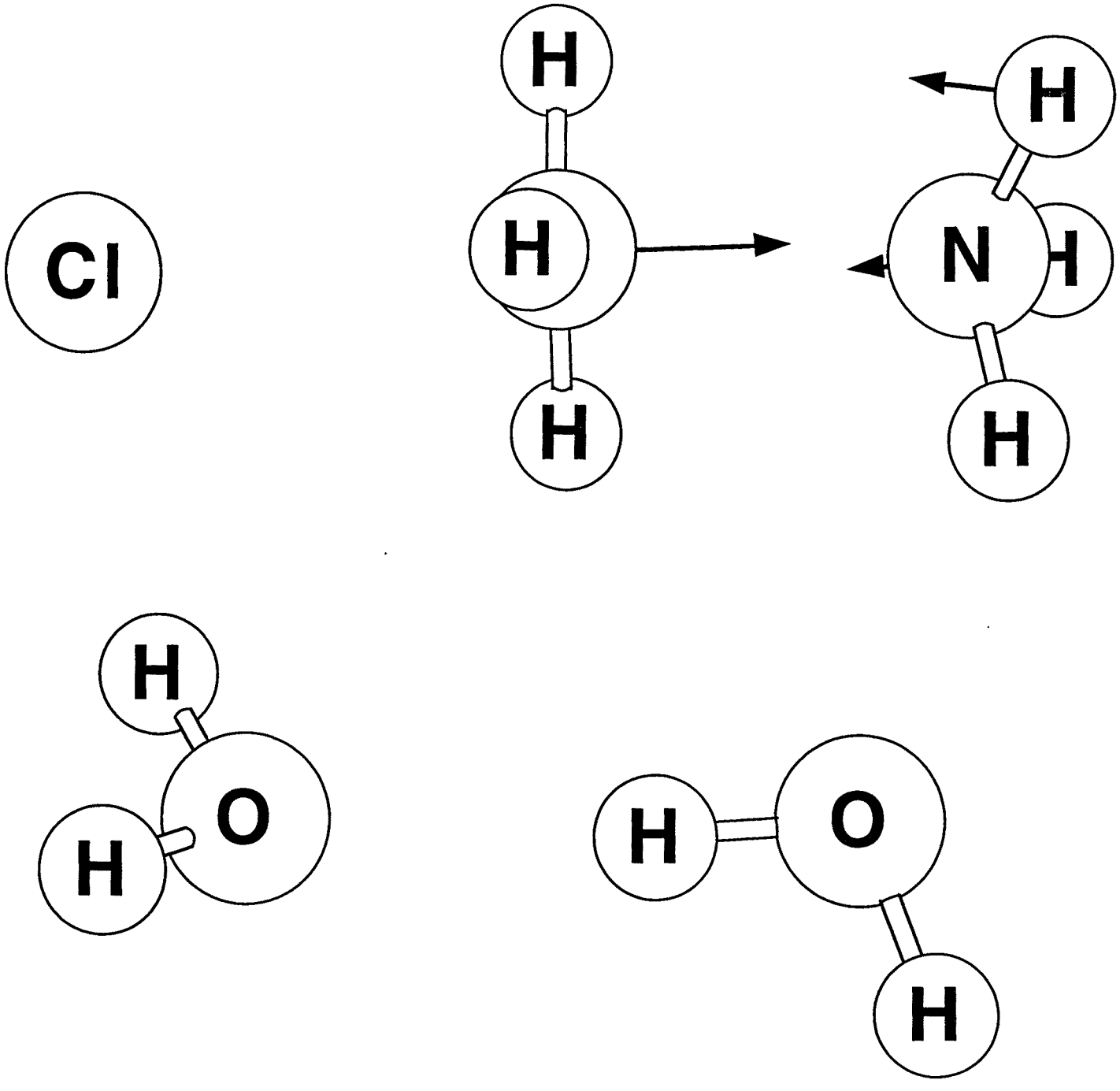
Cl
H
H
H
H
N
H
H
H
O
H
H
O
H

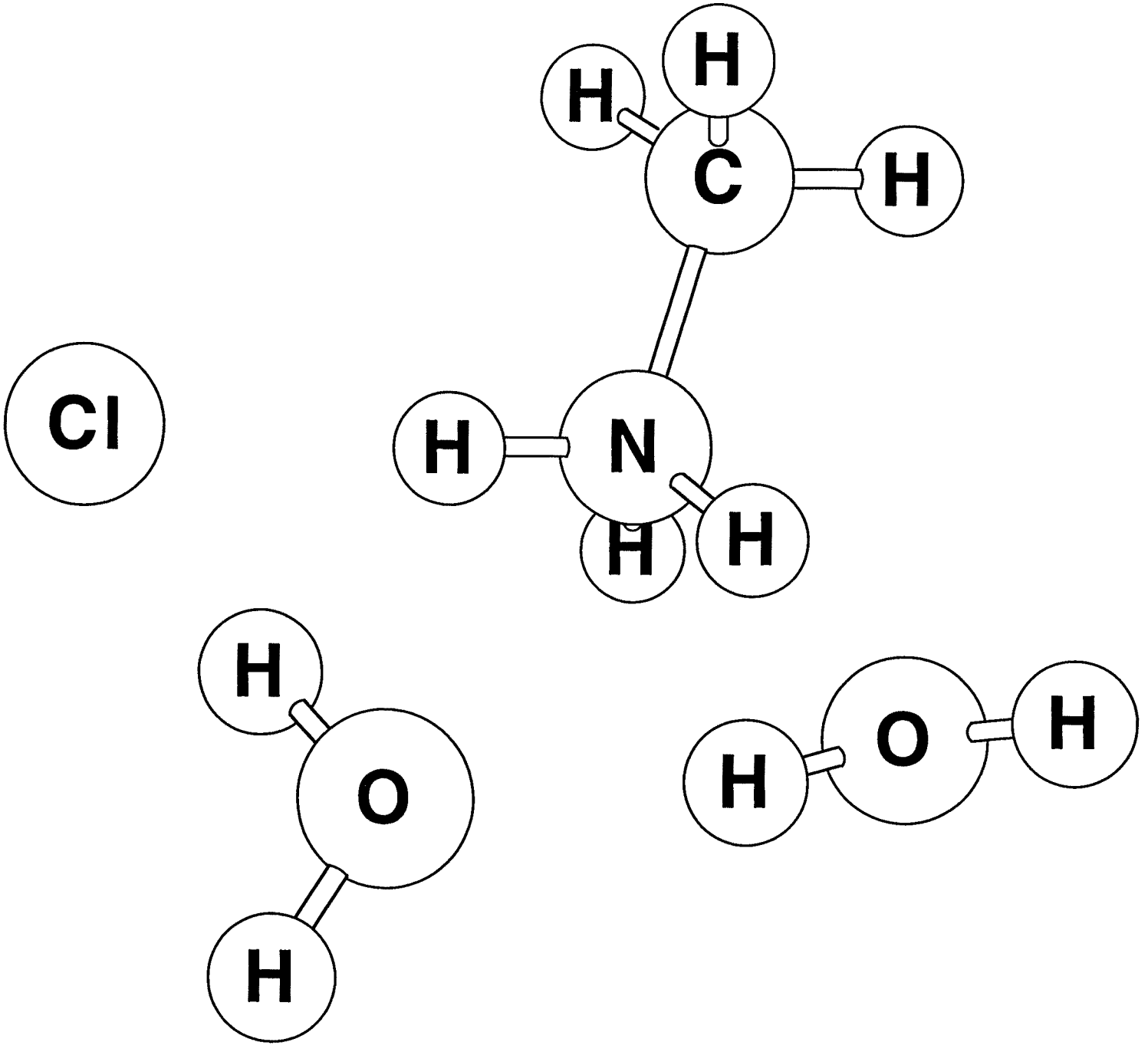
Cl
H
H
H
C
H
H
N
H
H
H
O
H
H
O
H

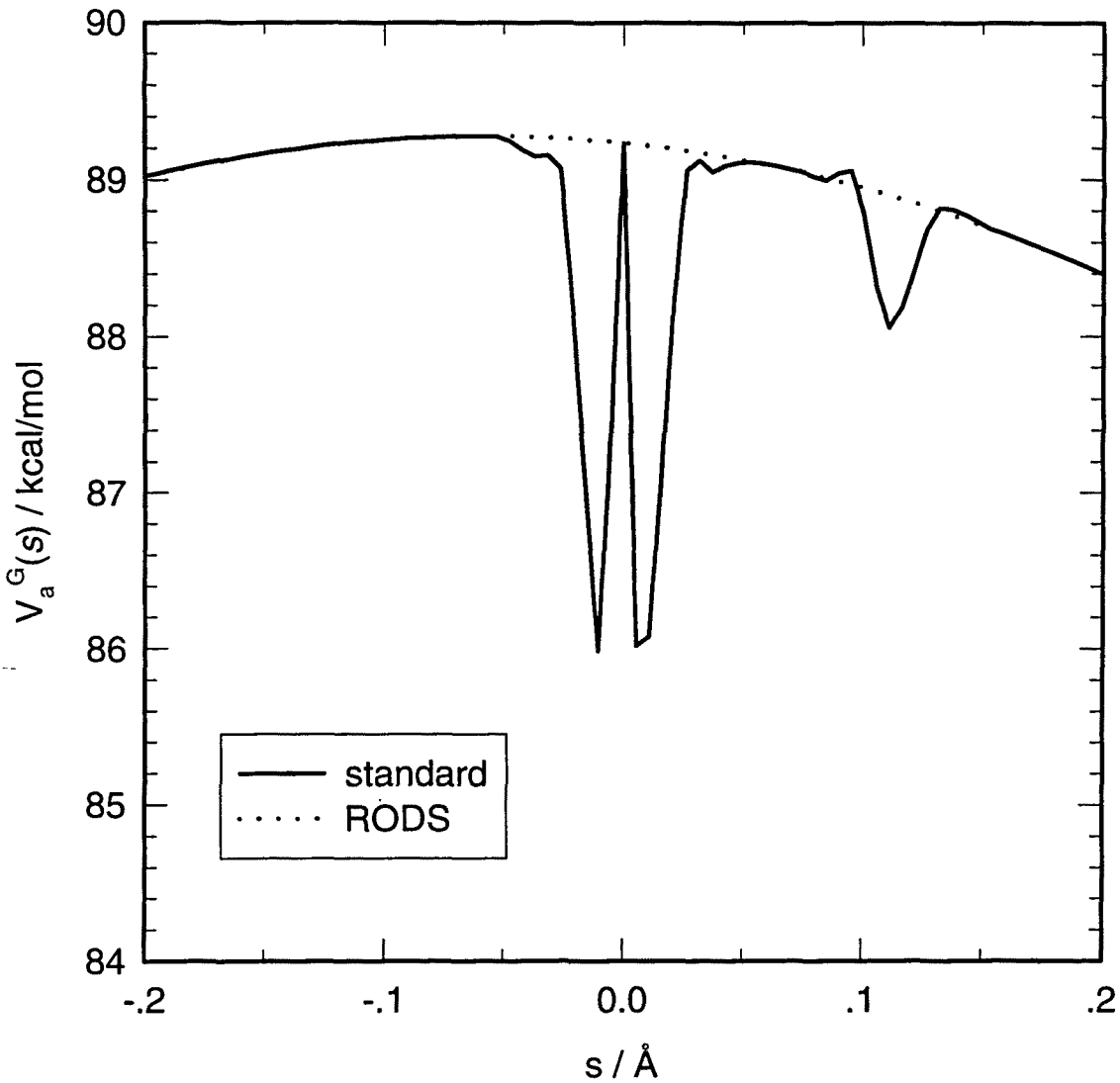

Figure 5a

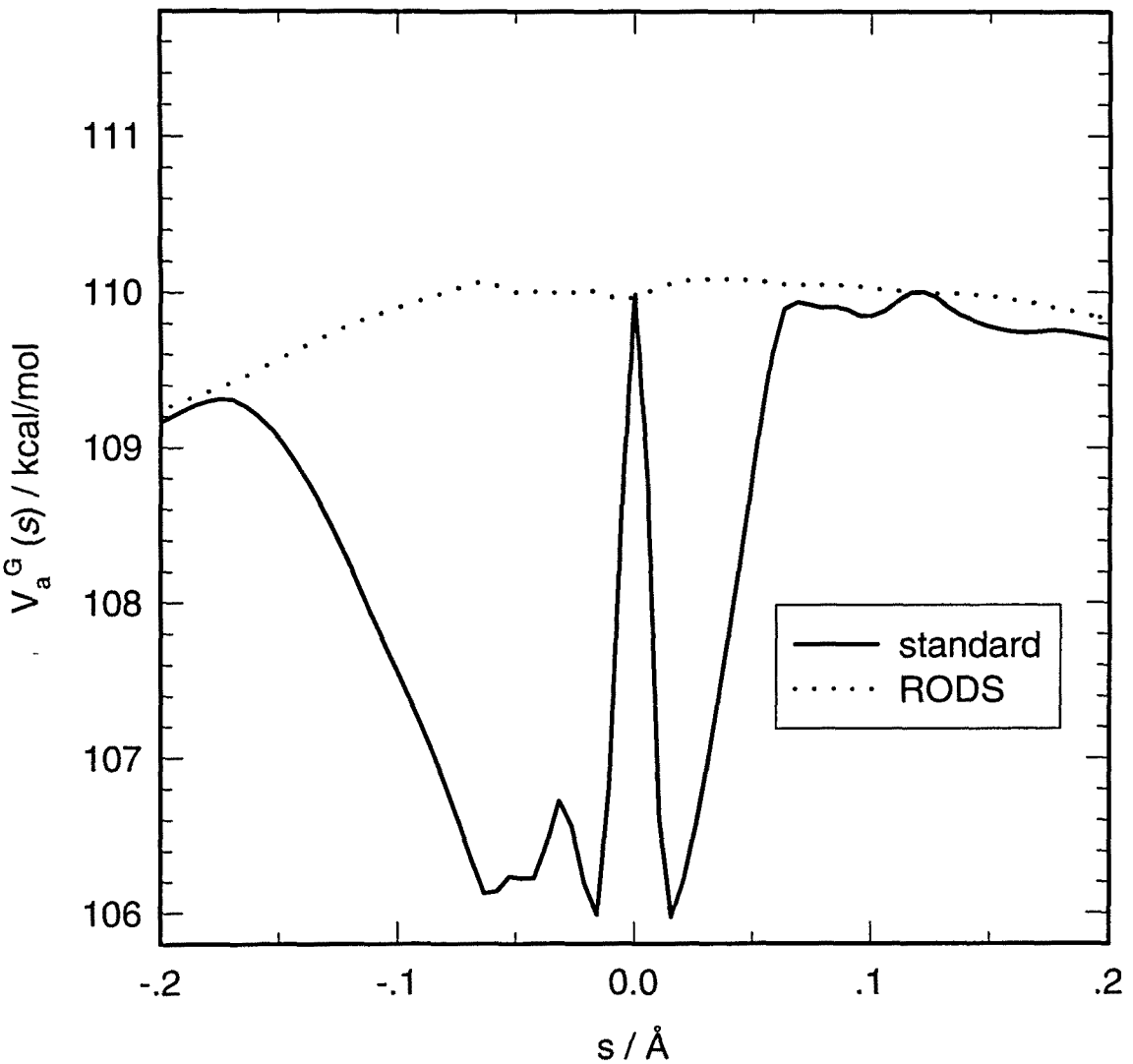

Figure 5b

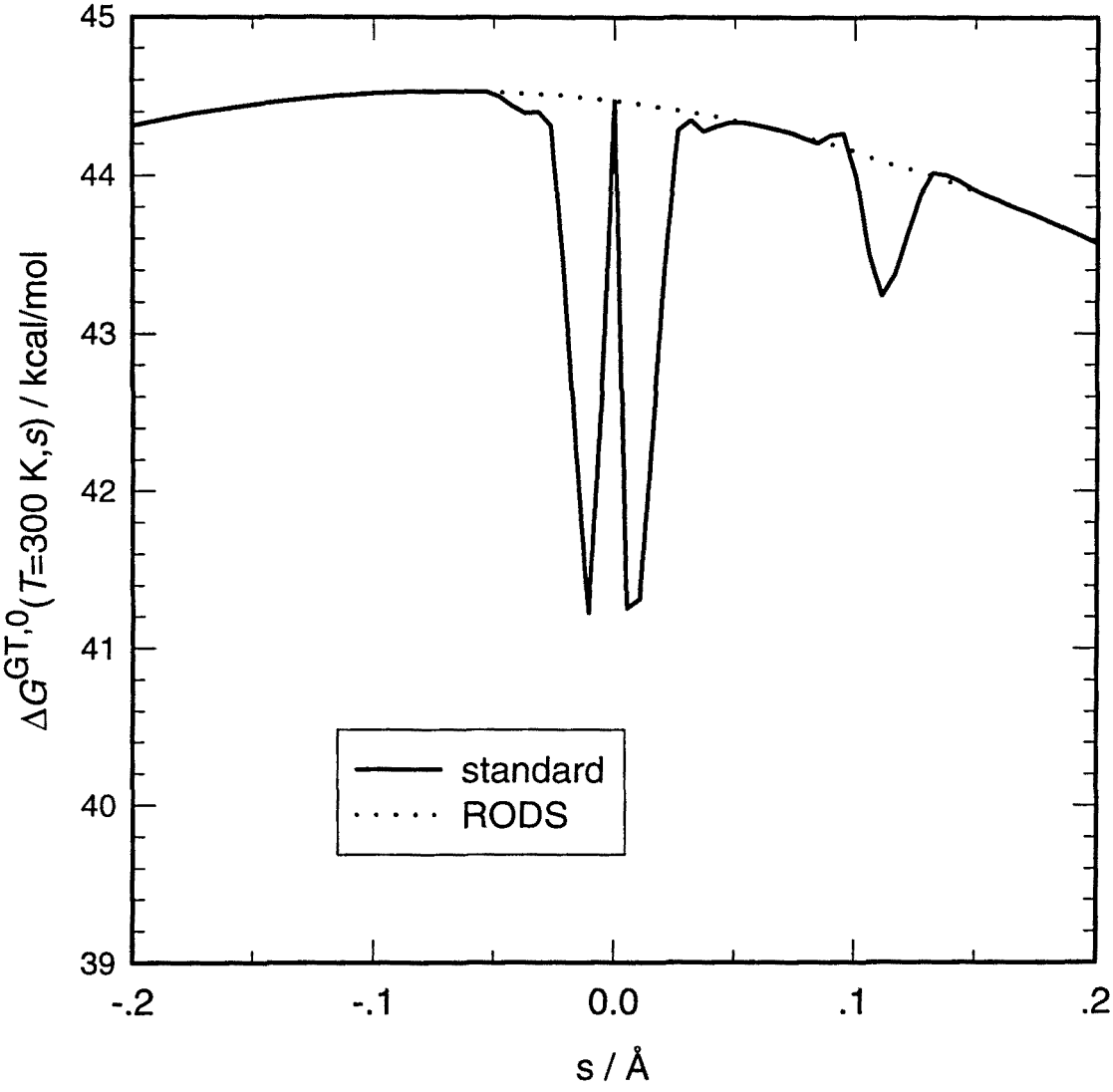
45
44
43
42
41
40
39
-.2
-.1
0.0
.1
.2
s / Å
ΔG^GT,0(T=300 K,s) / kcal/mol
standard
RODS

Figure 6a

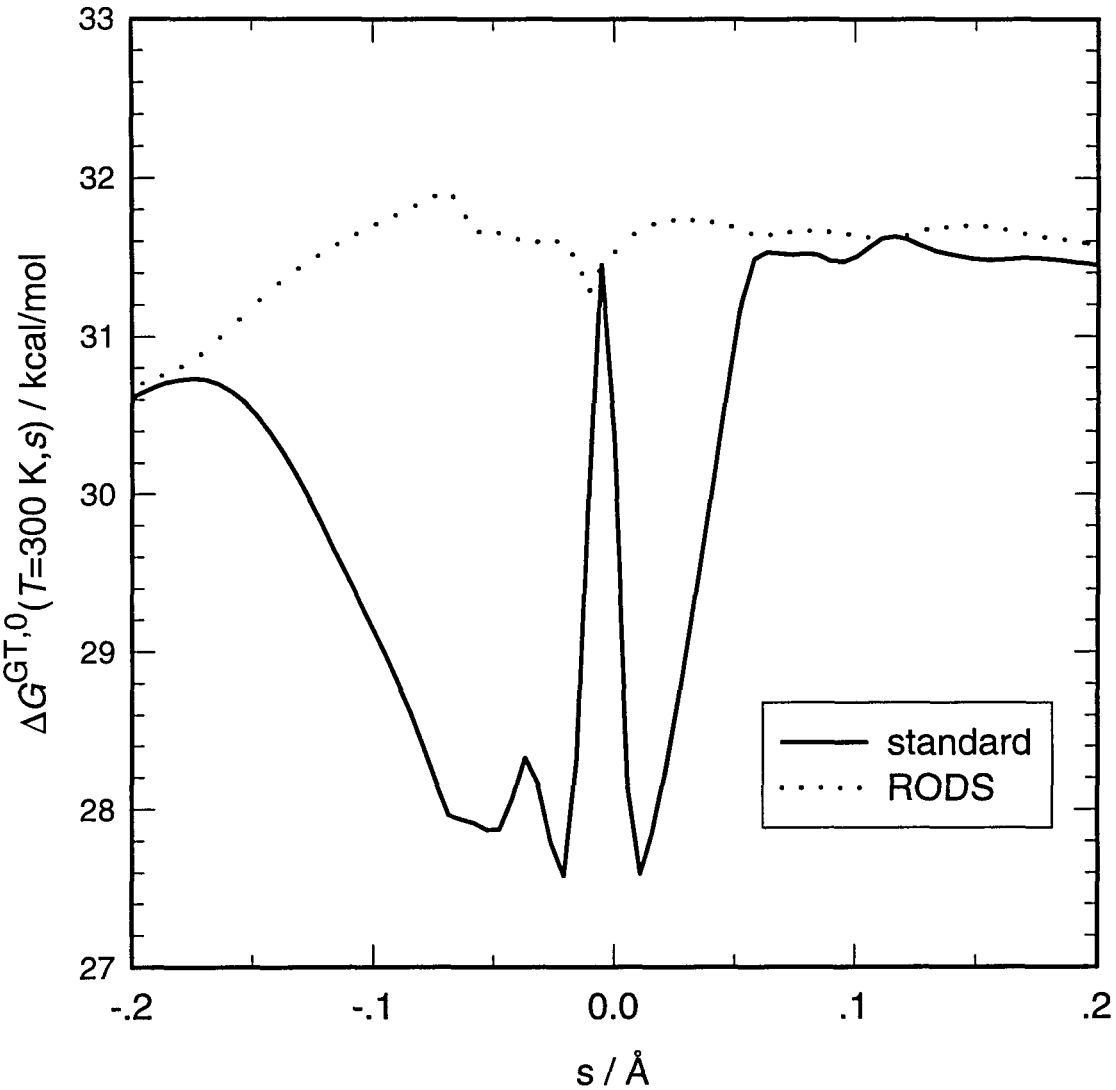
33
32
31
30
29
28
27
-.2
-.1
0.0
.1
.2
s / Å
ΔG^GT,0(T=300 K,s) / kcal/mol
standard
RODS

Figure 6b

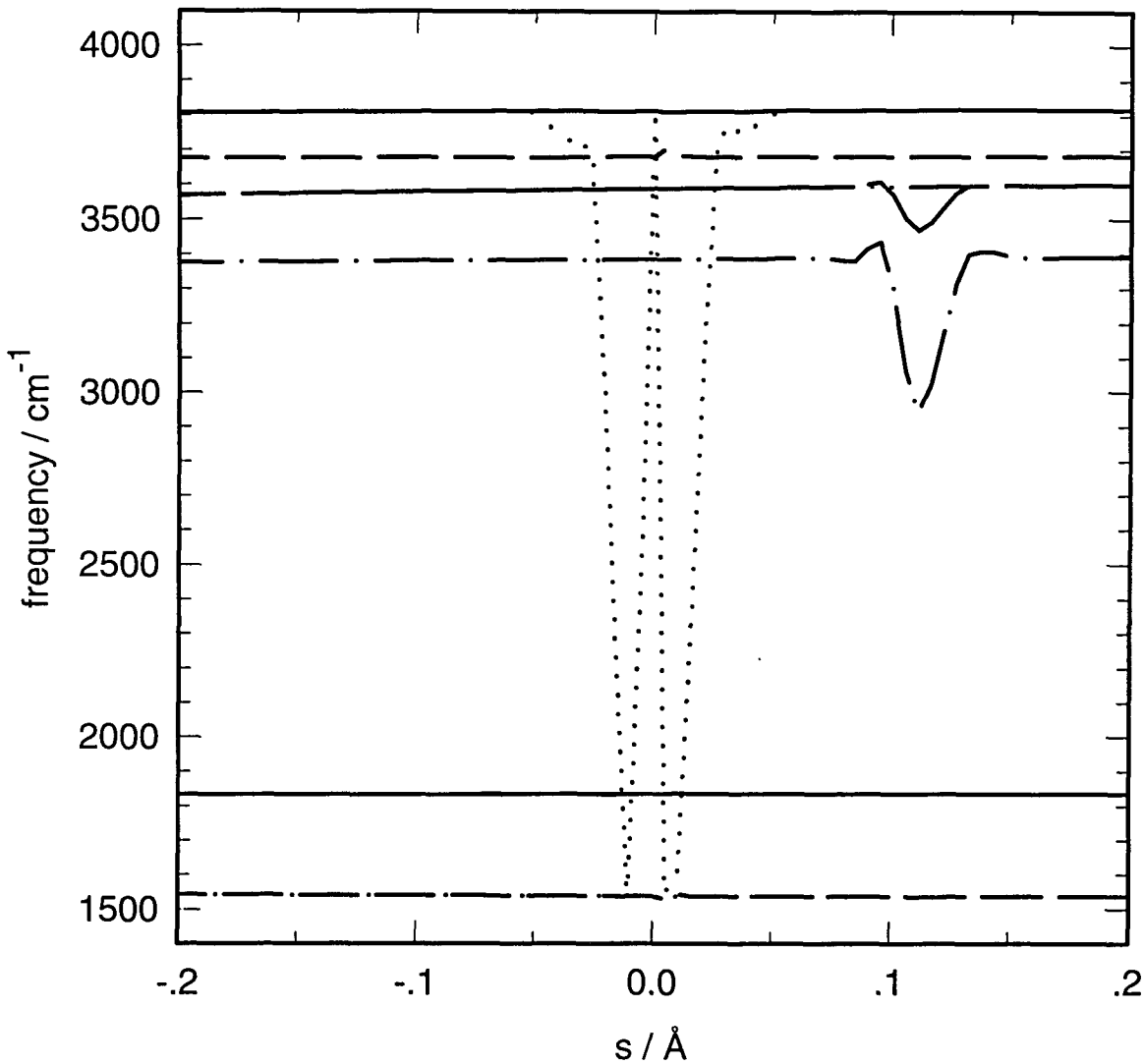

Figure 7

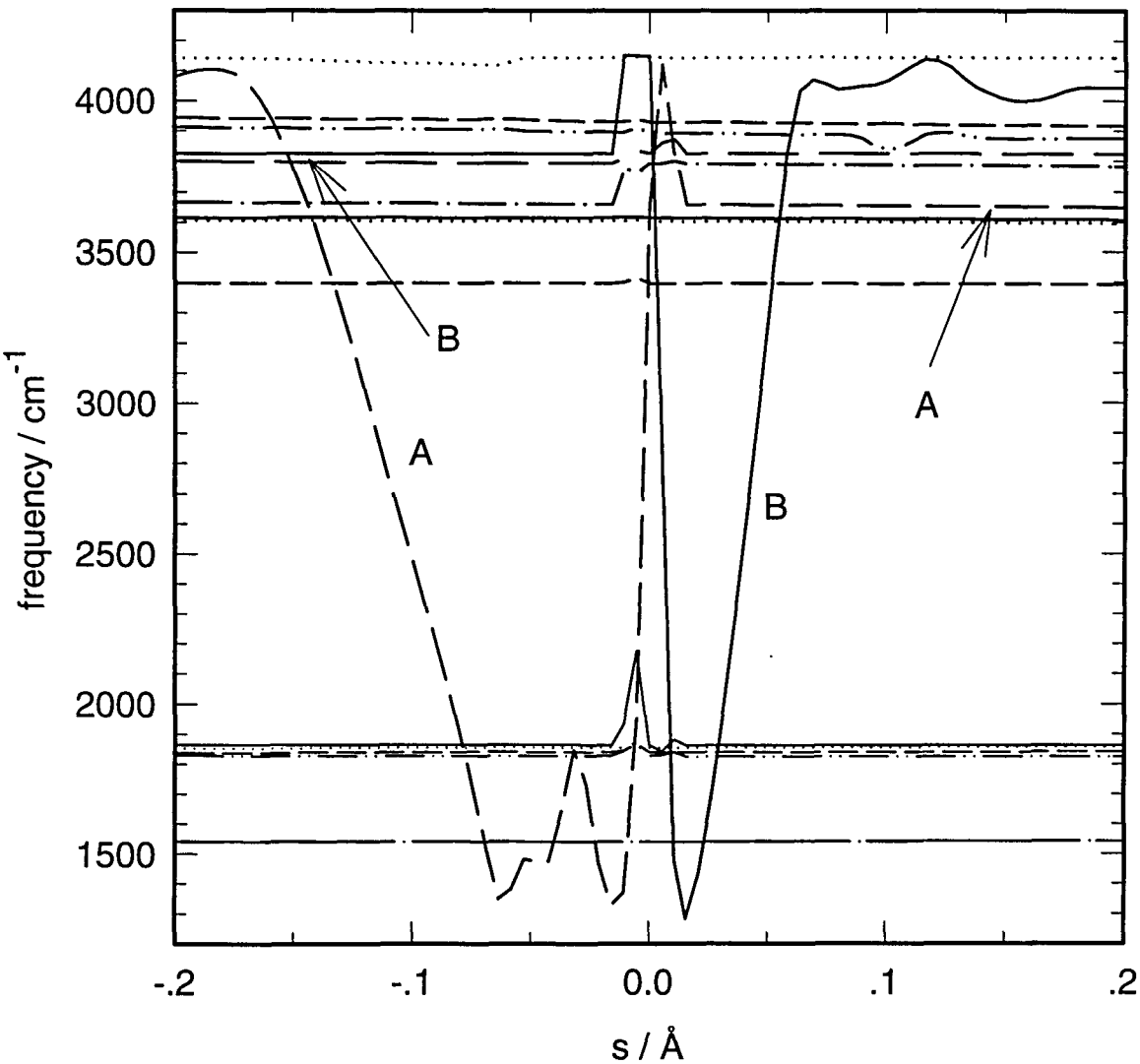

Figure 8

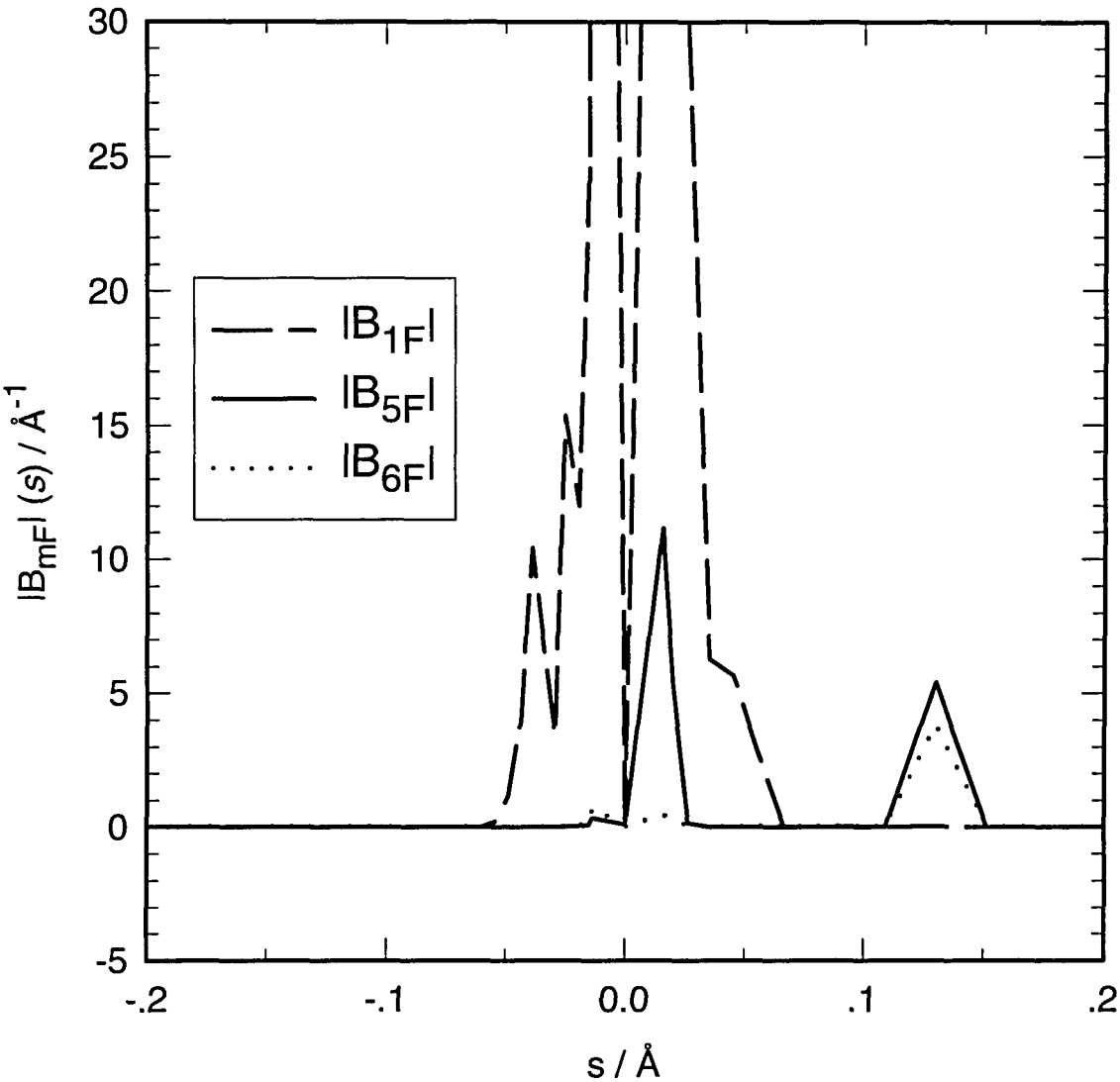

Figure 9

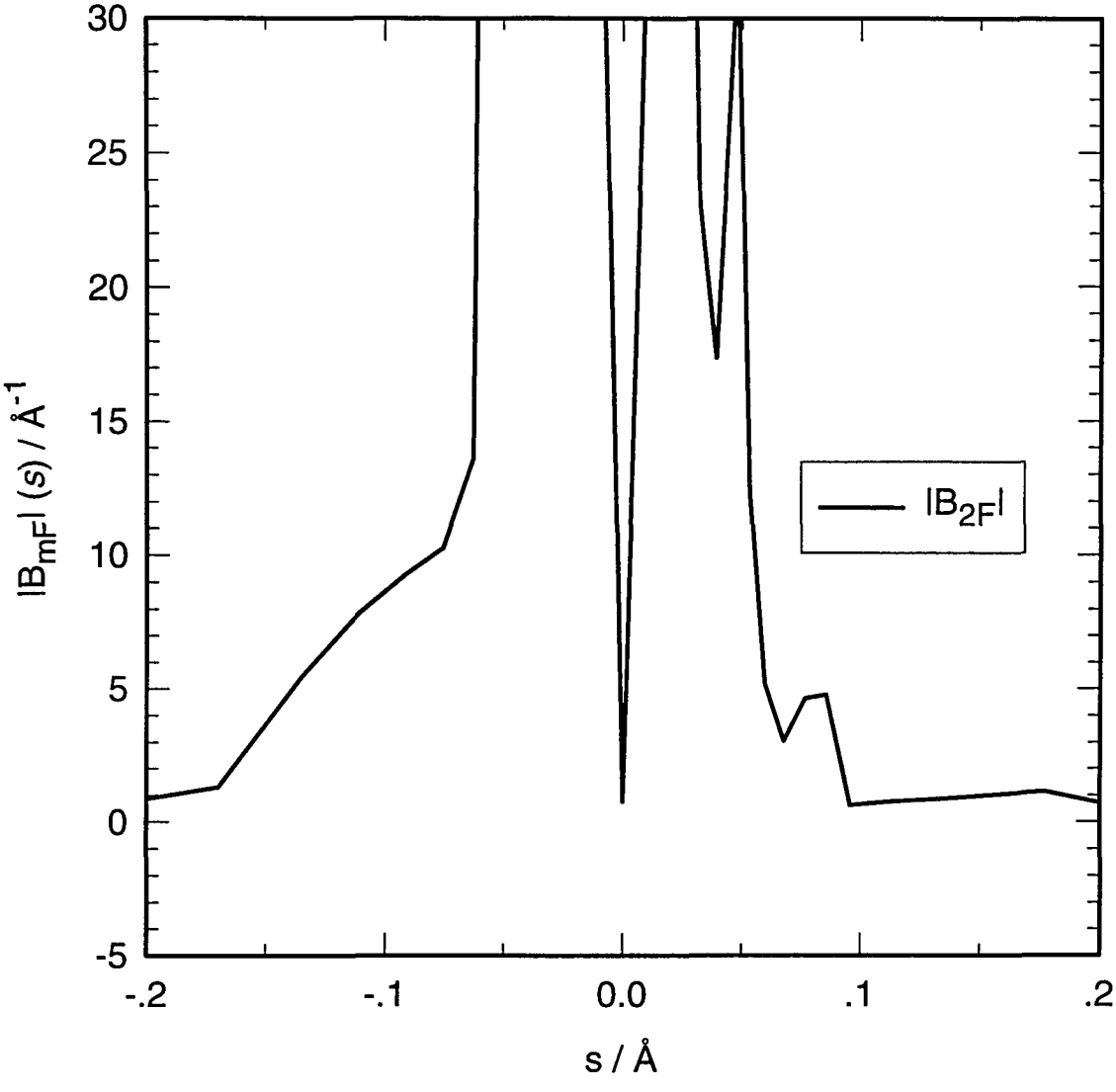

Figure 10

Article 4

"Kinetic isotope effects as tools to reveal solvation changes accompanying a proton transfer. A canonical unified statistical theory calculation"

Jordi Villà, Angels González-Lafont, José M. Lluch

The Journal of Physical Chemistry, **1996**, *100*, 19389.

Kinetic Isotope Effects as Tools To Reveal Solvation Changes Accompanying a Proton Transfer. A Canonical Unified Statistical Theory Calculation

Jordi Villà, Angels González-Lafont, and José M. Lluch*

Departament de Química, Universitat Autònoma de Barcelona, 08193 Bellaterra, Barcelona, Spain

Received: May 8, 1996; In Final Form: August 7, 1996[⊗]

Primary and solvent kinetic isotope effects (KIEs) for the proton transfer between a butanone molecule and the microsolvated ion $OH^-(H_2O)_{n=0,1,2}$ to give the $(H_2O)_{n+1}\cdots$butenolate complex have been theoretically calculated in order to study solvation changes that take place along the proton transfer process. To take into account in the transition state calculations the two dynamical bottlenecks involved in those cluster reactions (one corresponding to the ion−dipole approach and the other one to the actual proton transfer), the canonical unified statistical theory has been used. Only for the $n = 2$ case, the local bottleneck in the proton transfer region controls the global process at the whole range of temperatures studied. The different values of the KIEs as a function of temperature and depending on the relative weight of the two dynamical bottlenecks are analyzed. The degree of coupling between the motion of solvent molecules and the motion of the proton that is being transferred is studied by testing the rule of the geometrical mean. This empirical rule holds very well when only one bottleneck governs the global process, but an important breakdown of this rule is found when the two bottlenecks are comparable. Assuming a monotonical variation of solvent isotope effect from reactants to product, the solvent KIE, by comparison with the equilibrium solvent isotope effect, indicates that the hydroxide ion is 44% desolvated at the transition state of the reaction with $n = 2$ at 298 K. All these results have been obtained without including tunneling effects. A first estimation of the tunneling contribution to kinetic isotope effects has been evaluated by interpolated variational transition state theory.

Introduction

Solvation changes that take place in the course of a proton transfer reaction are of critical importance in order to understand the microscopic dynamics of those kind of chemical processes when they occur in solution.[1] Those solvation changes will be analyzed here from two different perspectives: (1) the extent of solvent reorganization along the transference process and (2) the degree of coupling between the motion of solvent molecules and the motion of the proton that is being transferred, in other words, to which extent the solvent atoms participate in the proton transfer reaction coordinate.

Experimentally, the reorganization attained by the solvent at the transition state of a proton transfer event is inferred from the comparison of the values of solvent kinetic isotope effects (KIEs) and the appropiate values of solvent equilibrium isotope effects.[2] If both kinds of isotope effects match, this is the indication of an important or complete reorganization of solvent at the transition state of the reaction. On the other hand, the degree of coupling has been related to the validation of an empirical rule denominated the rule of the geometrical mean (RGM)[3] that evaluates the KIEs of multiple isotopic substitution (isotope effects on isotope effects) as a product of the different kinds of kinetic isotope effects involved. Violations of the RGM have been used as an indication of coupling between different types of motions in the reaction coordinate.[4]

Recently, Casamassina and Huskey have reported their experimental results on primary hydrogen kinetic isotope effects and solvent isotope effects (with the undeuterated substrate) for the elimination of 4-nitrophenol from 4-(4-nitrophenoxy)-2-butanone in aqueous hydroxide.[5] As shown in Scheme 1, the elimination of the aromatic group consists of two consecutive reactions, with the first one rate limiting the overall kinetics of the mechanism. The authors conclude that their observations

SCHEME 1

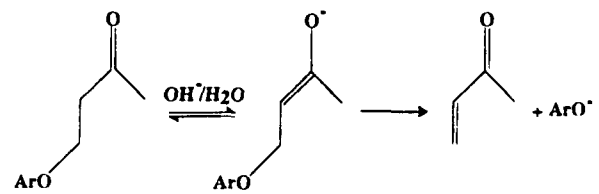

Ar=4-nitrophenyl

of primary isotope effects that are unchanged upon isotopic substitution in protonic sites of the solvent clearly indicate that solvent reorganization is not coupled to proton transfer in the reaction coordinate. In fact, the constancy of substrate KIEs with the isotopic composition of solvent is another way to verify the rule of the geometrical mean. Concerning the degree of reorganization of the solvent attained for this elimination reaction at the transition state for the proton transfer event, the authors conclude that a transition state structure consistent with their kinetic isotope effects would have the transferring proton halfway between the acid and the base (the primary isotope effects are large) and partial desolvation of hydroxide ion (ca. 50% desolvated).

Besides those experimental results, Casamassina and Huskey[5] present some theoretical calculations of isotope effects based on a very simple approach due originally to Bigeleisen and Wolfsberg.[6] Models for reactants and transition states are specified in terms of harmonic valence force fields. The model chosen for reactants resembles a hydroxide ion solvated by three water molecules with a nonbonded carbon acid represented by C−H. The transition state model includes a new partial bond between the oxygen atom of the hydroxide ion and the proton being transferred from the carbon acid. Through these vibrational analysis calculations, the authors show that RGM violations in models for coupled desolvation and proton transfer can

[⊗] Abstract published in *Advance ACS Abstracts*, November 15, 1996.

S0022-3654(96)01319-6 CCC: $12.00

SCHEME 2

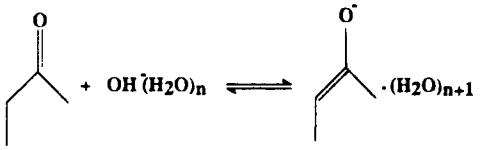

n=0,1,2

SCHEME 3

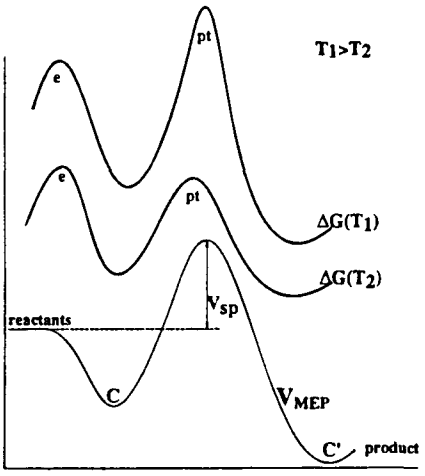

e = entrance channel
pt = proton transfer region

be large enough to be experimentally observed. Those calculations are then a numerical exercise to assess the degree of desolvation participation in reaction coordinate motion, and no kind of direct comparison can be established with the experimental results for the proton transfer process.

The main chemical purpose of the present work was to theoretically analyze, by means of quantum mechanical and dynamics calculations, the solvation changes accompanying the proton transfer rate-limiting step of the elimination reaction studied by Casamassina and Huskey. With this study we also intended to theoretically justify the empirical rules used by experimentalists to explain solvation changes that may occur between the reactant and the transition state of a reaction. Due to the computational cost involved in the quantum mechanical calculations, primary and solvent KIEs were evaluated on a cluster model of the real system in solution. The model reactions finally chosen are shown in Scheme 2.

It has to be emphasized here that the present work does not involve tunneling. However, as a first estimation of the tunneling contribution to kinetic isotope effects, we have performed interpolated variational calculations.

Experimental results for cluster reactions, as well as theoretical calculations carried out on cluster systems, have shown in the past, for several kinds of processes, that cluster studies can bridge the gap between unsolvated gas phase reactions, on one hand, and condensed phase reactions, on the other hand.[7] Our aim was to analyze the principal trends of solvation changes accompanying proton transfer in the cluster reactions of Scheme 2, in order to discuss what may happen in solution.

Many ion−molecule reactions studied in clusters present a potential energy function along the minimum energy path (V_{MEP}) with the general shape shown in Scheme 3. This potential energy function has two wells, labeled C and C′, corresponding to reactant and product ion−dipole complexes, respectively, on either side of a saddle point. In the processes analyzed in this paper, the saddle point corresponds to the proton transfer event. The ion−dipole approach (from reactants to complex C) takes place without a potential energy barrier, while the actual proton transfer has a classical barrier (V_{sp}) that depending on cluster size can be either positive or negative. In the low-pressure limit, the free energy profile may present two maxima (see Scheme 3): one at the entrance channel, a bottleneck to formation of the reactant ion−dipole complex, and another at the proton transfer region. Depending on temperature, the best single dynamical bottleneck for the complete process may be located either at the entrance channel or at the proton transfer region.

Conventional transition state theory (TST) assumes that the phase space dividing surface containing the saddle point provides a perfect dynamical bottleneck. In classical language that means that trajectories do not recross that bottleneck dividing surface centered at the saddle point.[8] Canonical variational transition state theory (CVT) again assumes a single dynamical bottleneck with no recrossing trajectories, but the location of the configuration space dividing surface is variationally optimized and may depend on temperature.[9] If the reaction under study presents multiple bottleneck regions, its dynamics has to be analyzed using the unified statistical theory (US,[10] in its canonical version CUS [11]) on the basis of the branching analysis of Hirschfelder and Wigner.[12] Only within this theory local fluxes are calculated and compared through the various dividing surfaces at the different bottlenecks of the chemical process.[13] The present chemical problem provides then an excellent opportunity to test and discuss the applicability of the CUS model to the study of KIEs. This is, in fact, the methodological aim of this paper.

Method of Calculation

In order to theoretically evaluate kinetic isotope effects (KIEs), an exploration of the potential energy surface (PES) followed by a dynamical treatment is required. In this section the technical details corresponding to both kinds of calculations, as well as to kinetic isotope effect evaluation, are successively described.

PES Exploration. To solve the electronic Schrödinger equation, *ab initio* restricted Hartree−Fock calculations were carried out using the split valence 6-31+G basis set,[14] which includes diffuse functions on the heavy atoms. Full geometry optimization and direct location of stationary points, minima and saddle points, were performed. The characterization of these stationary points has been carried out by diagonalizing their Hessian (force constant) matrices and looking for zero or one negative eigenvalues, respectively. Within the Born−Oppenheimer approximation, this characterization of the stationary points is independent of the isotopic composition of the system. The Gaussian 94 package[15] has been used to carry out these calculations.

When it was required, the minimum energy path (MEP) was calculated in mass-weighted Cartesian coordinates by using the fourth-order Runge−Kutta method.[16] Each MEP was built up with a step size of 0.0025 bohr·amu$^{1/2}$, being extended enough around the saddle point at the proton transfer barrier region in such a way that the corresponding local maximum of free energy is localized. Analytic Hessians were calculated at every point along the MEP. In mass-weighted Cartesian coordinates both the MEP and analytic Hessians along it have to be performed for each substitution. The Gamess 94 program[17] has been used for the MEP calculations.

Dynamical Calculations. As mentioned in the Introduction, we will study the $HO^-(H_2O)_n$ + butanone reaction to give the $(H_2O)_{n+1}$···butenolate complex, an ion-polarizable dipole sys-

tem. As a consequence, the PES contains two wells, labeled C and C′, corresponding to reactant and product ion−dipole complexes, respectively, on either side of the saddle point involved in the proton transfer (note that C′ is taken as the final product of the reaction). Then, there are two possible locations for the dynamical bottleneck to reaction (Scheme 3): (a) in the entrance channel, a bottleneck to formation of the reactant ion−dipole complex C, and (b) in the proton transfer region. The rate constants for passage through these two bottleneck regions will be labeled k_e and k_{pt}, respectively. k_C and $k_{C'}$ will denote the one-way flux rate constants evaluated at the ion−dipole complexes.

According to the CUS model, the final reaction rate constant $k^{CUS}(T)$ is given by:

$$k^{CUS}(T) = k_{MIN}(T)\, R^{CUS}(T) \tag{1}$$

where

$$k_{MIN}(T) = \min\{k_e(T), k_{pt}(T)\} \tag{2}$$

and

$$R^{CUS}(T) = \left(\frac{k_{MIN}(T)}{k_e(T)} - \frac{k_{MIN}(T)}{k_c(T)} + \frac{k_{MIN}(T)}{k_{pt}(T)} - \frac{k_{MIN}(T)}{k_{C'}(T)}\right)^{-1} \tag{3}$$

As it will be seen in the results section, the two C and C′ minima turn out to be at least 10 kcal/mol deep for the three cases studied in this paper. Then, the second ($k_{MIN}(T)/k_C(T) \ll 1$) and fourth ($k_{MIN}(T)/k_{C'}(T) \ll 1$) terms in eq 3 can be neglected, so that $R^{CUS}(T)$ will depend only on k_e and k_{pt}.

The ion-polarizable dipolar molecule association rate constant, $k_e(T)$, is estimated on the basis of the ion−dipole capture approximation of Celli *et al.*,[18] which has been shown to yield good results on similar systems[13]

$$k_e(T) = k_L\left(1 + \frac{P^2}{4}\right)^{1/2} \tag{4}$$

where

$$P = \frac{\mu}{(\alpha k_B T)^{1/2}} \tag{5}$$

μ, α, and k_B being the dipolar moment and the polarizability of the neutral reactant and the Boltzmann constant, respectively, and

$$k_L = 2\pi e\left(\frac{\alpha}{m}\right)^{1/2} \tag{6}$$

e and m being the electron charge and the ion−molecule reduced mass, respectively. The dipolar moment and the polarizability used to calculate k_e are, respectively, 2.78 D and 8.13×10^{-24} cm^3 for butanone.[19]

The rate coefficient k_{pt} can be obtained by carrying out direct dynamics calculations of the canonical variational transition state theory (CVT) rate constant. CVT yields hybrid (i.e., classical reaction path motion with other degrees of freedom quantized) rate constants. However, since the rotational energy levels are generally closely spaced, little accuracy is lost if we approximate the quantal rotational partition functions by means of the classical ones. For vibrations, in the present study, the partition functions were calculated quantum mechanically within the harmonic approximation.

The potential energy information (energies, gradients, and Hessians), calculated at every point along the generated MEP, was input in Polyrate (v.5.1),[20,21] which uses mass-scaled Cartesian coordinates.[22] However, if in this program we choose the reduced mass to be 1 amu in the mass-scaled Cartesian coordinate system, then both the mass-weighted and mass-scaled Cartesian coordinate systems yield numerically identical results.

KIE Calculations. KIEs and, in particular, hydrogen/deuterium KIEs, are defined as the ratios k_H/k_D, where k_H is the rate constant for the unsubstituted molecular system and k_D is the rate constant for the system in which one or several protiums have been substituted for deuteriums. By definition, a KIE is "normal" if it is greater than unity when the rate constant for the lighter isotope is in the numerator, and it is an "inverse" isotope effect if it is less than unity.

In this work, we have calculated KIEs for each one of the three model cluster reactions presented in Scheme 2. In the first place, we have evaluated primary deuterium KIEs corresponding to the isotope substitution of the hydrogen being transferred from the butanone molecule to the hydroxide ion. Secondly, kinetic solvent isotope effects have also been calculated by changing to deuterium atoms all the hydrogens of the water molecules and that of the reactant hydroxide ion which is not a direct participant of the proton transfer process. Finally, we will call kinetic isotope effects on kinetic isotope effects the values of the k_H/k_D ratios obtained by introducing at the same time the two kinds of isotopic substitutions just mentioned, thus corresponding to both primary and secondary KIEs evaluated all together.

In accordance with the free energy profile shown in Scheme 3, KIEs will be given for each model reaction at each one of the two individual local free energy maxima, that is, at the entrance channel (as ratios of k_e rate coefficients) and at the proton transfer region (as ratios of k_{pt} rate coefficients). KIEs obtained according to the CUS model, i.e., as ratios of CUS rate constants (k^{CUS}), will also be reported.

As it has already been mentioned in the Introduction, a measure of solvent reorganization in a proton transfer process has usually been derived from the comparison of solvent KIEs with solvent equilibrium isotope effects. In this work, solvent equilibrium isotope effects have been calculated as the ratios between the equilibrium constants (K_H) of the unsubstituted processes, $OH^-(H_2O)_{n=0,1,2}$ + butanone $\rightleftharpoons$ $(H_2O)_{n+1}\cdots$butenolate complex, and the corresponding equilibrium constants (K_D) for the isotopically substituted processes. For this case, as in the calculation of solvent KIEs, all the hydrogens of water molecules and that of the hydroxide ion which is not a direct participant of the proton transfer process have been changed to deuteriums.

In order to include in our dynamical calculations the tunneling contribution, when necessary the k_{pt} rate constant has been corrected by a transmission coefficient that accounts for the quantum mechanical tunneling in the direction along the reaction coordinate and is calculated by the semiclassical zero-curvature ground-state (ZCT) method.[23] In this approach, the proton is restricted to tunnel along the minimum energy path and the bound motions are assumed to adjust adiabatically to their ground states. To evaluate the transmission coefficient, we need the vibrationally adiabatic ground-state potential energy curve that has been obtained in this work following the zero-order interpolation algorithm (IVTST-0).[24,25] In this scheme, the classical energy and the zero-point energy along the reaction coordinate are interpolated from information at reactants, products, and the saddle point. Then, the potential energy curve and the adiabatic curve are modeled by two Eckart functions of the same range parameter (i.e., with the same width). This range parameter is obtained from the imaginary frequency at the saddle point. Our first estimation of the tunneling contribu-

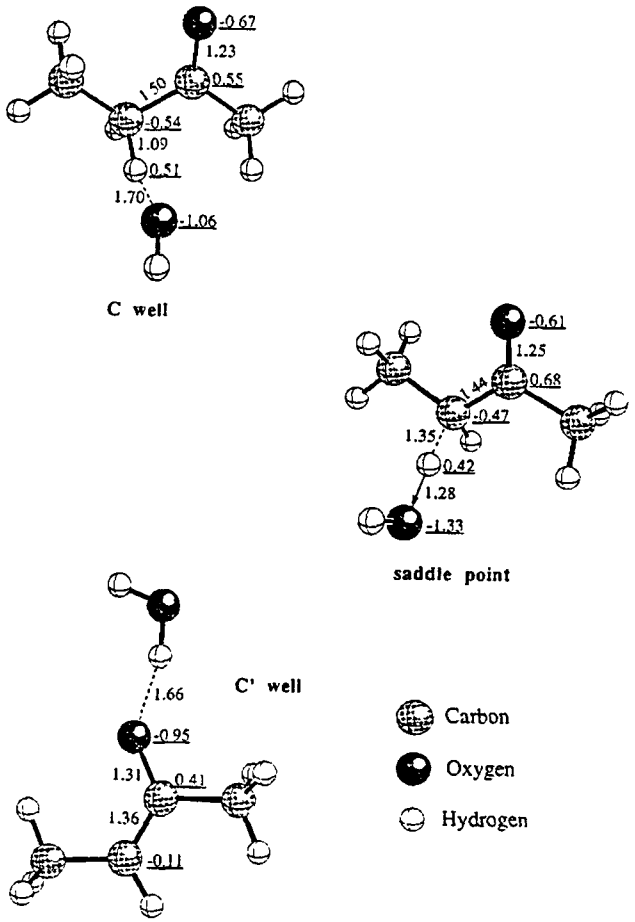

Figure 1. Main geometrical parameters (Å) along with Mulliken net charges (underlined numbers, in au) for the three stationary points of the butanone + OH^- reaction. The transition vector at the saddle point is depicted too.

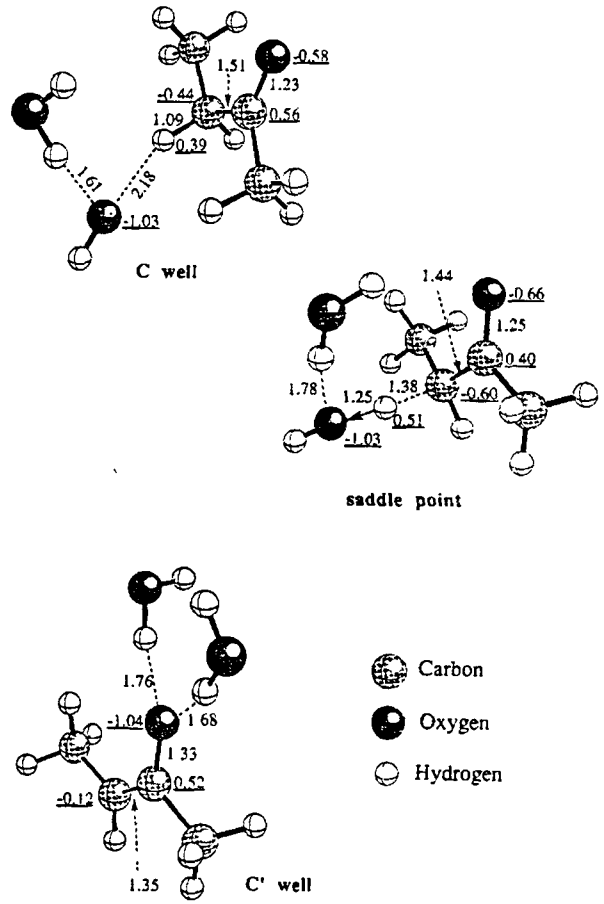

Figure 2. Main geometrical parameters (Å) along with Mulliken net charges (underlined numbers, in au) for the three stationary points of the butanone + $OH^-(H_2O)$ reaction. The transition vector at the saddle point is depicted too.

tion to the different KIEs considered in this study has been finally calculated as the ratios of the transmission coefficients corresponding to the unsubstituted system and each deuterated system.

Results and Discussion

In this section we will present the results obtained for the three reactions studied (n = 0, 1, and 2) according to the following sequence: We will firstly describe the main geometrical and energetic features of the stationary points of the potential energy surfaces; then we will list the CUS rate constants; we will thirdly evaluate the kinetic isotope effects (KIEs) and discuss their usefulness to reveal information about solvation changes accompanying the proton transfer.

Stationary Points of the PES. Apart from reactants at infinite distance, we have located three stationary points (the two C and C′ wells and the saddle point separating them) on each potential energy surface. The main geometrical parameters of these nine structures are given in Figures 1−3.

Several common geometrical features for the three reactions can be seen:

(1) At the reactant wells (C structures), the hydroxide oxygen ·ydrogen bonded to the butanone hydrogen atom that will ·ransferred. The hydroxide ion is nonsolvated (n = 0) or vated by one (n = 1) or two (n = 2) water molecules, and, · this reason, the hydrogen bond length increases from n = 0 to n = 2. On the other hand, the angles between the three atoms intervening in the hydrogen bond are 146° (n = 0), 149° (n = 1), and 173° (n = 2).

(2) At the saddle points, the shifting proton is more than halfway between the carbon acid and the hydroxide oxygen base, the three atoms being almost in linear disposition (only a deviation of about 6° exists). Although the hydrogen donor−hydrogen acceptor distance is practically identical for the three reactions, it is clear that the saddle point becomes closer to the product well (C′ structure) as n increases. Also shown in these figures are the main components of the transition vector at the saddle point, that is, the eigenvector associated with the negative eigenvalue, which indicates the MEP direction at that point. It is noteworthy that it entirely corresponds to the proton transfer itself, with no contribution of the rest of atoms of the system.

(3) Upon going from C to C′ structures, the C−C central bond of butanone shortens while the C−O bond lengthens. This is due to the fact that the first bond passes from single to double while the C−O bond, on the contrary, evolves from double to single, a negative net charge appearing on the oxygen atom in the butenolate. As a consequence, the new water (formed by the addition of the proton to hydroxide ion), alone or accompanied by one or two waters (depending on the reaction), migrates finally toward the butenolate oxygen atom.

(4) For both the n = 1 and n = 2 reactions, a clear desolvation of the hydroxide ion takes place upon going from C to C′.

Let us focus on the energetic aspects. Classical energies (that is, without zero-point correction) of the stationary points relative to reactants at infinite distance are displayed in Table 1. From those values it is evident that the entire reaction path is raised relative to reactants at infinite distance as n increases. As a consequence, the exothermicity decreases and the energy of the saddle point increases with respect to both reactants and C

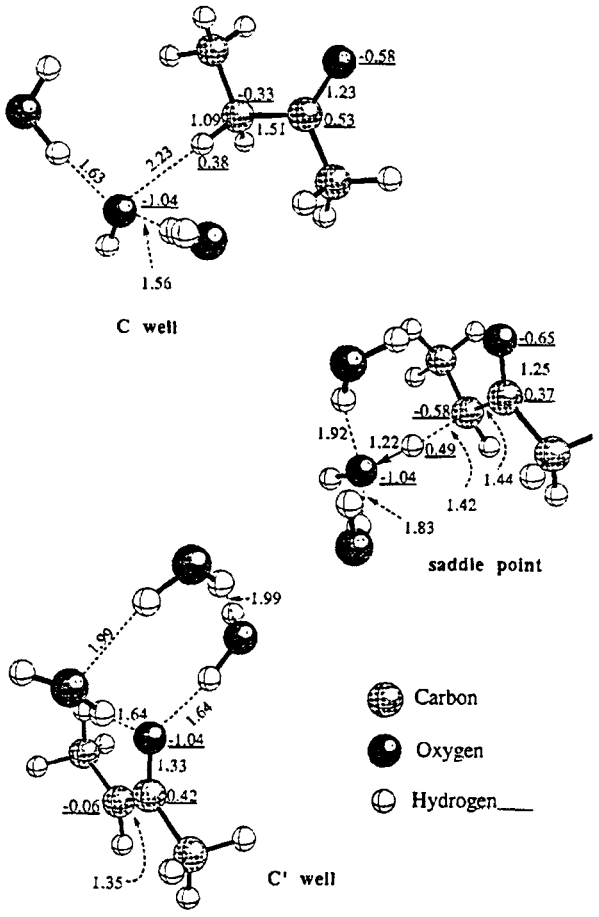

Figure 3. Main geometrical parameters (Å) along with Mulliken net charges (underlined numbers, in au) for the three stationary points of the butanone + $OH^-(H_2O)_2$ reaction. The transition vector at the saddle point is depicted too.

TABLE 1: Classical Energies (in kcal/mol) Relative to Reactants at Infinite Distance of Stationary Points for the Butanone + $OH^-(H_2O)_n$ Reactions

n	reactant well (C)	saddle point	product well (C')
0	−22.1	−12.1	−35.9
1	−18.2	−5.2	−27.6
2	−14.1	2.1	−20.4

structure when solvation is added. This behavior is due to the fact that the nonsolvated hydroxide ion is quite unstable, the potential energy going down as the reaction for the case $n = 0$ progresses and the negative charge is delocalized in the butenolate anion. However, the addition of one or two water molecules solvating the hydroxide ion diminishes its instability, in this way modifying the shape of the PES for $n = 1$ and $n = 2$. Not surprisingly, and in good agreement with the Hammond postulate, the smaller the exothermicity, the later the saddle point and the higher its energy. Interestingly, a saddle point that involves a positive energy barrier (2.1 kcal/mol) relative to reactants at infinite distance only appears for the reaction with $n = 2$. To test the accuracy of the basis set used, we have relocalized this saddle point employing the 6-31+G(d,p) basis set. The new structure is very similar from a geometrical point of view and imposes an energy barrier only slightly higher (2.8 kcal/mol). Then it seems that the inclusion of polarization functions does not improve significantly the results.

On the other hand, it has to be noted that the well depth of C and C' minima is 10 kcal/mol or more for the three reactions, so justifying the above mentioned simplification of eq 3.

CUS Rate Constants. Let us analyze the importance of variational effects in the proton transfer region. The corresponding results at different temperatures are displayed in Tables 2, 3, and 4 for the reactions with $n = 0$, 1, and 2, respectively. The location (measured as the arc length along the MEP in mass-scaled Cartesian coordinates) of the variational transition state is shown in the second column. Note that negative or positive values indicate that the bottleneck appears before or after the saddle point. k_{pt} rate constants calculated according to the conventional and the canonical variational transition state theory (TST and CVT, respectively), along with the ratio between them, are presented in columns three to five. It can be seen that variational transition state moves away from the saddle point toward the C structure (when $n = 0$) or the C' structure (when $n = 1$ or $n = 2$) as temperature increases. In any case, variational effects are small for $n = 0$ and $n = 2$, being somewhat more important for $n = 1$. To analyze the source of variational effects on the rate constants in this last system (that is, the one that presents the maximum variational effect), we have decomposed in Table 5 the ratio of TST to CVT k_{pt} rate constants over a range of temperatures for this last reaction according to the following equation

$$\frac{k_{pt}^{TST}}{k_{pt}^{CVT}} = \frac{Q_{vib}^{TST}}{Q_{vib}^{CVT}} \frac{Q_{rot}^{TST}}{Q_{rot}^{CVT}} e^{-(V_{MEP}^{TST} - V_{MEP}^{CVT})/RT} = \kappa_{vib}\kappa_{rot}\kappa_{pot} \quad (7)$$

where Q_{vib} denotes a vibrational partition function with the zero of energy at the local value of V_{MEP} (the classical energy along the MEP relative to reactants at infinite distance), Q_{rot} stands for a rotational partition function, and R is the gas constant.

TABLE 2: Variational Effects in the Proton Transfer Region for the Butanone + OH^- Reaction

T (K)	$s^*CVT(T)^a$	$k_{pt}^{TST\ b,c}$	$k_{pt}^{CVT\ b,c}$	$k_{pt}^{TST}/k_{pt}^{CVT}$
500	−0.0350	4.52(−08)	4.33(−08)	1.04
400	−0.0281	1.35(−06)	1.30(−06)	1.04
350	−0.0278	1.64(−05)	1.58(−05)	1.04
298	−0.0234	5.71(−04)	5.51(−04)	1.04
250	−0.0228	6.04(−02)	5.83(−02)	1.04
200	−0.0215	9.24(+01)	8.94(+01)	1.03
150	−0.0183	2.16(+07)	2.10(+07)	1.03
100	−0.0159	1.47(+18)	1.43(+18)	1.03

[a] In bohr. [b] In cm^3 $molecule^{-1}$ s^{-1}. [c] Power of 10 in parentheses.

TABLE 3: Variational Effects in the Proton Transfer Region for the Butanone + $OH^-(H_2O)$ Reaction

T (K)	$s^{*CVT}(T)^a$	$k_{pt}^{TST\ b,c}$	$k_{pt}^{CVT\ b,c}$	$k_{pt}^{TST}/k_{pt}^{CVT}$
500	0.0588	3.05(−13)	2.34(−13)	1.30
400	0.0560	1.02(−12)	7.99(−13)	1.28
350	0.0545	2.65(−12)	2.09(−12)	1.27
298	0.0330	1.08(−11)	8.67(−12)	1.25
250	0.0501	7.31(−11)	5.96(−11)	1.23
200	0.0396	1.60(−09)	1.33(−09)	1.20
150	0.0307	3.30(−07)	2.82(−07)	1.17
100	0.0284	1.87(−02)	1.67(−02)	1.12

[a] In bohr. [b] In cm^3 $molecule^{-1}$ s^{-1}. [c] Power of 10 in parentheses.

TABLE 4: Variational Effects in the Proton Transfer Region for the Butanone + $OH^-(H_2O)_2$ Reaction

T (K)	$s^{*CVT}(T)^a$	$k_{pt}^{TST\ b,c}$	$k_{pt}^{CVT\ b,c}$	$k_{pt}^{TST}/k_{pt}^{CVT}$
500	0.0364	1.53(−17)	1.36(−17)	1.13
400	0.0335	6.97(−18)	6.26(−18)	1.11
350	0.0303	4.34(−18)	3.92(−18)	1.11
298	0.0231	2.43(−18)	2.21(−18)	1.10
250	0.0221	1.26(−18)	1.15(−18)	1.10
200	0.0216	5.17(−19)	4.75(−19)	1.09
150	0.0210	1.39(−19)	1.29(−19)	1.08
100	0.0204	1.32(−20)	1.26(−20)	1.05

[a] In bohr. [b] In cm^3 $molecule^{-1}$ s^{-1}. [c] Power of 10 in parentheses.

TABLE 5: Contributions of the Different Factors to Variational Effect for the Butanone + $OH^-(H_2O)$ Reaction (TST to CVT Ratios)

T(K)	κ_{vib}	κ_{low}[a]	κ_{mid}	κ_{high}[b]	κ_{rot}	κ_{pot}
500	1.38	1.39	0.98	1.02	1.00	0.95
400	1.36	1.40	0.96	1.01	1.00	0.94
350	1.36	1.39	0.96	1.02	1.00	0.93
298	1.34	1.38	0.95	1.02	1.00	0.93
250	1.33	1.35	0.96	1.02	1.00	0.92
200	1.28	1.33	0.95	1.02	1.00	0.94
150	1.23	1.27	0.95	1.02	1.00	0.95
100	1.20	1.28	0.92	1.02	1.00	0.94

[a] Low-frequency modes are taken as those whose frequencies are below 600 cm^{-1} over all or most of the calculated MEP. [b] High-frequency modes are taken as those whose frequencies exceed 3000 cm^{-1} over all or most of the calculated MEP.

TABLE 6: Rate Constants (in cm^3 $molecule^{-1}$ s^{-1}) for the Butanone + $OH^-(H_2O)_n$ Reactions (Power of 10 in Parentheses)

T(K)	k_e	k_{pt}^{CVT}	R^{CUS}	k_{CVT}^{CUS}
		$n = 0$		
500	3.80(−09)	4.33(−08)	1.00	3.49(−09)
400	4.15(−09)	1.30(−06)	1.00	4.13(−09)
350	4.67(−09)	1.58(−05)	1.00	4.67(−09)
298	4.69(−09)	5.51(−04)	1.00	4.69(−09)
250	5.06(−09)	5.83(−02)	1.00	5.06(−09)
200	5.58(−09)	8.94(+01)	1.00	5.58(−09)
150	6.36(−09)	2.10(+07)	1.00	6.36(−09)
100	7.68(−09)	1.43(+18)	1.00	7.68(−09)
		$n = 1$		
500	2.90(−09)	2.34(−13)	1.00	2.34(−13)
400	3.17(−09)	7.99(−13)	1.00	7.99(−13)
350	3.57(−09)	2.09(−12)	1.00	2.09(−12)
298	3.58(−09)	8.67(−12)	1.00	8.65(−12)
250	3.86(−09)	5.96(−11)	0.98	5.87(−11)
200	4.26(−09)	1.33(−09)	0.76	1.01(−09)
150	4.86(−09)	2.82(−07)	0.98	4.78(−09)
100	5.87(−09)	1.67(−02)	1.00	5.87(−09)
		$n = 2$		
500	2.55(−09)	1.36(−17)	1.00	1.36(−17)
400	2.78(−09)	6.26(−18)	1.00	6.26(−18)
350	3.14(−09)	3.92(−18)	1.00	3.92(−18)
298	3.15(−09)	2.21(−18)	1.00	2.21(−18)
250	3.39(−09)	1.15(−18)	1.00	1.15(−18)
200	3.75(−09)	4.75(−19)	1.00	4.75(−19)
150	4.27(−09)	1.29(−19)	1.00	1.29(−19)
100	5.16(−09)	1.26(−20)	1.00	1.26(−20)

Furthermore we have factorized κ_{vib} into contributions from high-, mid-, and low-frequency modes

$$\kappa_{vib} = \kappa_{high}\kappa_{mid}\kappa_{low} \quad (8)$$

It is seen that overestimation of TST k_{pt} rate constants is due to low-frequency modes, their importance growing with increasing temperature.

Table 6 successively exhibits rate constants for passage through the entrance channel (k_e) and proton transfer (k_{pt}^{CVT}) bottlenecks, R^{CUS} factors, and CUS rate constant (k_{CVT}^{CUS}) as a function of temperature. Note that the R^{CUS} factor provides the recrossing correction of the best single bottleneck (the one corresponding to k_{MIN}) in the case of a complex region involving multiple bottlenecks. From the analysis of this table, we observe that the ion-polarizable dipolar molecule association rate constants decrease only slightly with increasing temperature in all cases. However, the proton transfer rate constants undergo a very significant variation as a function of temperature. For the reactions with $n = 0$ and $n = 1$, k_{pt}^{CVT} decreases as temperature increases (within the range of studied temperatures), as a consequence of the corresponding negative energy barriers.

TABLE 7: Kinetic Isotope Effects for the Butanone + OH^- Reaction

T(K)	KIE_{TST}	KIE_{CVT}	KIE_{CVT}^{CUS}
		Primary	
500	2.72	2.69	1.14
400	3.40	3.38	1.01
350	3.99	3.96	1.00
298	5.01	4.96	1.00
250	6.70	6.63	1.00
200	10.55	10.44	1.00
150	22.50	22.34	1.00
100	103.52	102.14	1.00
		Solvent	
500	0.87	0.86	1.01
400	0.82	0.82	1.02
350	0.78	0.79	1.02
298	0.74	0.74	1.02
250	0.68	0.68	1.02
200	0.58	0.58	1.02
150	0.44	0.45	1.02
100	0.25	0.25	1.02
		Isotope Effect on Isotope Effect[a]	
500	2.37 (2.37)	2.34 (2.31)	1.13 (1.15)
400	2.80 (2.79)	2.77 (2.77)	1.03 (1.03)
350	3.15 (3.11)	3.12 (3.13)	1.03 (1.02)
298	3.68 (3.71)	3.67 (3.67)	1.02 (1.02)
250	4.51 (4.56)	4.48 (4.51)	1.02 (1.02)
200	6.12 (6.12)	6.12 (6.06)	1.02 (1.02)
150	10.00 (9.90)	10.00 (10.05)	1.02 (1.02)
100	25.74 (25.88)	25.86 (25.54)	1.02 (1.02)

[a] In parentheses is the product $KIE_{primary}KIE_{solvent}$ in each case.

On the contrary, as mentioned above, the $n = 2$ reaction has a positive energy barrier, leading to the usual increase of k_{pt}^{CVT} as temperature goes up. The entrance bottleneck controls the global process for $n = 0$ at all studied temperatures and for $n = 1$ at low temperatures. On the other hand, the proton transfer bottleneck controls the global reaction for $n = 1$ at high temperatures and for $n = 2$ at the whole range of temperatures. It has to be noted that the R^{CUS} factor is 1.00 except when k_e and k_{pt}^{CVT} get comparable values. In other words, if k_e or k_{pt}^{CVT} is much lower than the other one, the bottleneck associated with the lowest rate constant completely determines the final reaction rate constant (k_{CVT}^{CUS}), no additional recrossing correction being needed. When k_e and k_{pt}^{CVT} have comparable values, there exists a significant recrossing through the best single bottleneck, the R^{CUS} factor becoming important for obtaining the final reaction rate constant.

Kinetic Isotope Effects. Let us turn our attention to kinetic isotope effects. The corresponding results over a range of temperatures are shown in Tables 7−9. The term primary refers to the substitution of the shifting hydrogen by deuterium, giving rise to a primary substrate isotope effect. The term solvent is applied to the secondary kinetic isotope effect that appears when the hydroxide hydrogen and all the water hydrogens (in the reactions with $n = 1$ and $n = 2$) are changed by deuterium atoms. Finally, the term isotope effect on isotope effect stands for the kinetic isotope effect (primary and secondary together) that occurs when all the above mentioned hydrogen atoms are replaced by deuterium atoms. The arrangement of Tables 7 and 8, which correspond to the unsolvated and the monosolvated reactions, respectively, is identical. The KIEs calculated as if only the proton transfer bottleneck exists, using both TST (KIE_{TST}) and CVT (KIE_{CVT}), are shown in columns two and three, respectively. The actual KIEs accounting for the two bottlenecks (KIE_{CVT}^{CUS}), that is, derived from variational k_{CVT}^{CUS}, are exhibited in the last column. As it will be commented below, no significant change in the KIEs is provided by variational calculations for the reactions with $n = 0$ and n

TABLE 8: Kinetic Isotope Effects for the Butanone + $OH^-(H_2O)$ Reaction

T(K)	KIE_{TST}	KIE_{CVT}	KIE_{CVT}^{CUS}
		Primary	
500	2.93	2.98	2.98
400	3.66	3.73	3.73
350	4.31	4.40	4.40
298	5.40	5.56	5.55
250	7.24	7.47	7.37
200	11.43	11.77	9.21
150	24.63	25.64	1.42
100	113.33	121.90	1.00
		Solvent	
500	0.65	0.66	0.66
400	0.58	0.59	0.59
350	0.54	0.54	0.54
298	0.48	0.48	0.48
250	0.41	0.41	0.42
200	0.31	0.31	0.48
150	0.19	0.20	1.01
100	0.07	0.07	1.03
		Isotope Effect on Isotope Effect[a]	
500	1.91 (1.91)	1.97 (1.96)	1.97 (1.96)
400	2.13 (2.12)	2.21 (2.19)	2.21 (2.19)
350	2.32 (2.32)	2.38 (2.38)	2.38 (2.38)
298	2.57 (2.57)	2.65 (2.68)	2.65 (2.68)
250	2.94 (2.94)	3.03 (3.07)	3.00 (3.10)
200	3.54 (3.55)	3.64 (3.69)	3.02 (4.45)
150	4.72 (4.75)	4.88 (5.02)	1.10 (1.44)
100	7.96 (8.00)	8.31 (8.81)	1.03 (1.03)

[a] In parentheses is the product $KIE_{primary}KIE_{solvent}$ in each case.

TABLE 9: Kinetic Isotope Effects and Equilibrium Solvent Isotope Effect for the Butanone + $OH^-(H_2O)_2$ Reaction

T(K)	KIE_{TST}	KIE_{TST}^{CUS}	$KIE_{TST}^{CUS/ZCT}$	K_H/K_D
		Primary		
500	2.80	2.80	2.66	
400	3.50	3.50	3.21	
350	4.13	4.13	3.64	
298	5.15	5.15	4.27	
250	6.89	6.89	5.19	
200	10.84	10.84	6.72	
150	23.17	23.17	9.30	
100	105.60	105.60	13.42	
		Solvent		
500	0.60	0.60	0.72	0.32
400	0.53	0.53	0.69	0.23
350	0.48	0.48	0.67	0.19
298	0.42	0.42	0.65	0.14
250	0.34	0.34	0.63	0.09
200	0.25	0.25	0.60	0.05
150	0.14	0.14	0.54	0.02
100	0.04	0.04	0.47	1.8×10^{-3}
		Isotope Effect on Isotope Effect[a]		
500	1.70 (1.69)	1.70 (1.69)	1.79 (1.92)	
400	1.86 (1.86)	1.86 (1.86)	2.02 (2.22)	
350	1.98 (1.99)	1.98 (1.99)	2.20 (2.45)	
298	2.15 (2.15)	2.15 (2.15)	2.44 (2.78)	
250	2.35 (2.36)	2.35 (2.36)	2.75 (3.26)	
200	2.65 (2.68)	2.65 (2.68)	3.24 (4.02)	
150	3.13 (3.16)	3.13 (3.16)	3.97 (5.06)	
100	4.07 (4.14)	4.07 (4.14)	4.95 (6.32)	

[a] In parentheses is the product $KIE_{primary}KIE_{solvent}$ in each case.

$= 1$. Since variational effects for $n = 2$ are in between those corresponding to $n = 0$ and $n = 1$, no significant variational effect in the KIEs for the reaction with $n = 2$ would be expected either. So, because CVT calculations involve a considerable increase of computer time (recall that a distinct IRC and a different set of Hessians have to be built for each isotopomer), we have decided to use only conventional transition state theory to determine KIEs for $n = 2$. For this reaction KIEs coming from just the proton transfer bottleneck (KIE_{TST}) and including the two bottlenecks (KIE_{TST}^{CUS}) are shown in the second and third columns, respectively, of Table 9.

From the analysis of those tables, the following points merit to be commented on:

(1) As mentioned above, no significant difference between the proton transfer bottleneck KIEs calculated by means of TST or CVT (comparison between the second and third columns, respectively) appears for reactions with $n = 0$ and $n = 1$, this way justifying the use of TST for the $n = 2$ case.

(2) Proton transfer bottleneck KIEs show similar trends for the three reactions, in spite of their different energy barriers (recall that two of them are negative and the third is positive). The fact that the direct effect of the barrier height cancels out in the kinetic isotope effect has been already reported.[26] Primary KIEs are always normal and quite high (very high at low temperatures), so confirming that the breaking of the C−H bond is quite advanced at the transition state. On the contrary, solvent KIEs are inverse. Finally, isotope effect on isotope effect is clearly smaller than primary KIE, especially at low temperatures. As expected, the three kinds of KIEs approach to unity as temperature increases.

(3) When the two bottlenecks are taken into account through the CUS model, each reaction leads to different results depending on whether just one (and which one) bottleneck or both of them control the global process (see Table 6).

(a) The primary KIE for the unsolvated reaction is unity below 350 K. At this range of temperatures, the process is entirely governed by k_e, whose dependence on mass is through the ion−molecule reduced mass (m) in eq 6. Since the replacement of one hydrogen atom of butanone (the heavy partner) by one deuterium does not significantly affect the value of m, k_e does not change and does not lead to any primary KIE. At higher temperatures, a small primary KIE begins to appear due to the onset of some contribution of k_{pt}. Conversely, the reaction with $n = 2$ is always controlled by the proton transfer bottleneck, in such a way that $KIE_{TST}^{CUS} = KIE_{TST}$ at the whole range of temperatures. Finally, the monosolvated reaction shows an intermediate behavior. Above 298 K, $KIE_{CVT}^{CUS} = KIE_{CVT}$ as a consequence of the fact that the global process is governed by k_{pt}. However, below 298 K, KIE_{CVT}^{CUS} is progressively smaller than KIE_{CVT} as the temperature decreases, due to the enhancing contribution of k_e.

(b) The solvent KIE follows the same trends as the primary KIE with two differences. Firstly, substitution of the hydrogen atoms of hydroxide ion (the light partner) and waters changes slightly the m value, in such a way that the solvent KIE due to k_e is 1.02 (for $n = 0$) or 1.03 (for $n = 1$). Secondly, the solvent KIE due to k_{pt} is inverse, so that the contribution of k_e (when it exists) makes KIE_{CVT}^{CUS} greater than KIE_{CVT}.

(c) The isotope effect on the isotope effect behaves as the primary KIE, taking into account that when the entrance bottleneck is dominant, it is entirely coming from the solvent KIE.

Let us now discuss the validity of the RGM. This rule has been theoretically tested here by comparing the product of the primary and the solvent kinetic isotope effects (these values are shown in parentheses in Tables 7−9) with the isotope effect on isotope effect. This is equivalent to comparing primary KIEs in light and heavy isotopic solvents. From the CUS results it can be seen that the RGM holds in general very well. This is evident when k_e governs the global process, since that rate constant is not significantly affected by substitution of the butanone hydrogen atom (that is, because the primary KIE does not exist, the isotope effect on isotope effect is reduced to solvent

KIE). Cases controlled by the proton transfer bottleneck are more interesting from a chemical point of view. Now the transferring hydrogen atom and the hydrogen atoms whose substitution originate solvent KIEs do not contribute to the same vibrational normal mode, either at reactants or at the transition state (recall that the transition vector is just the proton transfer motion). In other words, proton transfer and solvent reorganization are not coupled in the reaction coordinate (at least at reactants and transition state). Both kinds of isotope substitutions exert their effects independently (on the zero-point energy and on the vibrational partition function), verifying the RGM. However, it has to be emphasized that some deviations of the RGM appear when both bottlenecks are comparable ($R^{CUS} \neq 1$). This phenomenon already has been experimentally observed in several reactions.[27,28] Note especially the RGM breakdown for the case with $n = 1$ at 200 K. This is due to the fact that the R^{CUS} factors (that is, the recrossing corrections) are very sensitive to isotope changes when the two bottlenecks rule the global process. Then, the effects on eq 3 of the different isotope substitutions are not independent. As expected, the RGM would hold if KIE_{CVT} (only one bottleneck) is used.

As mentioned in the Introduction, a second experimental feature concerns the extent of solvent reorganization, that is, the progress of solvation changes that have occurred between reactants and the transition state. A measure of this can be experimentally obtained by comparing the solvent KIE with the corresponding equilibrium solvent isotope effect (solvent EIE). So, Casamassina and Huskey[5] use the equation

$$\text{solvent KIE} = (\text{solvent KIE})^x \qquad (9)$$

where x stands for the extent of hydroxide ion desolvation. In the present work (see the last column in Table 9), using solvent KIE_{TST}^{CUS}, we have obtained $x = 0.44$ (44% desolvated at the transition state) for the reaction with $n = 2$ at 298 K, in very good agreement with the corresponding experimental value in solution (ca. 50% desolvated). However, the estimation of solvent reorganization by means of this method has to be taken with caution. Firstly, it has to be assumed that the solvent isotope effect varies monotonically from reactants to products. Secondly, this method only accounts for solvent reorganization related to changes of bonds in which the isotopically substituted atoms intervene. Unfortunately, solvent reorganization sometimes involves a migration of solvent molecules as well. This is the case for the clusters studied here, for which desolvation of hydroxide ion is accompanied by a migration of the water molecules toward the butenolate oxygen atom (it is expected that this migration does not occur in solution).

It has to be mentioned here that in all the calculations presented so far no tunneling contributions to the KIEs have been included. Experimental results[4] in the literature suggest that tunneling can produce deviations from the RGM and secondary KIEs more important than the corresponding equilibrium secondary effects.[29] The RGM breakdown is thought to occur when solvent motions are coupled to the proton transfer event in a motion that involves tunneling. To analyze the relative importance in our system of those quantum mechanical tunneling effects, we present here, as a first estimation, the results obtained with the IVTST-0 methodology. This is done for the $n = 2$ case, which is the only system that presents a positive barrier to tunneling. The final corrected values of the KIEs are presented in the fourth column of Table 9. It is a common view that as protium has smaller mass than deuterium, it tunnels faster and has higher tunneling probability. Consequently, tunneling would always make KIEs more important. Aside from the transfer mass, tunneling probability also depends on the adiabatic ground-state potential along the tunneling path, in such a way that the larger the adiabatic barrier, the larger the transmission coefficient. As shown in Table 9, the values of primary and solvent KIEs, which are corrected including the tunneling contribution (as explained in the method of calculation), are closer to unity at the whole range of temperatures; i.e., the tunneling contribution makes KIEs less significant. For primary KIEs this is a result of the larger effective barrier for deuterium than for protium (2.3 vs 1.4 kcal/mol), while in the case of solvent KIEs proton transfer in the deuterated system presents a lower barrier than in the non deuterated one (0.7 vs 1.4 kcal/mol). Finally, we can observe that the isotope effect on isotope effect values, when corrected for tunneling, show increasing deviations from the RGM as temperature is lowered. In any case, that deviation is slight at 298 K in accordance with the experimental results of Cassamassina and Huskey.[5]

At this point, it is worth pointing out that in all the calculations which are presented in this paper, correlation effects have been neglected. For that reason, the quantitative values of the calculated rate constants must be viewed with caution. Nevertheless, we believe that our KIE results[26] as well as the main physical conclusions of our work would not basically change by the inclusion of correlation.

Conclusions

In this paper we have theoretically studied different kinetic deuterium isotope effects in butanone + $OH^-(H_2O)_n$ proton transfer reactions (with $n = 0, 1, 2$) to give the $(H_2O)_{n+1}\cdots$ butenolate complex, in order to analyze solvation changes accompanying proton transfer. Since there are two dynamical bottlenecks to reaction (one in the entrance channel, the other in the proton transfer region), we have used the canonical unified statistical theory (CUS). A saddle point in the proton transfer region that involves a positive energy barrier relative to reactants at infinite distance only appears for the reaction with $n = 2$. For this reaction the proton transfer bottleneck controls the global process at the whole range of temperatures. On the other hand, the CUS theory appears to be a very useful tool to calculate the recrossing correction of the best single bottleneck, which is only significant when the two bottlenecks have similar importance.

As for kinetic isotope effects (KIEs), the main difference between the three reactions arises from the relative weights of the two bottlenecks at each temperature, and CUS theory is also indispensable for the corresponding discussion. For the reaction with $n = 2$, the primary substrate KIE is normal and quite high, indicating that the breaking of the C−H bond is quite advanced at the transition state. On the contrary, solvent KIE is inverse. Isotope effect on isotope effect (primary and solvent KIEs together) is clearly smaller than primary KIE.

The rule of the geometrical mean (RGM) holds very well if just one bottleneck governs the global process, although it fails if the two bottlenecks are comparable. The first situation corresponds to the reaction with $n = 2$, in which case the lack of proton transfer and solvent reorganization coupling in the reaction coordinate is the cause of the RGM fulfillment. On the other hand, and assuming a monotonical variation of solvent isotope effect from reactants to product, the solvent KIE, by comparison with the equilibrium solvent isotope effect, indicates that the hydroxide ion is 44% desolvated at the transition state of the reaction with $n = 2$ at 298 K.

It has to be noted that along the series of clusters with $n = 0$, 1, and 2, we are approaching the behavior of the reaction in solution, for which the proton transfer bottleneck should be dominant. Then, it is expected that the main qualitative trends

of the reaction with $n = 2$ hold for the reaction in solution. As a matter of fact, experimental conclusions of Casamassina and Huskey[5] about the rate-limiting proton transfer step in the elimination of 4-nitrophenol from 4-(4-nitrophenoxy)-2-butanone in aqueous hydroxide at 298 K coincide quite well with our theoretical calculations for the reaction with $n = 2$: large normal primary KIE (exptl, 7.54; theor, 5.15), inverse solvent KIE (exptl, 0.66; theor, 0.42), partial desolvation of hydroxide ion at the transition state (exptl, ca. 50%; theor, 44%), and fulfillment of the RGM.

All these results have been obtained without including tunneling effects. A first estimation of the tunneling contribution to kinetic isotope effects has been evaluated by interpolated variational transition state theory. A slight deviation of the RGM due to tunneling is observed, although a wider study of tunneling effects should be performed to support this conclusion.

Acknowledgment. Financial support from DGICYT ("Ministerio de Educación y Ciencia" of Spain) through Project No. PB95-0637 and the use of the computational facilities of the "Centre de Supercomputació de Catalunya" (CESCA) are gratefully acknowledged.

References and Notes

(1) Grunwald, E.; Eustace, D. In *Proton Transfer Reactions*; Caldin, E. F., Gold, V., Eds.; Chapman and Hall: London,1975; pp 103−120.

(2) Quinn, D. M.; Sutton, L. D. In *Enzyme Mechanisms from Isotope Effects*; Cook, P. F., Ed.; CRC Press: Boca Raton, FL, 1991; Chapter 3.

(3) Bigeleisen, J. *J. Chem. Phys.* **1955**, *23*, 2264.

(4) (a) Klinman, J. P. In *Enzyme Mechanisms from Isotope Effects*; Cook, P. F., Ed.; CRC Press: Boca Raton, FL, 1991; Chapter 4. (b) Amin, M.; Price, R. C.; Saunders, W. H., Jr. *J. Am. Chem. Soc.* **1988**, *110*, 4085.

(5) Casamassina, T. E.; Huskey, W. P. *J. Am. Chem. Soc.* **1993**, *115*, 14.

(6) (a) Bigeleisen, J.; Wolfsberg, M. *Adv. Chem. Phys.* **1958**, *1*, 15. (b) Melander, L.; Saunders, W. H., Jr. *Reaction Rates of Isotopic Molecules*; Wiley: New York, 1980.

(7) (a) Castleman, A. W., Jr.; Keesee, R. G. *Chem. Rev.* **1986**, *86*, 589. (b) Leutwyler, S.; Bösiger, J. *Chem. Rev.* **1990**, *90*, 489. (c) Tucker, S. C.; Truhlar, D. G. *J. Am. Chem. Soc.* **1990**, *112*, 3347. (d) Zhao, X. G.; Tucker, S. C.; Truhlar, D. G. *J. Am. Chem. Soc.* **1991**, *113*, 826. (e) González-Lafont, A.; Truong, T. N.; Truhlar, D. G. *J. Phys. Chem.* **1991**, *95*, 4618. (f) Zhao, X. G.; Lu, D.-h.; Liu, Y.-P.; Lynch, G. C.; Truhlar, D. G. *J. Am. Chem. Soc.* **1992**, *97*, 6369.

(8) (a) Wigner, E. *Trans. Faraday Soc.* **1938**, *34*, 29. (b) Keck, J. C. *Adv. Chem. Phys.* **1967**, *13*, 85.

(9) Truhlar, D. G.; Isaacson, A. D.; Garrett, B. C. In *Theory of Chemical Reaction Dynamics*; Baer, M., Ed.; CRC Press: Boca Raton, FL, 1985; Vol. 4, pp 65−137.

(10) Miller, W. H. *J. Chem. Phys.* **1976**, *65*, 2216.

(11) Garrett, B. C.; Truhlar, D. G. *J. Chem. Phys.* **1982**, *76*, 1853.

(12) Hirschfelder, J. O.; Wigner, E. *J. Chem. Phys.* **1939**, *7*, 616.

(13) (a) Hu, W.-P.; Truhlar, D. G. *J. Am. Chem. Soc.* **1995**, *117*, 10726. (b) Hu, W.-P.; Truhlar, D. G. *J. Am. Chem. Soc.* **1996**, *118*, 860.

(14) Frisch, M. J.; Pople, J. A.; Binkley, J. S. *J. Chem Phys.* **1984**, *80*, 3265.

(15) Frisch, M. J.; Trucks, G. W.; Schlegel, H. B.; Gill, P. M. W.; Johnson, B. G.; Robb, M. A.; Cheeseman, J. R.; Keith, T. A.; Petersson, G. A.; Montgomery, J. A.; Raghavachari, K.; Al-Laham, M. A.; Zakrzewski, V. G.; Ortiz, J. V.; Foresman, J. B.; Cioslowski, J.; Stefanov, B. B.; Nanayakkara, A.; Challacombe, M.; Peng, C. Y.; Ayala, P. Y.; Chen, W.; Wong, M. W.; Andres, J. L.; Replogle, E. S.; Gomperts, R.; Martin, R. L.; Fox, D. J.; Binkley, J. S.; Defrees, D. J.; Baker, J.; Stewart, J. P.; Head-Gordon, M.; González, C.; Pople, J. A. *Gaussian 94 (version B.3)*; Gaussian Inc.: Pittsburgh, PA, 1995.

(16) Baldrige, K. K.; Gordon, M. S.; Steckler, R.; Truhlar, D. G. *J. Phys. Chem.* **1989**, *93*, 5107.

(17) Schmidt, M. W.; Baldrige, K. K.; Boatz, J. A.; Gordon, M. S.; Jensen, J. H.; Koveki, S.; Matsunaga, N.; Nguyen, K. A.; Su, S.; Windus, T. L.; Elbert, S. T. *J. Comput. Chem.* **1993**, *14*, 1347.

(18) Celli, F.; Weddle, G.; Ridge, D. P. *J. Chem. Phys.* **1980**, *73*, 801.

(19) Lide, D. R., Ed. *Handbook of Chemistry and Physics*, 73rd ed.; CRC Press: Boca Raton, FL, 1992-1993.

(20) Lu, D.-h.; Truong, T. N.; Melissas, V. S.; Lynch, G. C.; Liu, Y.-P.; Garrett, B. C.; Steckler, R.; Isaacson, A. D.; Rai, S. N.; Hancock, G. C.; Lauderdale, J. G.; Joseph, T.; Truhlar, D. G. *Comput. Phys. Commun.* **1992**, *17*, 235.

(21) Liu, Y.-P.; Lynch, G. C.; Hu, W. P.; Melissas, V. S.; Steckler, R.; Garrett, B. C.; Lu, D.-h.; Truong, T. N.; Isaacson, A. D.; Rai, S. N.; Lauderdale, J. G.; Joseph, T.; Truhlar, D. G. POLYRATE-version 5.1, University of Minnesota, Minneapolis, MN, 1993 (unpublished).

(22) Truhlar, D. G.; Kupperman, A. *J. Am. Chem. Soc.* **1971**, *93*, 1840.

(23) Garrett, B. C.; Truhlar, D. G.; Magnusson, A. W.; Grev, R. S. *J. Phys. Chem.* **1980**, *84*, 1730.

(24) Truong, T. N.; Truhlar, D. G. *J. Chem. Phys.* **1990**, *93*, 1761.

(25) González-Lafont, A.; Truong, T. N.; Truhlar, D. G. *J. Chem. Phys.* **1991**, *95*, 8875.

(26) Liu, Y.-P.; Lynch, G. C.; Truong, T. N.; Lu, D.-h.; Truhlar, D. G.; Garret, B. C. *J. Am. Chem. Soc.* **1993**, *115*, 2408.

(27) Cleland, W. W. In *Enzyme Mechanisms from Isotope Effects*; Cook, P. F., Ed.; CRC Press: Boca Raton, FL, 1991; Chapter 9.

(28) Huskey, W. P. *J. Phys. Org. Chem.* **1991**, *4*, 361.

(29) Saunders, W. H., Jr. *J. Am. Chem. Soc.* **1985**, *107*, 164.

JP9613192

Article 5

"Variable scaling of external correlation energy for association reactions. Entropic effects on the dynamical bottleneck location and tunneling contributions for $C_2H_4 + H \rightarrow C_2H_5$"

Jordi Villà, Angels González-Lafont, José M. Lluch, Donald G. Truhlar

Journal of the American Chemical Society, enviat.

Variable Scaling of External Correlation Energy for Association Reactions. Entropic Effects on the Dynamical Bottleneck Location and Tunneling Contributions for $C_2H_4 + H \rightarrow C_2H_5$

Jordi Villà, Angels González-Lafont, and José M. Lluch*

Departament de Química, Universitat Autònoma de Barcelona, 08193-Bellaterra, Spain

Donald G. Truhlar*

Department of Chemistry and Supercomputer Institute, University of Minnesota, Minneapolis, MN 55455-0431, USA

Abstract. A new way to extrapolate electronic structure calculations to the limit of full configuration mixing and a complete electron basis set is proposed. The method, called variable scaling of external correlation (VSEC) uses a scale factor that varies with geometry to combine a complete-active-space self-consistent-field (CASSCF) calculation with a calculation including an appreciable amount of the dynamical correlation energy. The parameters in the scaling factor are adjusted to experimental or high-quality theoretical data at critical points. The method is applied here to the prototype olefin addition process $H + C_2H_4$. We find excellent agreement with experiment at all temperatures both for the association reaction and its reverse dissociation, and we use the resulting model to infer critical details of the dynamics. In particular, we find that dynamical bottlenecks are about 0.06–0.15 Å tighter than the saddle point, with bending frequencies 1.2–1.8 times higher than at the saddle point. Furthermore we conclude that tunneling effects account quantitatively for the curvature of the Arrhenius plots.

1. INTRODUCTION

The addition of a free radical to an olefin to form an alkyl radical is a prototype class of association reactions. The simplest of these reactions is addition of a hydrogen atom to ethylene, which is of great fundamental and applied importance. For example it is the simplest reaction involving addition to a double bond, and the reaction and its reverse are critical steps in the industrially important pyrolysis (cracking) of ethane feedstock,[1,2] which is a major source of ethylene. The reverse reaction is also important in low-temperature combustion, where it competes with the oxidation of ethyl radical.[2] This reaction has been extensively studied both experimentally[1–21] and theoretically,[22–32] but is still not completely understood. Overall rate constants for both association and dissociation (k_a and k_d, respectively) have been reported in the literature, including their pressure dependence and the temperature dependence of their high-pressure values. We consider the well known mechanism

$$H + C_2H_4 \rightleftarrows C_2H_5^* \quad (1)$$

$$C_2H_5^* + M \rightleftarrows C_2H_5 + M \quad (2)$$

where the asterisk indicates vibrational and rotational excitation. The high-pressure association is of special interest because it corresponds to the rate constant for the elementary step (1), and the high-pressure dissociation is of special interest because RRKM theory reduces to transition state theory in the high-pressure limit. High-pressure rate constants k_a^∞ and k_d^∞ have been measured in the ranges 198–800 K[4,6–9,11,12,17,20] and 673–913 K, respectively.[3,15,16,18,21] Recently, Feng *et al.*[21] developed an RRKM transition state model, based on previously experimental data in the range 198–800 K, for extrapolating k_a^∞ up to 1100 K. The model leads to the following recommended rate expression for k_a^∞:

$$k_a^\infty(T) = 1.795 \times 10^{-12}\, T^{0.454} \exp(-917/T)\ \text{cm}^3\ \text{mol}^{-1}\ \text{s}^{-1} \quad (3)$$

Values obtained from eq. 3 by the same authors, when used together with thermodynamic properties of C_2H_5 yield a new recommended expression of the high-pressure dissociation rate constant in the same temperature range, 198–1100 K:

$$k_d^\infty(T) = 1.11 \times 10^{10}\, T^{1.037} \exp(-18504/T)\ \mathrm{s}^{-1} \qquad (4)$$

Feng *et al.*[21] used k_d^∞ values from eq. 4 to test agreement of their theoretical results with experiment in the 673–913 K range and to interpret their experimental results near the low-pressure limit from 875 to 1094 K.

Besides these experimental results and experimentally based models, several theoretical studies of the association and dissociation reactions have been carried out.[22–32] A major subject of discussion has been the question of whether transition state and RRKM theory can simultaneously fit the rates of the $C_2H_4 + H$ addition and the C_2H_5 unimolecular dissociation. Considerable progress was reported in 1982 by Hase and Schlegel,[25,26] who proposed a loose transition state model based on *ab initio* calculations of the geometry and vibrational frequencies for the transition state. Their model appeared to give an acceptable fit to available experimental data. However, in the above mentioned study by Feng *et al.*[21] it was concluded that a tighter transition state than that used by Hase and Schlegel is required for a good fit to the temperature dependence of the experimental k_d^∞. In view of this finding, Hase *et al.*[29] reassessed the kinetics of the $C_2H_4 + H \rightleftarrows C_2H_5$ system, and they tried to use high-level *ab initio* calculations to develop a definitive transition state model that fits the most reliable experimental results. The main conclusions of this new work are that it is very difficult to obtain quantitative *ab initio* predictions of the energetics for this reaction (so the forward barrier height was taken as an adjustable parameter in fitting the experimental rates, and it was combined with the enthalpy of reaction proposed in previous work[20] for the best estimate of the reverse barrier), and that the loose model proposed in the earlier

paper[25] is good enough to describe the geometry and frequencies for the transition state. With regard to the former conclusion, we note that several other studies have also shown the difficulty of calculating the barrier heights of radical addition reactions (see, for example, Refs. 31–37). One of the aims of the present work is to find a reliable method to evaluate enough of the potential energy surface to perform more sophisticated dynamics calculations than have been carried out so far. In this regard we note that Hase *et al.*[29] used conventional transition state theory, that is, the transition state position was assumed to be fixed at the saddle point structure. In this way, the same loose transition state model was used for the entire range of temperatures studied. One justification for this is an early study[38] in which the 0 K variational transition state was found to be close to the saddle point. We believe though that more definitive studies including finite-temperature dynamical bottlenecks are required to answer this question since entropic effects on the location of the dynamical bottleneck should be considered whenever the intrinsic barrier is small, and the potential is relatively flat in its vicinity.[39]

One objective in this work is to re-examine the addition and unimolecular dissociation rate constants under the more flexible assumption that the location of the transition state along the reaction path is optimized by variational transition state theory. This will allow more definitive conclusions about the looseness or tightness of the transition state as a function of temperature as well as an answer to the question of whether the dynamical bottleneck location is temperature dependent. A second goal is carry out a multidimensional tunneling calculation. To accomplish these objectives we will use a new method presented here called variable scaling of external correlation energy.

2. METHODS AND CALCULATIONS

Geometries, energies, and first and second energy derivatives were calculated using the GAUSSIAN94 system of programs.[40] We recall the general notation X//Y[41] to denote geometry optimization and Hessian evaluation (for frequencies) at level Y followed by a single-point energy calculation at level X. As usual, we omit //Y if Y is the same as X. A consequence of this standard notation is that X//Y calculations involve a level-Y Hessian whereas X calculations involve a level-X Hessian. As usual, X and Y each have the form L/B, where L denotes the Hartree-Fock or correlation level, and B denotes the one-electron basis.

Stationary point geometries (reactants, product, and saddle point) were optimized, and the harmonic vibrational frequencies were calculated using the 6-31G(*d*,*p*) basis set[41] (called B1 in this work) at two levels: Hartree-Fock[41] (HF) and Møller-Plesset second-order perturbation theory[41,43] (MP2). These geometries were also optimized with the 6-311G(*d*,*p*) basis set[41] (called B2) at four levels: HF, MP2, complete active space multiconfiguration SCF[44] (CASSCF) and quadratic configuration interaction with single and double excitations and a perturbative estimate of the effect of triple excitations[45] (QCISD(T)). For the CASSCF calculations we used the same active space (three electrons distributed among three orbitals) as used by Hase *et al.*[29]

Starting from the MP2/B1 saddle point geometry we have calculated the minimum energy path[46,47] (MEP) and the potential energy along the minimum energy path, $V_{MEP}(s)$, where s denotes the distance along the MEP in an isoinertial mass-weighted or mass-scaled coordinate system,[46-50] by following the Gonzalez-Schlegel mass-weighted internal-coordinates reaction-path algorithm[51] at the MP2/Bl level. Note that although this algorithm carries out the calculation in internal coordinates, it does correctly yield the true MEP[46,47] through isoinertial coordinates. A gradient step size, δs, of 0.0319 Å (in mass-scaled coordinates with the scaling mass equal to 1 amu) was used to follow the MEP. For 22 points along this MEP (reactants, product, saddle point, and 19

nonstationary points with values of s from –0.083 Å to 0.344 Å, which correspond to R_1 distances between 1.793 and 2.171 Å) we have also calculated the force constant matrix at the same MP2/B1 level. Then, a generalized normal-mode analysis was performed in rectilinear[46,48–50,52,53] coordinates, which allows us to calculate both the vibrational partition function along the MEP and the vibrationally adiabatic potential energy curve[46,49,50,53–59]

$$V_a^G(s) = V_{MEP}(s) + \varepsilon_{tran}^G(s) \qquad (5)$$

where $\varepsilon_{tran}^G(s)$ is the zero-point energy (ZPE) at s from the generalized normal-mode vibrations transverse to the reaction path. Use of the re-oriented dividing-surface (RODS) algorithm[60] in order to improve these generalized frequencies does not produce any significant change in the $V_a^G(s)$ curve, which indicates that the relatively large step size used to follow the MEP was accurate enough for this reaction. The use of curvilinear coordinates[61,62] was also explored, but they did not lead to significant improvement in the important range of s, so all results presented here were obtained with rectilinear coordinates.

For the above mentioned 22 points, we have also made single-point calculations at the two highest levels used in this work, obtaining improved values of $V_{MEP}(s)$ at the CASSCF(3,3)/B2//MP2/B1/// and QCISD(T)/B2//MP2/B1/// levels. (In this notation, the // indicates that geometries were obtained at the MP2/B1 level, and the /// at the end indicates that these single-point calculations were used to improve the properties all along the MEP, calculated at the // level, not just at the stationary points.) In addition, at the stationary points we carried out PMP2/B1//MP2/B1 calculations, where PMP2 denotes the spin-projected MP2 method:[36] this correction could be important because unrestricted Møller-Plesset perturbation theory suffers from serious spin contamination problems for radical addition reactions to ethylene.[28,33,34]

Rate constants were calculated by direct multidimensional semiclassical dynamics, that is, including multidimensional quantum effects on the nuclear motion by a semiclassical method and obtaining all required information about the potential energy surface directly from electronic structure calculations without the intermediacy of an analytic potential energy function.[63] Canonical variational transition state theory (CVT) rate constants[39,48–50,53,59,64] and semiclassical transmission coefficients[50,53,59,64] for addition and unimolecular dissociation reactions were calculated using a modified version of version 7.0 of the POLYRATE computer program[65–67] that includes the RODS algorithm mentioned above. Bound vibrational and rotational motions were assumed to be separable, and the vibrational partition functions were computed quantum mechanically within the harmonic approximation, except for the torsion around the C–C bond, which is considered a hindered rotor[68,69] in the generalized transition states and C_2H_5 product. Five-point Lagrange interpolation of the reaction-path data was used to obtain properties (geometry, energy, and generalized normal mode frequencies) at every 0.00529 Å along the path from the saddle point to the equilibrium structures. The generalized free energy of activation was then calculated at each of these points, and the location of the variational transition state and the CVT rate constants (k_a^{CVT} and k_d^{CVT}) were determined by interpolating to the maximum of this function for each temperature. Frequencies between consecutive points along the reaction path were correlated adiabatically.[50,70]

Quantum mechanical tunneling effects were included by multiplying $k_a^{CVT}(T)$ and $k_d^{CVT}(T)$ by a transmission coefficient[50,53,59,64] $\kappa(T)$. In particular, the zero-curvature tunneling (ZCT) semiclassical adiabatic ground-state approximation[46,50,53,59,64] $\kappa^{CVT/ZCT}(T)$ has been employed. (Note that in our earlier papers the ZCT approximation is sometimes called the vibrationally adiabatic zero curvature (VAZC) approximation or the minimum-energy-path semiclassical adiabatic

ground-state (MEPSAG) approximation.) The ZCT transmission coefficient is calculated as the Boltzmann average of the semiclassical probability, $P(E)$, of tunneling along the MEP through or over the ground-state vibrationally adiabatic potential barrier, $V_a^G(s)$, at energy E. The ZCT approximation is a multidimensional tunneling method because V_a^G includes the variation with s of the zero point energy of all 14 vibrational modes that are orthogonal to the reaction coordinate.

3. RESULTS

3.1. Geometries

The optimized geometries for the equilibrium and saddle point structures are presented in Table 1. The coordinates used in Table 1 are defined in Figure 1. The overall agreement among the various calculational methods is good, as is the agreement with previous calculations and experimental[71] values (where available). The carbon-carbon distance in ethylene is somewhat underestimated at the HF level whereas the post-HF geometries have the C–C distance closer to the experimental distance of 1.339 Å. The same trends are observed for the carbon-hydrogen distance, with the exception of the CASSCF calculation, which does not improve the HF value. Even though the best calculation energy-wise is the QCISD(T) one, the MP2 optimized geometries are in better agreement with the experimental geometry. For ethyl radical, all methods reflect the expected lengthening of the carbon-carbon distance. In all the optimized geometries of C_2H_5, the R_1 and R_3 distances are clearly longer than R_2 which maintains the value it has in ethylene.

In the saddle point structures, the C_2H_4 moiety resembles ethylene. At the QCISD(T) level the carbon-carbon distance is only 0.013 Å longer than in ethylene, and at the CASSCF and at HF levels there is a greater increase, whereas at the MP2 level the carbon-carbon distances has not

changed from ethylene to the saddle point structure. The distance, R_1, for the attacking/departing hydrogen is 1.967 Å at the QCISD(T) level; the MP2 and CASSCF levels give smaller values for this distance by about 0.1 Å, while the HF R_1 distance is longer. Thus the MP2 and CASSCF potential energy hypersurfaces have a saddle point structure that is more similar to the C_2H_5 system than is the saddle point of the QCISD(T) hypersurface. The bond angles are quite consistent across all levels of theory considered.

3.2. Energies and reaction path

Table 2 summarizes the results for the energetics of the $C_2H_4 + H \rightarrow C_2H_5$ reaction. (The last row of this table will be explained in Section 3.3.)

The quantity ΔV is the classical energy of reaction, i.e., the potential energy of the product of association, C_2H_5, relative to the potential energy of the reactants, $C_2H_4 + H$. The QCISD(T)/B2//MP2/B1 and QCISD(T)/B2 values coincide, indicating that the geometric differences between MP2/B1 and QCISD(T)/B2 minimum-energy structures are not energetically significant. The correction of spin contamination at the PMP2/B2//MP2/B1 level changes the MP2/B1 value of the reaction energy by 1.3 kcal/mol and provides an energy of reaction of –39.2 kcal/mol, in very good agreement with the QCISD(T)/B2 result, which is the highest level reported here. However the CASSCF calculations underestimate the exoergicity by about 8–9 kcal/mol. Since CASSCF includes internal (static) correlation energy, but a negligible portion of the external (dynamic) correlation energy, we conclude that the latter changes very appreciably over the course of reaction.

The quantity ΔH_0 is the 0 K heat of reaction. Our highest-level calculation of this quantity is the QCISD(T) value, –33.4 kcal/mol. This theoretical value is 2 kcal/mol different from the best

experimental result of –35.5 ± 1 kcal/mol, obtained by using the value[72] of 28.0 ± 1 kcal/mol for the 300 K C_2H_5 heat of formation. The discrepancy is understandable due mainly to the small size of the B2 basis set, with only a single set of polarization functions, although corrections for higher-level electron correlation effects could also be important.

The forward and reverse potential energy barriers, $V^{\ddagger}$ and $V^{\ddagger} - \Delta V$, evaluated in the usual ways, i.e., by geometry optimization of the saddle point and evaluation of the energy at the optimized structure, are the first six rows of Table 2. The approximate spin projection technique PMP2 lowers the MP2 addition and dissociation barriers by 6–8 kcal/mol. The PMP2 values are in fair agreement, 0.5–0.7 kcal/mol, with the QCISD(T)/B2 calculations, while the CASSCF calculations overestimate the addition barrier and underestimate the unimolecular dissociation barrier with respect to the QCISD(T)/B2 ones by about 4–5 kcal/mol. Table 2 also gives the zero-point-inclusive barrier height for the forward reaction, $\Delta H_0^{\ddagger}$, and for the reverse reaction, $\Delta H_0^{\ddagger} - \Delta H_0$. These values are evaluated at the MP2/B1 saddle point location for rows 1, 2, 3, and 5, at the CASSCF(3,3)/B2 saddle point for row 4, and at the QCISD(T)/B2 saddle point for row 6.

Rows 7, 8 and 9 of Table 2 show the result of carrying out higher-level single-point calculations along the MP2/B1 reaction path and finding the maximum potential energy along the path. A calculation involving single-point level-X calculations along a reaction path at level Y is called X//Y///. The deviations of these X//Y/// calculations from the most accurate result, QCISD(T)/B2, are comparable to the deviations found at the X//Y levels. The saddle point location is estimated by finding the highest X//Y/// energy along the path calculated at level Y. The maximum of the CASSCF/B2//MP2/B1/// potential energy curve is displaced toward C_2H_5, and the other two X//Y/// curves show a displacement of their maxima from the MP2/B1 saddle

point structure towards the C_2H_4 + H structure. The QCISD(T)/B2//MP2/B1/// forward classical barrier height, 4.3 kcal/mol, is only 0.7 kcal/mol above the QCISD(T)/B2 value calculated with full optimization. Despite the differing locations of the approximate saddle point geometries, the zero point energies of the three X//Y/// saddle points are all in the range 34.3–34.6 kcal/mol. The zero point energy difference between the maximum energy structure at the QCISD(T)/B2//MP2/B2/// level and the saddle point optimized at the QCISD(T)/B2 level is only 1.3 kcal/mol. These results and the geometries in Section 3.1 suggest that, although it is inadequate from an energetic perspective, the MP2/B1 level may be useful for providing a reaction path that connects C_2H_4 + H and C_2H_5. (When the maximum energy point of a series of single-point calculations along a reaction path does not agree well with full optimization of the saddle point at the higher level, which is often the case,[73] then the more complete VTST-IC version[74] of the /// approach, i.e., X///Y instead of X//Y///, may be preferred since in that approach the barrier height calculated by the full optimization is employed.)

Our highest-level unextrapolated result for the zero-point-inclusive barrier, $\Delta H_0^{\ddagger}$, is the full QCISD(T) result, 3.7 kcal/mol. The previous estimate of Hase *et al.*[29] is 2.7 kcal/mol.

If results in any of the first nine rows Table 2 are used to calculate the rate constants for the title reaction, the computed values do not match the experimental results. At all levels, the computed $k_a^{\infty}(T)$ are too low relative to the experimental values. This strongly implies that the calculated *ab initio* energy barriers for the addition reaction are too high. One strategy to fix this problem was suggested by Hase *et al.*,[29] who used the barrier height for C_2H_4 + H addition as an adjustable parameter in conventional transition state theory calculations (including a transmission coefficient based on a one-dimensional Eckart tunneling approximation) to fit the experimental rate constants. We shall suggest an alternative way to proceed in the next section.

3.3 Parameter adjustment

We now propose a new fitting procedure that allows both for a realistic shape of the reaction-path energy profile and also for the change in location of the variational transition state along the reaction path as a function of temperature. By using canonical variational transition state theory with semiclassical tunneling coefficients, we will fit the experimental k_a^∞ and k_d^∞ at the same time.

The basis of the new model is the Scaled External Correlation (SEC) method,[75,76] which is based on combining the results of two *ab initio* calculations: a complete active space self-consistent-field (CASSCF) calculation that accounts for internal (or static) correlation effects and a multi-reference configuration interaction[77] (MRCI) that accounts for an appreciable fraction of the external (or dynamical) correlation. Then, the accurate energy is approximated by:[75]

$$E_{SEC} = E_{CASSCF} + \frac{E_{MRCI} - E_{CASSCF}}{F} \tag{6}$$

where we assume that the non-dynamical correlation is correctly introduced by the CASSCF term[78] and that the fraction of the dynamical correlation energy recovered by the MRCI calculation can be represented by a constant[75] or simple function F.

In the present paper we replace MRCI by QCISD(T). Although QCISD(T) is technically a single-reference method, it shares with coupled cluster methods a relative insensitivity to orbital basis,[79] and it has a major advantage over MRCI that it is size consistent.[45,80] Furthermore the QCI approach is much less affected by spin contamination than the MP2 method. It has been shown previously that in the system under study, the QCISD(T) methodology yield similar

energetic results to multi-reference configuration interaction methods,[29] while having the advantage of being computationally more convenient.

The major new feature introduced in the present paper is that in eq. 6, F is assumed to be a function of geometry. In particular we assume that F is a function of a distinguished coordinate that indicates the degree of advance of the reaction. This accounts for the fact that non-dynamical correlation is not fully included in the QCISD(T) calculation as well as for the fact that the fraction of dynamical correlation energy recovered is not completely constant. To distinguish the new approach from the original SEC method[75,76] in which F was constant, we will call the new approach in which F is a function of geometry Variable Scaling of External Correlation or VSEC.

In the present application the functional form of F is based on the bond energy-bond order (BEBO)[39,81,82] scheme, in which the bond order of a bond depends exponentially on distance, as originally postulated by Pauling.[83] Thus we take

$$F = F_0 + F_1 \exp\left(-\frac{R_1 - R_{1,e}}{\gamma}\right) \tag{7}$$

where F_0, F_1, and γ are adjustable parameters, R_1 is defined in Fig. 1, and $R_{1,e}$ is the R_1 distance at the MP2/B1 C_2H_5 equilibrium geometry ($R_{1,e}$ = 1.095 Å). In the present work the three parameters were adjusted to reproduce as accurately as possible the high-pressure experimental rate constants for the addition and the unimolecular dissociation. This procedure allows us to get a consistent energy profile for studying the location and temperature dependence of the variational transition state of this reaction.

At the C_2H_4 + H reactant (R) structure, R_1 is equal to infinity, yielding $F_R = F_0$. Analogously, at the C_2H_5 product (P) structure, eq. 7 reduces to $F_P = F_0 + F_1$. Using these values yields

$$E^P_{VSEC} - E^R_{VSEC} = E^P_{CASSCF} - E^R_{CASSCF} + \frac{E^P_{QCI} - E^P_{CASSCF}}{F_0 + F_1} - \frac{E^R_{QCI} - E^R_{CASSCF}}{F_0} \qquad (8)$$

where QCI is short for QCISD(T) in the present case. Note that the left-hand side of eq. 8 is the VSEC approximation to the quantity called ΔV in Table 2.

To use eq. 8 we require an estimate for ΔV, which is the classical energy difference between the C_2H_5 and C_2H_4 + H systems. Ideally this would be available from a reliable *ab initio* calculation, but, as we have pointed out above, energy differences in radical addition reactions are very difficult to compute reliably, even if we use very high-level *ab initio* calculations. For this reason we estimate ΔV by an iterative semiempirical method. A reasonable zeroeth iterate for this energy difference is the value that is deduced from the transition state model of Hase *et al.*[29] In Table 5 of Ref. 29 the authors used zero-point-inclusive barriers of 3.1 and 38.4 kcal/mol (the latter is the mean of all the values used) for the addition and the unimolecular dissociation, respectively. For the sake of consistency with our work we calculate ΔV from these values by using *ab initio* frequencies instead of using the scaled values in Table 5, Ref. 29. From the best *ab initio* frequency values of Table 2 in Ref. 29, a ZPE increment between C_2H_4 and C_2H_5 of 5.6 kcal/mol is obtained. Combining these three values yields –40.9 kcal/mol as an estimate of ΔV. This classical energy value is used in eq. 8 to provide a relation between F_0 and F_1; that is, for each trial value for F_0, a unique value of F_1 is calculated with eq. 8. In this way, a table with all the allowed (F_0,F_1) pairs for a given classical energy difference is constructed.

From inspection of the table obtained as just described, (F_0,F_1) pairs with F_0 close to 1.0 and F_1 close to zero are selected. Such a choice of F_0 follows from the high level of the QCISD(T)/B2 calculation, and such a choice of F_1 is made because the dependence of the electron correlation with the bond distance, R_1, although not negligible, is probably small. For each of these (F_0,F_1) pairs, various values of the γ parameter are selected. For a set of three parameters, an energy profile is computed, and we perform a canonical variational transition state theory calculation with semiclassical multidimensional tunneling. We reject those sets of parameters that produce a variational displacement of the transition state out of the region where high level *ab initio* calculations have been carried out, namely, the range of R_1 distances from 1.793 to 2.171 Å. If we cannot obtain a good fit with the variational transition states in this range, we should extend the range.

Comparison with experimental values is done by applying Student's *t* test[84] to the rate constants values. If none of the trial sets give satisfactory results for the Student's *t* test, we change ΔV and repeat the process. This is continued until good agreement with experiment is obtained.

After wide exploration, the parameters that were found to give theoretical rate constants close enough to experimental results (with a significance of 0.02 for Student's *t* test) were F_0 = 1.1, F_1 = –0.0268, and γ = 3.846 Å, with a classical energy difference for the addition process of ΔV = –43.0 kcal/mol. Although $F_0 + F_1$ would ideally be less than 1, a value slightly larger than 1 is acceptable in practical fitting. The maximum in the V_{MEP} curve obtained by the VSEC method (eqs. 7 and 8) with that set of parameters is located at an *s* increment 0.148 Å earlier than (looser than) the MP2/B1 saddle point location. This VSEC-estimated saddle point corresponds to R_1 = 2.011 Å, and the classical barrier height relative to the C_2H_4 + H system is 1.2 kcal/mol. The

bending frequencies of the forming bond at this location are 338 and 257 cm^{-1}. Including zero point changes raises the forward classical barrier height from 1.2 kcal/mol to 2.7 kcal/mol, in excellent agreement with the value of Hase *et al.*[29] (It is worthwhile to note that our calculations were complete before the appearance of the erratum that lowered their value to 2.7 kcal/mol, so this is an independent determination.) The good agreement is encouraging from an empirical point of view because our method is quite different from theirs, involving variational transition state theory and a multidimensional tunneling approximation. Since our treatment is based on higher-level dynamical theory with less assumptions, it can give insight into the nature of the dynamical bottleneck, as discussed in the next section.

Our classical barrier heights for the forward and reverse reaction are 1.2 and 44.2 kcal/mol, respectively. The zero-point-inclusive barrier heights measured at the saddle point are 2.7 and 39.8 kcal/mol, respectively. But since the saddle point is not the dynamical bottleneck, and the variational transition becomes tighter as temperature increases, it is necessary to consider finite-temperature entropic effects as well as zero point energy to get a correct physical model of the reaction. We shall see in the next section that it is necessary to consider more than just the reactants, product, and saddle point in order to model the dynamical bottlenecks for the thermal rate constants.

The energy of reaction and forward and reverse barrier heights as approximated by the VSEC method are given in the last row of Table 2. The value –37.1 kcal/mol that the VSEC treatment yields for ΔH_0, combined with a heat of formation of 12.548 kcal/mol[85] for ethylene at 298 K, implies a value of $\Delta H_{f,298}$ = 26.6 kcal/mol for the heat of formation of ethyl radical, which is in the range (25.8–28.8 kcal/mol) of experimental values,[20] but slightly lower than the values of 28.0–28.8 recommended by Hanning-Lee *et al.*[20] As noted by Hase *et al.*,[29] the data available for

the reverse reaction are not discriminating enough to predict reliable values for ΔV and the heat of formation of the products, and in this light the prediction of the product heat of formation within 1½ kcal/mol is acceptable confirmation that our reaction path model is globally realistic. In the next section we concentrate on the bottleneck properties on the reactant side of the reaction path and tunneling through the barrier region, which are the central points of this study.

3.4 Dynamics

The final calculated values of k_a^{∞} and k_d^{∞} are given in Arrhenius form in Figures 2 and 3, respectively, along with the experimental results. Dotted lines represent the CVT results, and solid lines stand for CVT/ZCT results. Figure 2 shows some dispersion in the oldest values at 298 K, probably due to the extrapolations from low-pressure results that were necessary to obtain estimates of the high-pressure-limit rate constants. Notice that the two figures cover different temperature ranges.

Figure 2 shows that tunneling is important for temperatures below ~500 K. The ZCT transmission coefficient is 1.14, 1.23, 1.44, and 2.37 at 500, 400, 300, and 200 K respectively. If tunneling is neglected, the deviation from experimental values is a factor of 1.6 and 2.8 at temperatures of 300 and 200 K, respectively, with a factor of 2.1 discrepancy at 250 K. Figure 2 illustrates very dramatically that the widely discussed curvature of the Arrhenius plot for this addition reaction is almost entirely due to tunneling. Thus the CVT calculation without tunneling yields nearly a straight line in Fig. 2, while the nonlinear CVT/ZCT curve incorporating the VSEC multidimensional tunneling contribution tracks the experimental results rather faithfully. Although it was concluded even in early work that the temperature dependence of the partition coefficients

were probably insufficient to account for the temperature dependence of the rate constants, only relatively crude tunneling calculations were available.[1,2]

Figure 3 shows a somewhat greater dispersion in the experimental values, and Trenwith's results[15] are significantly different from the rest. Inclusion of the semiclassical tunneling coefficient in the calculation is now less important because all the experimental values were obtained at high temperatures (600 K and higher); the ZCT transmission coefficient decreases from 1.09 at 600 K to 1.03 at 1000 K.

In Table 3 we present the properties corresponding to the variational transition states at several temperatures. In the second column of this table the displacements of the transition state with respect to the VSEC saddle point geometry are presented. Negative values of s correspond to the C_2H_4 + H side of the saddle point. Note that the variational transition state is tighter than the saddle point. This is expected[39] for an early saddle point in an exothermic reaction because the variational effect is controlled by the tightening of transitional bending modes, that is bending modes whose frequencies vanish asymptotically. Furthermore the variational transition state becomes tighter (moves toward the C_2H_5 product) as the temperature increases, also in accord with previous variational transition state theory results.[34,39,86–93] The maximum of the VSEC vibrationally adiabatic ground-state potential curve V_a^G, which is the maximum of the standard-state generalized transition state theory free energy of activation profile[39,48] at 0 K, also appears at positive s (s = 0.39 Å), corresponding to a geometry where R_1 is 1.971 Å. The movement of the variational transition state from s = 0.039 Å at 0 K to s = 0.149 Å at 1000 K corresponds to shortening of about 0.11 Å in the R_1 distance, with a concomitant change of 0.4 kcal/mol in V_{MEP} at the variational transition state. The V_a^G curve is rather flat in this region, dropping 0.3 kcal/mol from the saddle point value, but finite-temperature entropic effects are more important. The only

generalized normal mode frequencies that suffer important changes in the region that contains the variational transition states at the different temperatures are the C–C stretching and the two H–C–C bending frequencies about the forming bond. Values of these bending frequencies at the variational transition states are shown in column 5 of Table 3. These low frequencies have an important weight in the entropic term[34,39,70,85] of the CVT free energy of activation (last two columns of Table 3), and they have provoked considerable discussion in the literature concerning their loose or tight character. As shown in Table 3, as temperature increases from 200 to 1000 K, these two bending frequencies at the variational transition state increase by 99 and 132 cm^{-1}, respectively. However even at 1000 K, the variational transition state calculated here is looser than the one calculated by Hase *et al.*[27], which has bending frequencies of 399 and 369 cm^{-1}, or by Hase *et al.*,[29] values of 422 and 382 cm^{-1} for the same frequencies. Thus our study does not support the conclusions of Feng *et al.*[21]

The bending frequencies at the 200 K dynamical bottleneck are 17% and 30% larger than at the VSEC saddle point, and the bending frequencies at 1000 K are factors of 1.5 and 1.8 larger than at the VSEC saddle point. These ratios show that a proper understanding of association reactions cannot be based on calculations only at the saddle point; entropic bending effects that tend to tighten the dynamical bottleneck location are important, and they compete successful with energetic effects in determining that location, with the effect being quite large at 1000 K. Nevertheless these effects can be estimated using the present direct dynamics scheme based on variable scaling of external correlation energy.

4. SUMMARY AND CONCLUDING REMARKS

We have introduced a new method, VSEC (variable scaling of external correlation), for extrapolating electronic structure calculations to the limit of full configuration interaction and a complete one-electron basis set. The VSEC method assumes that separate estimates are available for the non-dynamical and total correlation energies, and that the fraction of correlation energy recovered is a smooth function of geometry. In the present application, that smooth function is taken as a monotonic function of a single internal coordinate corresponding to the breaking bond. The assumption that a single internal coordinate is appropriate is justified by the fact that radical addition reactions satisfy the Bell-Evans-Polanyi principle.[94a] According to this principle, if no bonding elements occur in the transition state that do not also occur in either the reactants or products, the delocalization energy correlates monotonically with a single reaction coordinate.[94b] It will be interesting in future work to explore the applicability of the VSEC model for other reaction types.

One of the principal advantages of the VSEC model is that it does not presume a particular shape or even a functional form for the reaction barrier. By parameterizing the fraction of dynamical correlation energy recovered rather than parameterizing the potential energy hypersurface, we allow an arbitrary shape of the reaction path energy profile. This is particularly important for the credibility of tunneling calculations.

We have employed variational transition state theory in which the dynamical bottleneck is equated to the variational transition state, which in turn is identified with the structure with the maximum free energy of activation for both the forward and reverse reaction. The variational displacement of the dynamical bottleneck from the location of the saddle point depends on temperature, and in the range of temperatures from 200 and 1000 K, it ranges from 0.06 to 0.15 Å, with the variational transition state being tighter than the saddle point. The potential energy

varies by only about 0.4 kcal/mol over the range of geometries where the dynamical bottlenecks are found, but the C–C–H bend frequencies are 156 and 210 cm^{-1} higher at the 1000 K variational transition state than at the saddle point location and over 100 cm^{-1} higher than at the 200 K variational transition state. Because these changes with temperature correspond to 25–40% increases in the bend frequencies, it means we must be very cautious about interpreting addition reactions in terms of a temperature-independent transition state. The fact that the frequencies at the variational transition states differ even more from the saddle point frequencies means that converging electronic structure calculations for stationary point energies and geometries is only a first step at providing true understanding of the dynamics, even if the goal is simply to understand thermal high-pressure-limiting rate constants. Nevertheless fully characterizing the saddle point is an important first step, and one that still eludes us in a fully *ab initio* sense. Thus we should remember that the present results are based on an electronic structure extrapolation method that, while suggestive and qualitatively stimulating, is surely susceptible to quantitative improvement.

Because the transition state occurs fairly early along the reaction path, tunneling was estimated by a zero-reaction-path-curvature scheme. The variation of zero point energies along the tunneling path was included for all 14 transverse vibrational modes. Tunneling is found to be important for temperatures below about 500 K, increasing the calculated rate constants by 23, 44, and 137 percent at 400, 300, and 200 K respectively, and accounting for the lion's share of the curvature observed in Arrhenius plots.

5. ACKNOWLEDGMENTS

This work was supported in part by the U. S. Department of Energy, Office of Basic Energy Sciences. Financial support from DGES (project No. PB95-0637) and the use of the

computational facilities of the "Centre de Computació i de Comunicacions de Catalunya" are also gratefully acknowledged.

References

(1) Pilling, M. J. In *Modern Gas Kinetics*; Pilling, M. J., Smith, I. W. M., Eds.; Blackwell Scientific: Oxford, 1987; p. 330.

(2) Davies, J. W.; Pilling, M. J. *Adv. Gas-Phase Photochem. Kinet.* **1989**, *2*, 105.

(3) (a) Lin, M. C.; Back, M. H. *Can. J. Chem.* **1996**, *44*, 505. (b) Lin, M. C.; Back, M. H. *Can. J. Chem.* **1966**, *44*, 505. (c) Loucks, L. F.; Laidler, K. J. *Can. J. Chem.* **1967**, *45*, 2795.

(4) Braun, W.; Lenzi, M. *Discussions Faraday Soc.* **1967**, *44*, 252.

(5) Westenberg, A. A.; deHaas, N. *J. Chem. Phys.* **1969**, *50*, 707.

(6) Kurylo, M. J.; Peterson, N. C.; Braun, W. *J. Chem. Phys.* **1970**, *53*, 2776.

(7) Eyre, J. A.; Hikida, T.; Dorfman, L. *J. Chem. Phys.* **1970**, *53*, 1281.

(8) Barker, J. R.; Keil, D. G.; Michael, J. V.; Osborne, D. T. *J. Chem. Phys.* **1970**, *52*, 2079.

(9) (a) Michael, J. V.; Cowfer, J. A.; Keil, D. G.; Yeh, C. *J. Phys. Chem.* **1971**, *75*, 1584. (b) Cowfer, J. A. Michael, J. V. *J. Chem. Phys.* **1975**, *62*, 3504.

(10) (a) Michael, J. V.; Osborne, D. T.; Suess, G. N. *J. Chem. Phys.* **1973**, *58*, 2300. (b) Jones, W. E.; Macknight, S. D.; Teng, L. *Chem. Rev.* **1973**, *73*, 407.

(11) Lee, J. H.; Michael, J. V.; Payne, W. A.; Stief, L. J. *J. Chem. Phys.* **1978**, *68*, 1817.

(12) Oka, K.; Cvetanović, R. J. *Can. J. Chem.* **1979**, *57*, 777.

(13) Pacey, P. D.; Wimalasena, J. H. *Chem. Phys. Lett.* **1980**, *76*, 433.

(14) (a) Sugawara, K.; Okazaki, K.; Sato, S. *Chem. Phys. Lett.* **1981**, *78*, 259. (b) Sugawara, K.; Okazaki, K.; Sato, S. *Bull. Chem. Soc. Jpn.* **1981**, *53*, 2872.

(15) Pacey, P. D.; Wimalasena, J. H. *J. Phys. Chem.* **1984**, *88*, 5657.

(16) Trenwith, A. B. *J. Chem. Soc., Faraday Trans.* **1986**, *82*, 457.

(17) Lightfoot, P. D.; Pilling, M. J. *J. Phys. Chem.* **1987**, *91*, 3373.

(18) Simon, Y.; Foucaut, J. F.; Scacchi, G. *Can. J. Chem.* **1988**, *66*, 2142.

(19) Garner, D. M.; Fleming, D. G.; Arseneau, D. J.; Senba, M.; Reid, I. D.; Mikula, R. J. *J. Chem. Phys.* **1990**, *93*, 1732.

(20) Hanning-Lee, M. A.; Green, N. J. B.; Pilling, M. J.; Robertson, S. H. *J. Phys. Chem.* **1993**, *97*, 860.

(21) Feng, Y.; Niiranen, J. T.; Bencsura, Á., Knyazev, V. D.; Gutman, D.; Tsang, W. *J. Phys. Chem.* **1993**, *97*, 871.

(22) Michael, J. V.; Suess, G. N. *J. Chem. Phys.* **1973**, *58*, 2807.

(23) (a) Sloane, C.; Hase, W. L. *Faraday Discuss. Chem. Soc.* **1977**, *62*, 210. (b) Hase, W. L.; Mrowka, G.; Brudzynski, R.; Sloane, C. S. *J. Chem. Phys.* **1978**, 69, 3548. (c) Hase, W. L.; Wolf, R. J.; Sloane, C. S. *J. Chem. Phys.* **1979**, *71*, 2911. (d) Hase, W. L.; Mrowka, G.; Brudzynski, R.; Sloane, C. S. *J. Chem. Phys.* **1980**, *72*, 6321.

(24) (a) Hase, W. L.; Ludlow, D. M.; Wolf, R. J.; Schlick, T. *J. Phys. Chem.* **1981**, *85*, 958. (b) Schlegel, H. B. *J. Phys. Chem.* **1982**, *85*, 4878. (c) Hase, W. L.; Buckowski, D. G. *J. Comput. Chem.* **1982**, *3*, 335.

(25) Hase, W. L.; Schlegel, H. B. *J. Phys. Chem.* **1982**, *86*, 3901.

(26) Schlegel, H. B.; Bhalla, K. C.; Hase, W. L. *J. Phys. Chem.* **1982**, *86*, 4883.

(27) (a) Hase, W. L.; Buckowski, D. G.; Swamy, K. N. *J. Phys. Chem.* **1983**, *87*, 2754. (b) Swamy, K. N.; Hase, W. L. *J. Phys. Chem.* **1983**, *87*, 4715.

(28) Sosa, C.; Schlegel, H. B. *Int. J. Quant. Chem.* **1986**, *29*, 1001.

(29) Hase, W. L.; Schlegel, H. B.; Balbyshev, V.; Page, M. *J. Phys. Chem.* **1996**, *100*, 5354; **1997**, *101*, 5026(E).

(30) Mole, S. J.; Zhou, X.; Liu, R. *J. Phys. Chem.* **1996**, *100*, 14665.

(31) Nguyen, M. T.; Creve, S.; Vanquickenborne, L. G. *J. Phys. Chem.* **1996**, *100*, 18422.

(32) Jursic, B. S. *J. Chem. Soc., Perkin Trans. 2* **1997**, *637*.

(33) Barone, V.; Orlandini, L. *Chem. Phys. Lett.* **1995**, *246*, 45.

(34) Villà, J.; González-Lafont, A.; Lluch, J. M.; Corchado, J. C.; Espinosa-García, J. *J. Chem. Phys.* **1997**, *107*, 0000.

(35) Schlegel, H. B. *J. Chem. Phys.* **1986**, *84*, 4530.

(36) Gonzalez, C.; Sosa, C.; Schlegel, H. B. *J. Phys. Chem.* **1989**, *93*, 2435, 8388(E).

(37) Wong, M.; Radom, L. *J. Phys. Chem.* **1995**, *99*, 8582.

(38) Hase, W. L. *Acc. Chem. Res.* **1983**, *16*, 258.

(39) (a) Garrett B. C.; Truhlar, D. G. *J. Am. Chem. Soc.* **1979**, *101*, 4534. (b) Garrett, B. C.; Truhlar, D. G. *J. Am. Chem. Soc.* **1979**, *101*, 5207.

(40) Frisch, M. J.; Trucks, G. W.; Schlegel, H. B.; Gill, P. M. W.; Johnson, B. G.; Robb, M. A.; Cheeseman, J. R.; Keith, T. A.; Petersson, G. A.; Montgomery, J. A.; Raghavachari, K.; Al-Laham, M. A.; Zakrzewski, V. G.; Ortiz, J. V.; Foresman, J. B.; Cioslowski, J.; Stefanov, B. B.; Nanayakkara, A.; Challacombe, M.; Peng, C. Y.; Ayala, P. Y.; Chen, W.; Wong, M. W.; Andres, J. L.; Replogle, E. S.; Gomperts, R.; Martin, R. L.; Fox, D. J.; Binkley, J. S.; Defrees, D. J.; Baker, J.; Stewart, J. P; Head-Gordon, M.; Gonzalez, C.; Pople, J. A. *GAUSSIAN94*; Gaussian, Inc.; Pittsburgh, PA, 1995.

(41) Hehre, W. J.; Radom, L.; Schleyer, P. v. R.; Pople, J. A. *Ab Initio Molecular Orbital Theory*; Wiley; New York, 1986.

(42) Corchado, J. C.; Espinosa-García, J.; Hu, W.-P.; Rossi, I.; Truhlar, D. G. *J. Phys. Chem.* **1995**, *99*, 687.

(43) Møller, C.; Plesset, M. S. *Phys. Rev.* **1934**, *46*, 618.

(44) Roos, B. O.; Taylor, P. R.; Siegbahn, P. E. M. *Chem. Phys.* **1980**, *48*, 152.

(45) Pople, J. A.; Head-Gordon, M.; Raghavachari, K. *J. Chem. Phys.* **1987**, *87*, 5968.

(46) Truhlar, D. G.; Kuppermann, A. J. *J. Am. Chem. Soc.* **1971**, *93*, 1840.

(47) Fukui, K. *Pure Appl. Chem.* **1982**, *54*, 1825.

(48) Garrett, B. C.; Truhlar, D. G. *J. Chem. Phys.* **1979**, *70*, 1593.

(49) Garrett, B. C.; Truhlar, D. G. *J. Phys. Chem.* **1979**, *83*, 1079.

(50) Isaacson A. D.; Truhlar, D. G. *J. Chem. Phys.* **1982**, *76*, 1380.

(51) Gonzalez, C.; Schlegel, H. B. *J. Phys. Chem.* **1990**, *94*, 5523.

(52) Miller, W. H.; Handy, N. C.; Adams, J. E. *J. Chem. Phys.* **1980**, *72*, 99.

(53) Truhlar, D. G.; Isaacson, A. D.; Garrett, B. C. In *Theory of Chemical Reaction Dynamics*; Baer, M., Ed.; CRC Press: Boca Raton, FL, 1985; Vol. 4; p. 65.

(54) Elaison, M. A.; Hirschfelder, J. O. *J. Chem. Phys.* **1959**, *30*, 1426.

(55) Hofacker, L. *Z. Naturforsch.* **1963**. *18a,* 607.

(56) Marcus, R. A. *J. Chem. Phys.* **1967**, *46*, 959.

(57) Truhlar, D. G. *J. Chem. Phys.* **1970**, *53*, 2041.

(58) Troe, J. In *Physical Chemistry: An Advanced Treatise, Vol. 6B*; Jost, W., Ed.; Academic press: New York, 1975; p. 835.

(59) Garrett, B. C.; Truhlar, D. G.; Grev, R. S.; Magnuson, A. W. *J. Phys. Chem.* **1980**, *84,* 1730.

(60) Villà, J.; Truhlar, D. G. *Theor. Chem. Acc.* **1997**, *97*, 317.

(61) (a) Nguyen, K. A.; Jackels, C. F.; Truhlar, D. G. *J. Chem. Phys.* **1996**, *104*, 6491. (b) Chuang Y.-Y.; Truhlar, D. G. *J. Phys. Chem.*, in press.

(62) Corchado, J. C.; Chuang, Y.-Y.; Fast, P.; Coitiño, E. L.; Hu, W.-P.; Liu, Y.-P.; Lynch, G. C.; Nguyen, K. A.; Jackels, C. F.; Gu, M. Z.; Rossi, I.; Clayton, S.; Melissas, V. S.; Steckler, R.; Garrett, B. C.; Isaacson, A. D.; Truhlar, D. G. POLYRATE-version 7.8, University of Minnesota, Minneapolis, MN 1997.

(63) (a) Gray, S. K.; Miller, W. H.; Yamaguchi, Y.; Schaefer, H. F. *J. Am. Chem. Soc.* **1981**, *103*, 1900. (b) Colwell, S. M. *Mol. Phys.* **1984**, *51*, 1217. (c) Colwell, S. M.; Handy, N. C. *J. Chem. Phys.* **1985**, *82*, 1281. (d) Nelson, H. H.; Adams, G. F., Page, M. *J. Chem. Phys.* **1990**, *93*, 479. (e) Baldridge, K. K.; Gordon, M. S.; Steckler, R.; Truhlar, D. G. *J. Phys. Chem.* **1989**, *93*, 5107. (f) Garrett, B. C.; Koszykowski, M. L.; Melius, C. F.; Page, M. *J. Phys. Chem.* **1990**, *94,* 7096. (g) Truhlar, D. G.; Gordon, M. S. *Science* **1990**, *249*, 491. (h) González-Lafont, A.; Truong, T. N.; Truhlar, D. G. *J. Phys. Chem.* **1991**, *95*, 4618. (i) Liu, Y.-P.; Lynch, G. C.; Truong, T. N.; Lu, D.-h.; Truhlar, D. G.; Garrett, B. C. *J. Am. Chem. Soc.* **1993**, *115*, 2408. (j) Liu, Y.-P.; Lu, D.-h.; González-Lafont, A. D.; Truhlar, G.; Garrett, B. C. *J. Am. Chem. Soc.* **1993**, *115*, 7806.

(64) (a) Truhlar, D. G.; Isaacson, A. D.; Skodje, R. T.; Garrett, B. C. *J. Phys. Chem.* **1982**, *86*, 2252. (b) Tucker, S. C.; Truhlar, D. G. In *New Theoretical Concepts for Understanding Organic Reactions*; Bertrán, J., Csizmadia, I. G., Eds.; Kluwer Academic Publishers: Dordrecht, 1989; p. 291.

(65) Lu, D.-h.; Truong, T. N.; Melissas, V. S.; Lynch, G. C.; Liu, Y.-P.; Garrett, B. C.; Steckler, R.; Isaacson, A. D.; Rai, S. N.; Hancock, G. C.; Lauderdale, J. G.; Joseph, T.; Truhlar, D. G. *Computer Phys. Commun.* **1992**, *71*, 235.

(66) Steckler, R.; Hu, W.-P.; Liu, Y.-P.; Lynch, G. C.; Garrett, B. C.; Isaacson, A. D.; Melissas, V. S.; Lu, D.-h.; Truong, T. N.; Rai, S. N.; Hancock, G. C.; Lauderdale, J. G.; Joseph, T.; Truhlar, D. G. *Computer Phys. Commun.* **1995**, *88*, 341.

(67) Steckler, R.; Chuang, Y.-Y.; Coitiño, E. L.; Hu, W.-P.; Liu, Y.-P.; Lynch, G. C.; Nguyen, K. A.; Jackels, C. F.; Gu, M. Z.; Rossi, I.; Fast, P.; Clayton, S.; Melissas, V. S.; Garrett, B. C.; Isaacson, A. D.; Truhlar, D. G. POLYRATE version 7.0, University of Minnesota, Minneapolis, MN, 199.

(68) Truhlar, D. G.; *J. Comp. Chem.* **1991**, *12*, 266.

(69) Sears, T. J.; Johnson, P. M.; Jin, P.; Oatis, S. *J. Chem. Phys.* **1996**, *104*, 781.

(70) Villà, J.; González-Lafont, A.; Lluch, J. M.; Bertrán, J. *Mol. Phys.* **1996**, *89*, 633.

(71) Duncan, J. L. *Mol. Phys.* **1974**, *28*, 1177.

(72) Castelhano, A. L.; Marriott, P. R.; Griller, D. *J. Am. Chem. Soc.* **1981**, *103*, 4262.

(73) (a) Espinosa-Garcia, J.; Corchado, J. C. *J. Phys. Chem.* **1995**, *99*, 8613. (b) Chuang, Y.-Y.; Truhlar, D. G. unpublished.

(74) (a) W.-P. Hu, Y.-P. Liu, and D. G. Truhlar, *J. Chem. Soc. Faraday Trans.* **1994**, *90*, 1715. (b) Chuang, Y.-Y.; Truhlar, D. G. *J. Phys. Chem. A* **1997**, *101*, 6911.

(75) Brown, F. B.; Truhlar, D. G. *Chem. Phys. Lett.* **1985**, *117*, 307.

(76) Corchado, J. C.; Truhlar, D. G. *ACS Symp. Ser.*, in press.

(77) Shavitt, I. In *Advanced Theories and Computational Approaches to the Electronic Structure of Molecules*; Dykstra, C. E., Ed.; Reidel: Boston, 1984, p.

(78) Mok, D. K. W.; Neumann, R.; Handy, N. C. *J. Phys. Chem.* **1996**, *100*, 6225.

(79) Lee, T. J.; Scuseria, G. E. In *Quantum Mechanical Electronic Structure Calculations with Chemical Accuracy*; Langhoff, S. R., Ed.; Kluwer: Dordrecht, 1995; p. 47.

(80) Raghavachari, K.; Anderson, J. B. *J. Phys. Chem.* **1996**, *100*, 12960.

(81) Johnston, H. S.; Parr, C. A. *J. Am. Chem. Soc.* **1963**, *85*, 2544.

(82) Truhlar, D. G. *J. Am. Chem. Soc.* **1972**, *94*, 7584.

(83) Pauling, L. *J. Amer. Chem. Soc.* **1947**, *69*, 542.

(84) Miller, J. C.; Miller, J. N. In *Statistics for Analytical Chemistry, 2nd Edition;* Ellis Horwood: London, 1988.

(85) Lide, D. R., Ed.; *Handbook of Chemistry and Physics*, 76th edition; CRC Press: Boca Raton, FL, p. 5-4.

(86) Hase, W. L. *J. Chem. Phys.* **1976**, *64*, 2442.

(87) Quack, M.; Troe, J. *Ber. Bunsenges. Phys. Chem.* **1977**, *81*, 329.

(88) Rai, S. N.; Truhlar, D. G. *J. Chem. Phys.* **1983**, *79*, 6046.

(89) Hase, W. L. *Accounts Chem. Res.* **1983**, *16*, 258.

(90) Hu, X.; Hase, W. L. *J. Phys. Chem.* **1989**, *93*, 6029.

(91) Hase, W. L.; Wardlaw, D. M. *Adv. Gas-Phase Photochem. Kinet.* **1989**, 2, 171.

(92) Klippenstein, S. J.; Marcus, R. A. *J. Chem. Phys.* **1990**, *93*, 2418.

(93) Wardlaw, D. M.; Marcus, R. A. *Adv. Chem. Phys.* **1987**, *70*, 231.

(94) Dewar, M. J. S.; Dougherty, R. C. *The PMO Theory of Organic Chemistry*; Plenum: New York, 1975; (a) p. 310; (b) pp. 219–220.

Table 1: *Ab initio* geometries (distances in Å and angles in degrees)[a]

		6-31G(*d*,*p*)		6-311G(*d*,*p*)			
	coordinate	HF	MP2	HF	MP2	CASSCF(3,3)	QCISD(T)
C_2H_4	R_{CC}	1.316	1.336	1.316	1.337	1.337	1.344
	R_{CH}	1.077	1.081	1.077	1.085	1.076	1.089
	Φ_{HCC}	121.7	121.6	121.7	121.7	121.6	121.5
SP[b]	R_{CC}	1.375	1.335	1.357	1.335	1.362	1.357
	R_1	2.009	1.864	1.983	1.869	1.880	1.967
	R_2	1.075	1.080	1.075	1.085	1.076	1.088
	R_3	1.076	1.080	1.076	1.084	1.075	1.088
	Φ	106.3	107.2	106.6	107.2	107.8	106.8
C_2H_5	R_{CC}	1.497	1.489	1.498	1.494	1.497	1.500
	R_1	1.086	1.089	1.086	1.094	1.086	1.098
	R_2	1.076	1.078	1.076	1.083	1.076	1.087
	R_3	1.091	1.095	1.091	1.100	1.114	1.104
	Φ	111.7	111.8	111.6	111.6	111.6	111.6

[a]Experimental values for C_2H_4: R_{CC} = 1.339 Å, R_{CH} = 1.085 Å, and Φ_{HCC} = 121.1 (Ref. 70)

[b]Saddle point

Table 2: Energetics (kcal/mol) for the $C_2H_4 + H \rightarrow C_2H_5$ reaction[a]

method[b]	ΔV	$V^{\ddagger}$	$V^{\ddagger} - \Delta V$	ΔH_0	$\Delta H_0^{\ddagger}$	$\Delta H_0^{\ddagger} - \Delta H_0$
MP2/B1	–37.9	11.0	48.9	–32.0	12.7	44.7
PMP2/B1//MP2/B1	–39.2	3.1	42.3	–33.3		
CASSCF(3,3)/B2//MP2/B1	–30.7	8.5	39.1	–24.8		
CASSCF(3,3)/B24	–30.8	7.9	38.8	–24.9	9.4	34.3
QCISD(T)/B2/MP2/B1	–39.3	3.9	43.1	–33.4		
QCISD(T)/B2	–39.3	3.6	43.0	–33.4	3.8	37.2
PMP2/B1//MP2/B1///	–39.2	4.0	43.2	–33.3	5.4	38.7
CASSCF(3,3)/B2//MP2/B1///	–30.7	8.5	39.1	–24.8	10.3	35.1
QCISD(T)/B2//MP2/B1///	–39.3	4.3	43.6	–33.4	5.7	39.1
VSEC//MP2/B1///	–43.0	1.2	44.2	–37.1	2.7	39.8

[a] ΔV is the classical energy of reaction. $V^{\ddagger}$ is the classical barrier height. $V^{\ddagger} - \Delta V$ is the classical barrier height of the reverse reaction. ΔH_0 is the zero-point-inclusive energy of reaction, which equals the enthalpy of reaction at 0 K. $\Delta H_0^{\ddagger}$ is the zero-point-inclusive barrier height evaluated at the conventional transition state (saddle point). $\Delta H_0^{\ddagger} - \Delta H_0$ is the zero-point-inclusive barrier height for the reverse reaction evaluated at the saddle point.

[b] B1: 6-31G(*d*,*p*); B2: 6-311G(*d*,*p*)

Table 3: Properties corresponding to the VSEC variational transition state at several temperatures

T(K)	s(Å)[a]	R_1(Å)[b]	V_{MEP}-ΔV[c]	freq. (cm^{-1})[d]	$\Delta G_a^{CVT,0}$ [e]	$\Delta G_d^{CVT,0}$ [f]
200	0.057	1.954	44.1	395, 335	2.4	39.8
300	0.078	1.932	44.1	417, 365	2.4	39.9
400	0.088	1.923	44.0	427, 379	2.5	40.0
500	0.095	1.916	44.0	435, 389	2.7	40.1
600	0.106	1.905	44.0	447, 405	2.7	40.2
700	0.144	1.868	43.7	488, 460	2.9	40.4
800	0.146	1.867	43.7	490, 463	3.1	40.5
900	0.147	1.865	43.7	492, 465	3.2	40.7
1000	0.149	1.864	43.7	494, 467	3.4	40.9

[a]Relative to the VSEC saddle point

[b]See Figure 1

[c]Potential energy relative to C_2H_5, in kcal/mol

[d]The two H...C = C bending frequencies about the rupturing bond

[e]CVT standard-state free energy of activation, in kcal/mol

[f]CVT standard-state free energy of activation, in kcal/mol

Figure captions

Figure 1. Definition of geometrical parameters for the C_2H_4 and C_2H_5 systems.

Figure 2. Arrhenius plot for the high-pressure limit of the addition rate constant, k_a^∞. The solid and dotted lines are the calculated rate constants with and without tunneling, respectively and the symbols are experimental results.[4,6-11,12,14,17,20]

Figure 3. Arrhenius plot for the high-pressure limit of the unimolecular dissociation rate constant, k_d^∞. The solid and dotted lines are the calculated rate constants with and without tunneling, respectively, and the symbols are experimental results.[3,15,16,18,21] Note that the dotted line is practically hidden by the solid line.

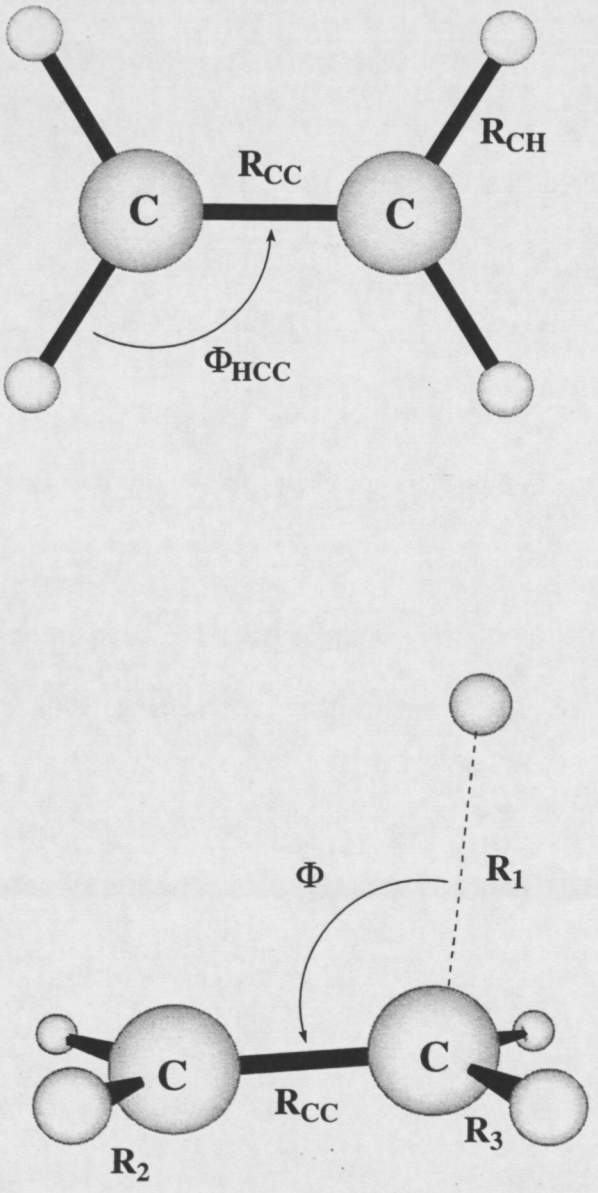

Figure 1

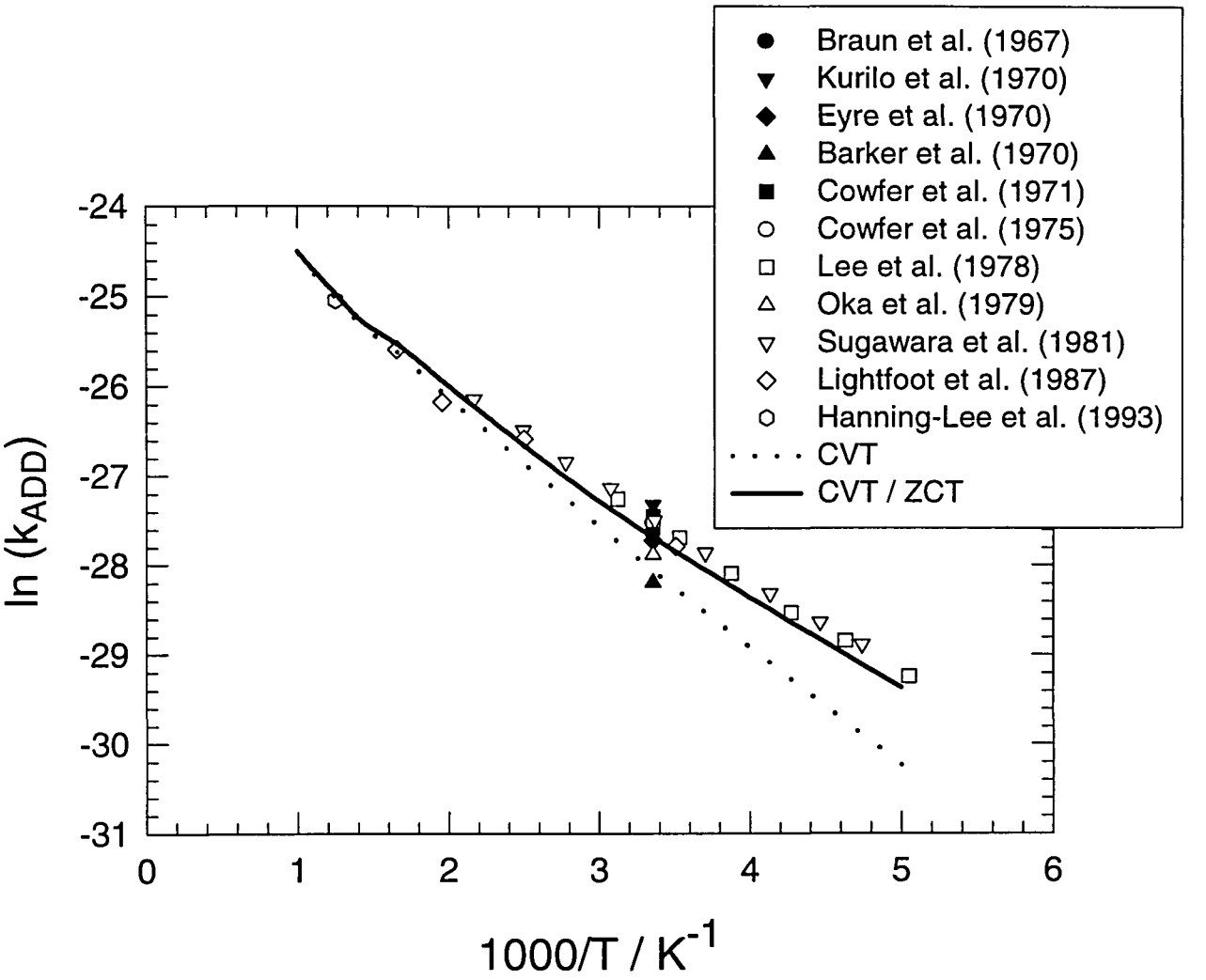
Braun et al. (1967)
Kurilo et al. (1970)
Eyre et al. (1970)
Barker et al. (1970)
Cowfer et al. (1971)
Cowfer et al. (1975)
Lee et al. (1978)
Oka et al. (1979)
Sugawara et al. (1981)
Lightfoot et al. (1987)
Hanning-Lee et al. (1993)
CVT
CVT / ZCT
ln (k_ADD)
-24
-25
-26
-27
-28
-29
-30
-31
0
1
2
3
4
5
6
1000/T / K^-1

Figure 2

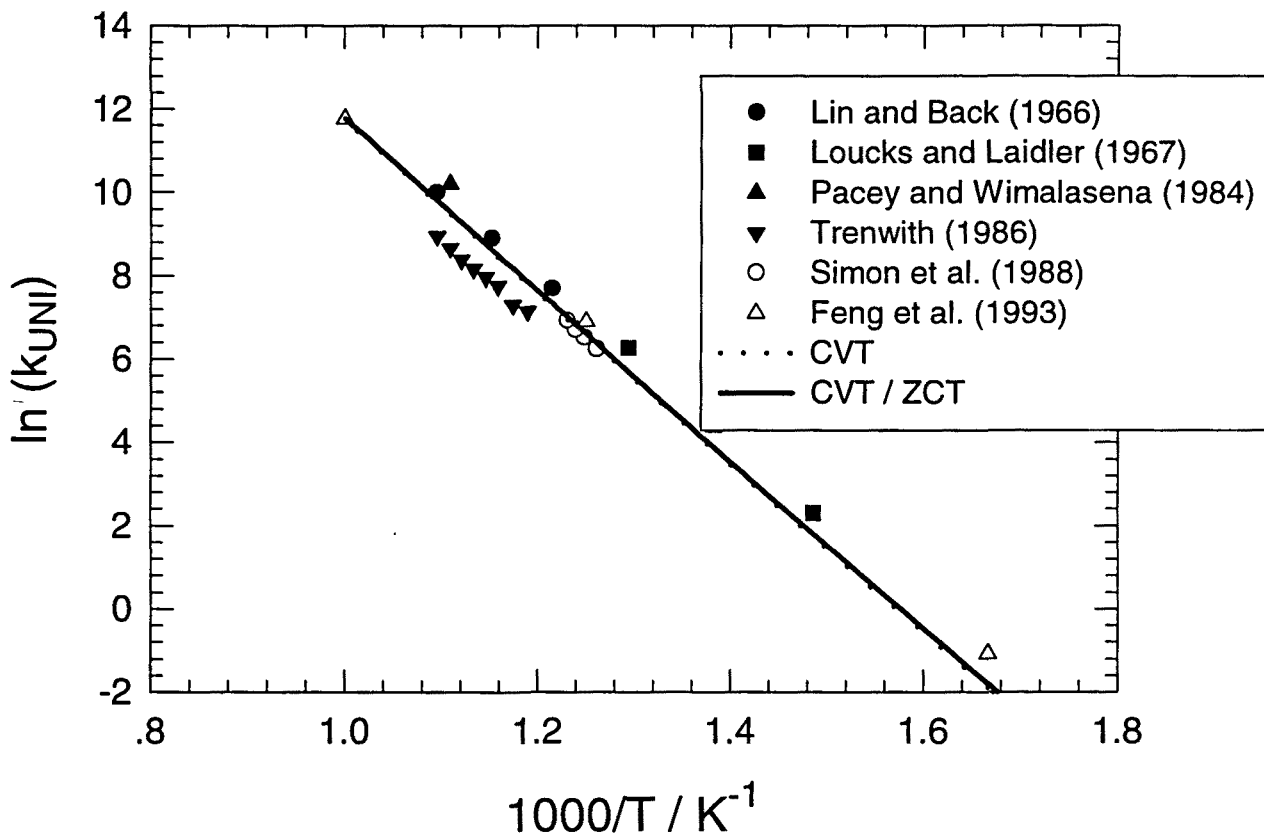
14
12
10
8
6
4
2
0
-2
.8
1.0
1.2
1.4
1.6
1.8
ln (k_UNI)
1000/T / K^-1
Lin and Back (1966)
Loucks and Laidler (1967)
Pacey and Wimalasena (1984)
Trenwith (1986)
Simon et al. (1988)
Feng et al. (1993)
CVT
CVT / ZCT

Figure 3

Article 6

"Understanding the activation energy trends for the $C_2H_4 + OH \rightarrow C_2H_4OH$ reaction by using canonical variational transition state theory"

Jordi Villà, Angels González-Lafont, José M. Lluch, José C. Corchado, Joaquín Espinosa-García

Journal of Chemical Physics, **1997**, *107*, 7266.

Understanding the activation energy trends for the $C_2H_4+OH \rightarrow C_2H_4OH$ reaction by using canonical variational transition state theory

Jordi Villà, Angels González-Lafont, and Jose M Lluch
Departament de Química Universitat Autònoma de Barcelona 08193 Bellaterra Barcelona Spain

José C Corchado and Joaquín Espinosa-García
Departamento de Química Física, Universidad de Extremadura 06071 Badajoz Spain

(Received 28 May 1997, accepted 8 August 1997)

The potential-energy hypersurface of the addition reaction $OH-C_2H_4$ was partially explored following two different approaches First, the stationary points were located at the MP2(FULL)/6-31G(d,p) level and then the minimum energy path (MEP) was built starting from the MP2 saddle-point geometry In order to improve the energetics along the MEP, single-point calculations were carried out at several higher levels, in particular, PMP2, MP4sdtq, PMP4sdtq, and QCISd(t) In a different approach, the C–O bond length was assumed to provide an accurate parametrization of the reaction path in the vicinity of the transition state The minimum energy structures at the MP4sdq/6-311+G(d,p) level for 16 points along the R_{C-O} coordinate have been calculated, followed by a generalized normal-mode analysis at the MP2(FULL)/6-311+G(d,p) level for each point The initial potential information from both approaches was used to calculate canonical variational transition state (CVT) association rate constants for the temperature range 200–1000 K Our calculations at the PMP4sdtq/6-311+G(d,p)//MP4sdq/6-311+G(d,p)[MP2(FULL)/6-311+G(d,p)] level reproduce the inverse dependence of the rate constant with temperature at $T<565$ K, in agreement with the experimental evidence that this reaction has a negative activation energy at room temperature The analysis of the enthalpic and entropic contributions to the Gibbs free-energy profile has allowed us to understand those negative values of the activation energy
 [S0021-9606(97)02842-0]

I. INTRODUCTION

Radical addition reactions are difficult to study experimentally, because they are very fast reactions, and theoretically, because the accurate description of the low-energy barriers they present needs a very high level of theory [1–3]

The very fast reaction of a hydroxyl radical with ethylene plays an important role in combustion processes and atmospheric chemistry Experimentally, this reaction has been extensively studied using a wide variety of detection techniques.[4–17] The reported high-pressure rate constants differ by a factor of about 2 (5.00×10^{-12}–9.96×10^{-12} cm^3 molecule^{-1} s^{-1}) at room temperature [4,5,7–11] A negative temperature dependence of the rate constant has been found in most studies yielding a negative activation energy of about -1 kcal mol^{-1} [4,9–11] On the other hand, an activation energy of $-(2.3\pm1.6)$ kcal mol^{-1} derived from fitting the experimental data with $P>500$ Torr and $T\leq590$ K has been recently reported by Diau *et al* [17] However, a careful analysis of this latter work shows a quite high dispersion of the rate constants for the title reaction, which introduces some doubts on the accuracy of the fitted activation energies

Negative temperature dependences appear to be a common feature of the reaction of a OH radical with olefins For these reactions, 20 years ago Atkinson *et al* [9] stated that it is possible that the activation energies are zero and that the observed negative temperature dependences arise from a temperature dependence of the preexponential factor On the other hand, the existence of a weakly bound complex prior to the formation of the adduct has been proposed in similar reactions to explain this negative dependence [18,19] In turn Zellner and Lorenz[11] proposed an explanation in terms of collision theory if one assumes a cross section which increases rapidly at threshold energy, reaches a sharp maximum, and then decreases as energy is increased

The extensive experimental literature on the addition of a OH radical to ethylene contrasts with the lack of theoretical studies, of which, to the best of our knowledge, there have only been two reported [2,20] Sosa and Schlegel studied this reaction with the Møller–Plesset perturbational method, both with and without spin projection They concluded that the barrier height is overestimated when spin projection is not performed, while annihilation of the largest spin contamination lowers this energy barrier by 7–9 kcal mol^{-1} All the stationary points and the reaction path were optimized at the Hartree–Fock level, followed by single-point calculations at several perturbational levels An interpolated energy barrier of -0.9 kcal mol^{-1} was obtained at the PMP4sdtq 6-31G*//6-31G* level of theory Using transition state theory they estimated a positive value for the activation energy of about 0.1 kcal mol^{-1} at the same level These results showed that, in accordance with other works,[13,21] it is theoretically difficult to obtain accurate energy barriers for radical addition reactions, even though a very high level of calculation is used

These practically barrierless reactions are an exciting challenge for theoretical calculations The aim of this paper is to study the $CH_2=CH_2+OH\rightarrow CH_2CH_2OH$ reaction in or

 0021-9606/97/107(18)/7266/9/$10 00

der to obtain kinetic information using canonical variational transition state theory (CVT). In particular we will try to reproduce and understand the negative temperature dependence of the rate constant experimentally found for this reaction. In Sec. II we give the theoretical methods and calculations details. Results and Discussion are given in Sec. III. Finally, conclusions are presented in Sec. IV.

II. METHODS AND CALCULATION DETAILS

Geometries, energies, and first and second energy derivatives were calculated using the GAUSSIAN 94 system of programs.[22]

Two different approaches were employed to calculate the initial information about the potential-energy surface for the title reaction that is needed to perform the dynamical study. From now on, we will use the convenient notation *X*//*Y*[*Z*], which denotes geometry optimization at level *Y* and energies calculated at level *X*, with frequencies at level Z.[23] When *Z* is the same as *Y*, it need not be mentioned. When *Y* is the same as *X* it need not be mentioned.

(i) In the first approach the stationary point geometries (reactants, product, saddle point, and complex) are optimized in restricted (*R*) or unrestricted (*U*) second-order Møller–Plesset perturbation theory,[24] MP2, with full electron correlation, using the 6-31G(d,p) basis set (b1). Starting from the saddle-point geometry we have constructed the minimum energy path (MEP)[25] following the González–Schlegel mass-weighted internal-coordinates reaction-path algorithm[26] at the MP2(FULL)/6-31G(d,p) level. In addition, for 29 points along this MEP (also including reactants, product, and saddle point) we obtain double information. First, we compute the force constant matrix at the same level [MP2(FULL)/6-31G(d,p)]. Then, a generalized normal-mode analysis projecting out frequencies is performed,[27] which allows us to calculate both the vibrational partition function along the MEP and the vibrationally adiabatic ground-state potential energy curve

$$V_a^G(k) = V_{\mathrm{MEP}}(k) + \epsilon_{\mathrm{int}}^G(k), \tag{1}$$

where $V_{\mathrm{MEP}}(k)$ is the classical energy along the MEP at the point k, and $\epsilon_{\mathrm{int}}^G(k)$ is the zero-point energy (ZPE) at point k from the generalized normal-mode vibrations orthogonal to the reaction path. Second, for the above mentioned 29 points, we make single-point calculations at higher levels:

(1) Fourth-order Møller–Plesset perturbation theory, MP4, with a frozen core (FC) approximation and single, double, triple, and quadruple replacements, with a somewhat larger basis set, namely, 6-311+G(d,p) (b2). We can denote the resulting energy as

MP4sdtq(FC)/b2//MP2(FULL)/b1.

To reduce the spin contamination, we use the spin projection operator as implemented in GAUSSIAN 94.[28] In addition, we have calculated the energies after spin decontamination, which will be denominated PMP2 and PMP4.

(2) Quadratic configuration interaction (QCI) with single and double substitutions and perturbative inclusion of connected triple substitutions,[29] with the b2 basis set. We can denote the resulting energy as

QCIsd(t)/b2//MP2(FULL)/b1.

(ii) In the second approach the reactants, product, and saddle point geometries are optimized at the restricted (*R*) or unrestricted (*U*) fourth-order Møller–Plesset perturbation theory, MP4, with frozen core (FC) approximation and single, double, and quadruple replacements (MP4sdq) with the b2 basis set. At this level we used a distinguished-coordinate path (DCP) approach[30] instead of an MEP approach to define the reaction path and reaction coordinate. Since the C–O bond has found to be the most significant varying parameter along the MP2 MEP in the transition-state region, the C–O bond length, R(CO), has been taken as the distinguished coordinate to define the MP4 reaction path in the vicinity of the variational transition states. The DCP is defined as the sequence of minimum energy structures obtained for 16 values of the C–O distance between 1.95 and 2.24 Å at the MP4sdq/b2 level of theory. To minimize spin contamination single-point calculations, using MP4sdtq, followed by projection of the spin contribution of higher electronic states, have been performed, yielding a final value of the energy which can be denoted as PMP4sdtq/b2//MP4sdq/b2 at stationary points and as PMP4sdtq/b2///MP4sdq/b2 at other points along the reaction path where[23] /// denotes "along a path calculated by" just as // denotes "at a stationary point optimized by." At each one of these geometries, a generalized normal-mode analysis of frequencies at the MP2(FULL)/b2 level has been performed. Since in this approach the true MEP has not been calculated, projecting out the frequencies using the local gradient obtained may lead to incorrect results.[31] For this reason, and taking into account that the gradient norm in this flat MP4 surface is very small in the region which contains the variational transition states over the temperature range studied, we can use, as a first approximation, the nonprojected frequencies. On the other hand, since the spin contamination is higher along the reaction path ($\langle S^2 \rangle$ between 0.9 and 0.999) than at reactants and products ($\langle S^2 \rangle$ equal to 0.756 and 0.762, respectively) we have scaled the generalized frequencies at the points with higher contamination by a factor of 0.925.

This initial information (optimized geometries, first and second energy derivatives, and the energies at higher levels) for both approaches allows us to calculate rate constants as a function of temperature in the framework of canonical variational transition state theory (CVT).[32] CVT yields hybrid rate constants (i.e., classical reaction path motion with other degrees of freedom quantized). However, in the present work, no significant quantitative error is introduced if rotational partition functions are calculated classically. For all vibrations, the partition functions are calculated quantum mechanically within the harmonic approximation and we include correctly the $^2\Pi_{1/2}$ excited state of OH (only 140 cm^{-1} above the electronic ground state)[33] in the reactant partition

function The extra information needed for the CVT calculation (potential energy, moments of inertia, and generalized vibrational frequencies) was calculated at intervals of $0.01a_0$, in mass-scaled Cartesian coordinates (using a reduced mass of 10.58 amu) by a three-point Lagrange interpolation The frequencies between consecutive points along the reaction paths were correlated adiabatically [34] Calculations were performed by using a slightly modified version of the general polyatomic rate constant POLYRATE computer program, version 7.0 [35]

Finally, in order to compare with the experimental reaction enthalpies we have performed additional single-point calculations with different basis sets at optimized MP2(FULL)/b1 geometries corresponding to reactants and product (a) PMP4sdtq(FC)/b3, (b) PMP4sdtq(FC)/b4, (c) CCsd(t)/b5, (d) CCsd(t)/b6, (e) B3LYP/b5 (f) B3LYP/b6 (g) B3LYP/b7, and (h) B3LYP/b8, where b3=6-311+G(2d,p), b4=6-311++G(2d,p), b5=cc-pVDZ, b6=aug-cc-pVDZ, b7=cc-pVTZ, and b8=aug-cc-pVTZ Also, a full optimization at the B3LYP/b5 level has been performed for reactants and products Note that CC stands for coupled cluster[36] calculations, while B3LYP[37] denotes the three-parameter hybrid functional of Becke and the LYP correlation functional which is used in density functional theory

III. RESULTS AND DISCUSSION

A. Stationary points

Some of the geometric parameters of reactants product, and saddle point at MP2(FULL)/b1 and MP4sdq/b2 levels are shown in Fig 1 Table I lists the harmonic vibrational frequencies at these levels When comparison is possible (at reactants) the MP2 and MP4 geometries and MP2 frequencies are in good agreement with the experimental values [33] Note, however, as is known,[38] that the frequencies calculated at the MP2 level are somewhat overestimated The saddle-point structure presents only small perturbations of the geometrical parameters relative to reactants, which suggests that the addition of the OH radical to ethylene proceeds via an "early" transition state This is the expected behavior from Hammond's postulate,[39] since the reaction is very exothermic This stationary point was characterized with one and only one imaginary frequency ($539i$ and $573i$ cm^{-1} at MP2(FULL)/b1 and MP4sdq/b2[MP2(FULL)/b2] levels of theory, respectively) These low values are in agreement with that calculated by Sosa and Schlegel,[2] and they suggest a flat potential energy surface in this region The classical energy values relative to reactants turn out to be 4.87 kcal mol^{-1} and 5.22 kcal mol^{-1} at MP2(FULL)/b1 and MP4sdq/b2 levels respectively

We performed a wider exploration of the potential-energy surface between the reactants and the saddle point and located a complex whose main properties at MP2(FULL)/b1 and MP4sdq/b2 levels are in good agreement with the ones obtained by Sosa and Schlegel [2] The complex has C_{2v} symmetry with the H of the hydroxyl attacking the π bond at a distance of 2.408 Å and 2.516 Å at MP2(FULL)/b1 and MP4sdq/b2 levels, respectively Table II shows the binding energy and the frequencies for this complex

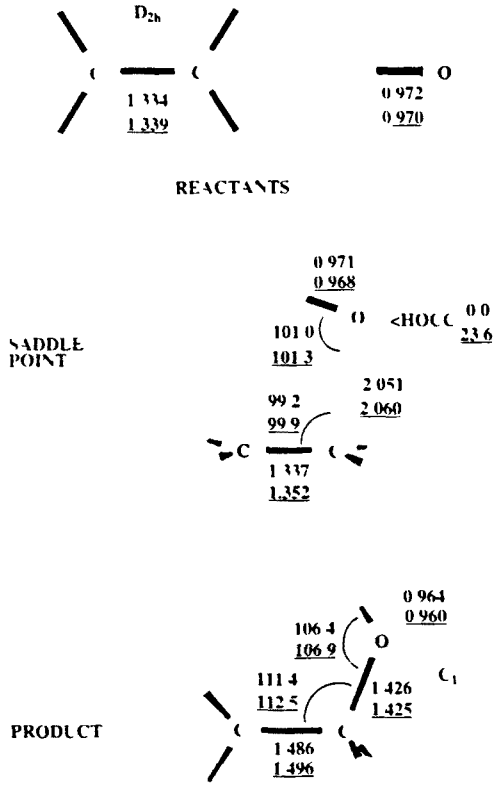

FIG 1 Geometries of reactants saddle point and product for the OH+CH_2—C H OH reaction at the MP2(FULL)/6-31Gd p (saddle point with C_s symmetry) and MP4sdq(FC)/6-311+Gd p) (C_1 symmetry) underlined values levels Distances and angles are given in Å and degrees respectively Experimental values for reactants (Ref 33) $R_{OH}=0.9700$ Å $R_{CC}=1.337$ Å

B. MP2 minimum energy path

We will now discuss the ab initio results obtained using the first approach mentioned in Sec II

The MEP initially consists in a shortening of the C–O interatomic distance leading to the saddle point at the MP2(FULL)/b1 level The C–C π-bond is being broken while the C–O σ-bond is simultaneously being formed Finally the reaction yields the product CH_2CH_2OH The MEP does not pass through the complex For this reason it does not influence the kinetics of the title reaction according to the treatment of the dynamics adopted here and we will not consider this complex further

Some MP2 vibrational frequencies along the MEP are shown in Fig 2 Because the MEP in the region near the saddle point is governed by the CO distance, R(CO) for the sake of clarity and for comparison with the second approach in this work we have chosen this distance to describe the degree of advance along the MEP In the reactant limit (large C–O distances) $OH+CH_2=CH_2$ only 13 vibrational frequencies are nonzero Most of these frequencies do not change significantly in going from the reactants to the tran

TABLE I. Harmonic frequencies (cm^{-1}) for reactants, saddle point, and product

$CH_2CH_2^a$		OH^b		Saddle point		Product	
A[c]	B[c]	A[c]	B[c]	A	B	A	B
3356	3280	3836	3813	3830	3821	3880	3906
3333	3254			3391	3317	3380	3302
3255	3184			3363	3285	3264	3183
3238	3166			3283	3210	3136	3082
1729	1675			3262	3185	3085	3038
1525	1484			1698	1625	1558	1517
1414	1382			1534	1494	1523	1486
1268	1237			1395	1342	1445	1425
1092	1066			1283	1257	1405	1383
995	975			1123	1109	1212	1196
943	900			1063	1066	1161	1147
850	834			965	973	1138	1115
				859	846	985	973
				797	760	870	856
				414	436	543	561
				239	246	439	440
				81	173	362	344
				539*i*	573*i*	230	249

[a]Experimental values (Ref. 33): 3105, 3102, 3026, 2988, 1622, 1443, 1342, 1222, 1023, 949, 943, and 826 cm^{-1}.
[b]Experimental values (Ref. 33): 3735 cm^{-1}.
[c]Method A corresponds to MP2(FULL)/6-31G(d,p)[MP2(FULL)/6-31G(d,p)] and method B to MP4sdq/6-311+G(d,p)[MP2(FULL)/6-311+G(d,p)]. See text.

sition state. Globally, there are 17 degrees of freedom corresponding to vibrational movements orthogonal to the MEP and one degree corresponding to the MEP itself (essentially, the C–O shortening). Figure 2 shows frequencies 6, 12, 14, 15, 16, and 17, which are the ones that change significantly along the reaction path. Note the significant change of frequency 6, which corresponds to the C–C stretching, within the interval represented in Fig. 2.

MP2(FULL)/b1 classical energies along the MEP, V_{MEP}, the ground-state vibrationally adiabatic potential curve, V_a^G, and zero-point energies (ZPE) as a function of the C–O distance are plotted in Fig. 3. The position of the maximum of the two energy curves is essentially the same at this level, because ZPE is practically constant as the C–O distance varies within the interval shown in Fig. 3. The classical and the adiabatic barrier heights are, respectively, 4.87 and 7.37 kcal mol^{-1} at this level.

TABLE II. Complex properties

Frequencies (cm^{-1})		Energy[a]	
A[b]	B[b]		
3828	3776		
3359	3280		
3336	3254		
3257	3182		
3241	3166	ΔV_{MEP}	
1722	1672	A[b]	B[b]
1537	1487	−5.04	−2.73
1412	1381		
1309	1240	ΔZPE	
1268	1071	A[b]	B[b]
1092	990	2.36	1.41
1008	924		
849	836		
696	383		
282	271		
133	120		
79	114		
77	88		

[a]Relative to reactants, in kcal mol^{-1}.
[b]Method A corresponds to MP2(FULL)/6-31G(d,p) and method B to MP4sdq/6-311+G(d,p)[MP2(FULL)/6-311+G(d,p)]. See text. Spin contamination effect is negligible.

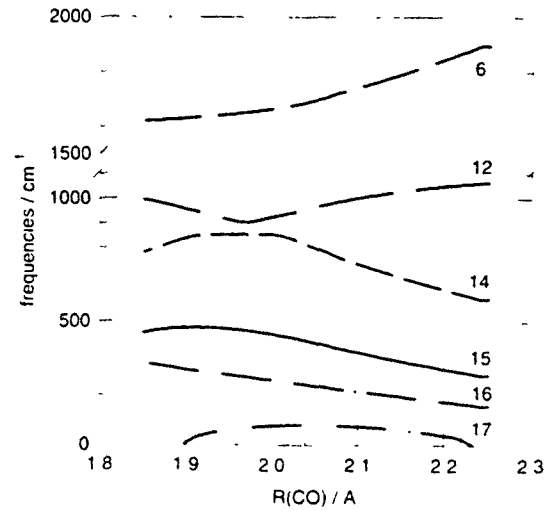

FIG. 2. Adiabatically correlated generalized-normal-mode vibrational frequencies corresponding to some modes at the MP2(FULL)/6-31G(d,p) level.

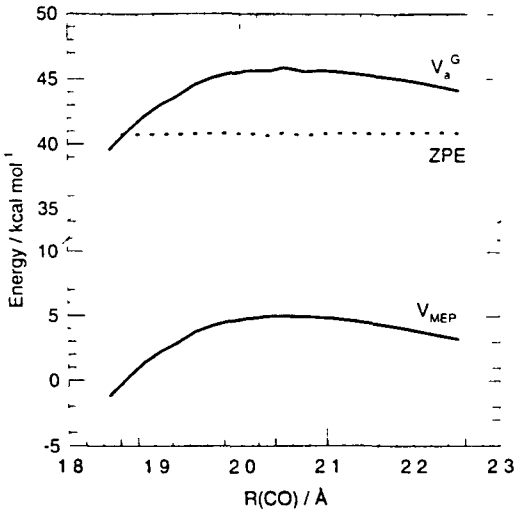

FIG 3 Classical energy profile $V_{MEP}(k)$, vibrationally adiabatic ground-state potential-energy curve $V_a^G(k)$, and zero-point energy from the generalized-normal-mode vibrational frequencies, along the MP2(FULL)/6-31G(d,p) minimum energy path At reactants, $V_a^G = \text{ZPE} = 37.53$ kcal mol^{-1}

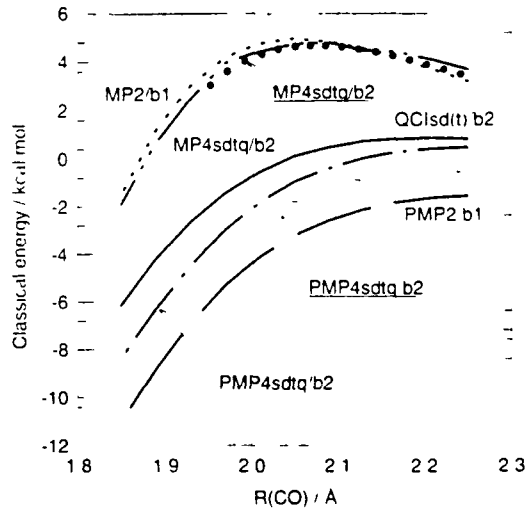

FIG 4 Classical energy profiles at different levels of calculation for both approaches adopted in this work Nonunderlined legends correspond to the first approach in Sec II underlined legends correspond to the second approach b1 6-31G(d,p), b2 6-311+G(d,p) All the values are given with respect to reactants

C. Improved reaction paths

If the energetic MP2 information were used to obtain thermal rate constants, poor agreement with experiment would be found, showing, in accordance with previous work,[1-3,21] the difficulty of obtaining theoretically accurate barrier heights for radical addition reactions. This poor agreement means that we have to improve the energy along our ab initio reaction path. Table III lists the relative energies, for both approaches presented in Sec. II, with respect to reactants at several levels of calculation, and Fig. 4 shows the changes in classical energy along the reaction path. The maximum value for the classical energy along the path a

TABLE III. Energies (in kcal mol^{-1}) relative to reactants[a]

Method	Maximum of V_{MEP}[b]	Product
MP2(FULL)/b1//MP2(FULL)/b1	4.87	−33.94
PMP2(FULL)/b1//MP2(FULL)/b1	0.0	−34.26
MP4sdtq/b2//MP2(FULL)/b1	4.81	−28.67
PMP4sdtq/b2//MP2(FULL)/b1	0.45	−28.75
QCIsd(t)/b2//MP2(FULL)/b1	0.85	−27.70
MP4sdq/b2//MP4sdq/b2	5.22	−27.98
MP4sdtq/b2//MP4sdq/b2	4.67	−28.81
PMP4sdtq/b2//MP4sdq/b2	0.0	−28.90
MP4sdtq/6-311+G(2d,p)//MP2(FULL)/b1	-[c]	−28.14
PMP4sdtq/6-311+G(2d,p)//MP2(FULL)/b1	-	−28.21
MP4sdtq/6-311++G(2d,p)//MP2(FULL)/b1	-	−28.12
PMP4sdtq/6-311++G(2d,p)//MP2(FULL)/b1	-	−28.18
B3LYP/cc-pVDZ//MP2(FULL)/b1	-	−31.39
B3LYP/aug-cc-pVDZ//MP2(FULL)/b1	-	−29.56
B3LYP/cc-pVTZ//MP2(FULL)/b1	-	−28.76
B3LYP/aug-cc-pVTZ//MP2(FULL)/b1	-	−28.14
CCsd(t)/cc-pVDZ//MP2(FULL)/b1	-	−26.52
CCsd(t)/aug-cc-pVDZ//MP2(FULL)/b1	-	−28.16
B3LYP/cc-pVDZ//B3LYP/cc-pVDZ	-	−27.72
ΔZPE[c]	2.73	4.23
ΔTC[d]	−1.19	−1.27

[a]b1 6-31G(d,p); b2 6-311+G(d,p)
[b]Maximum value of the classical potential energy at each level
[c]Zero-point energy differences at the MP4sdq/b2[MP2(FULL)/b2] level
[d]Differences in the thermal corrections to the enthalpy of activation or enthalpy of reaction at the MP4sdq/b2[MP2(FULL)/b2] level and 298 K.
[e](-) means the path was not calculated

each level of calculation is shown in the second column of Table III As has been analyzed in previous work,[28 40–43] spin contamination is a very important concern, and the use of the spin-projection technique lowers the barrier by ~5 kcal mol^{-1}, depending on the level of correlation and the basis set The correction for spin contamination is overestimated in the PMP2(FULL)/b1//MP2(FULL)/b1 case, whereas the PMP4sdtq/b2//MP2(FULL)/b1 results are in better agreement with the QCIsd(t)/b2//MP2(FULL)/b1 ones Lowering the barrier height by using better levels of calculation also provokes the displacement of the maximum towards reactants, which in turn provokes an important change in the vibrational modes of the MP2(FULL)/b1 structures that yield those barriers Higher levels of calculation yield earlier maximum energy points

Except for the PMP2 single-point calculations, all the other curves within the frame of our first approach yield maximum energies along the reaction path which are inconsistent with the expected negative values of the activation energies reported in the literature For this reason we will need to use the second approach introduced in Sec II in order to get classical and adiabatic energy profiles which, as we will see in the next subsection, reproduce the experimental negative dependence of the rate constant versus temperature.

On the other hand, some disagreement exists for the experimental values of the reaction enthalpy, which ranges from −29 to −36 kcal mol^{-1} [1 11 15 17 44 45] To our knowledge, the only direct experimental determination of ΔH^0 for the title reaction has been reported by Diau and Lee,[17] who obtained a value for the reaction enthalpy of −(30 7 ±0 9) kcal mol^{-1} By using the theoretical ZPE and thermal corrections from Table III we can derive an estimate of the reaction energy of about −33 66 kcal mol^{-1} Our theoretical reaction energy values shown in Table III drastically decrease on including the fourth-order correction, while the negligible spin contamination in the CH_2CH_2OH adduct results in equal projected and nonprojected values of the energy of the product for each level of calculation examined Convergence of the classical reaction energy is achieved at the higher levels of calculation when larger basis sets are used It is clear that experiment and theory disagree for the reaction energy, and additional work will be necessary to understand the origin of this discrepancy

D. Activation energy calculation

As stated in the previous subsection, calculations using the optimized geometries from the second approach provide a reaction path as a function of the C–O bond length which does not present either a classical or an adiabatic potential energy barrier Thus this approach is able to reproduce the experimental negative temperature dependence of the rate constant This fact can be seen in Fig 5, where our theoretical rate constants at the PMP4sdtq/b2//MP4sdq/b2[MP2(FULL)/b2] level at different temperatures, along with the corresponding experimental values obtained by several authors, are shown In general, there is good agreement among the results

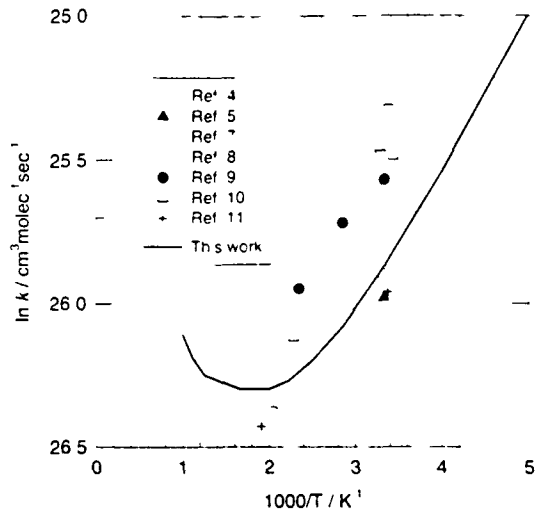

FIG 5 Comparison of calculated CVT rate constants at the PMP4sdtq/6 311+G(d p)//MP4sdq/6 311+G(d p)[MP2(FULL)/6 311+G(d p)] level and high pressure experimental rate constants for the OH+C H$_3$—C H$_3$OH reaction

Activation energies can be obtained from rate constants through the usual definition

$$E_a = -R \frac{d(\ln k)}{d(1/T)} \tag{2}$$

which is equivalent to determining the slope of the plot in Fig 5 Negative theoretical activation energies are obtained at temperatures below 565 K In particular, a value of −0 92 kcal mol^{-1} is found at 298 K, in very good agreement with the experimental values at room temperature (about −1 kcal mol^{-1}) On the other hand, as temperature increases, the activation energy first goes to zero (around 565 K) and then becomes positive Thus our calculations predict that a positive temperature dependence of the rate constant could be expected at high temperatures ($T>565$ K) This behavior should be experimentally observed, unless a competitive reaction becomes significant at those temperatures, which could mask the predicted augment of the rate constant for the title reaction As a matter of fact, a minimum in the temperature dependence of the rate of other fast reactions has been previously reported by Levine and other workers [46 47]

In order to understand the behavior of the activation energy, we have analyzed the evolution of the variational transition states as a function of temperature Gibbs free-energy profiles (obtained from the PMP4sdtq/b2//MP4sdq/b2[MP2(FULL)/b2] data) at several temperatures along with the location of transition states are displayed in Fig 6 By using the van't Hoff equation, Gibbs free energy can be decomposed into the enthalpic and the entropic contributions through equations

$$\Delta H^{GT\,0}(k) = -T^2 \frac{d(\Delta G^{GT\,0}(k)/T)}{dT} - RT \tag{3}$$

and

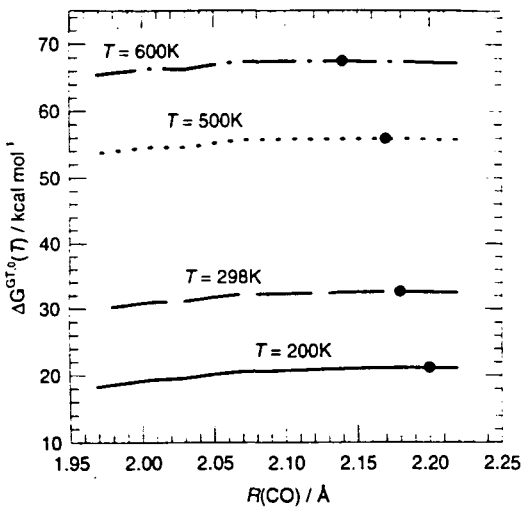

FIG. 6. Gibbs free-energy ($\Delta G^{GT,0}$) profiles along the reaction path at the PMP4sdtq/6-311+G(d,p)//MP4sdq/6-311+G(d,p)[MP2(FULL)/6-311+G(d,p)] level of calculation (second approach in Sec. II). The solid dot indicates the position of the generalized transition state at each temperature. All the values are taken versus reactants.

$$\Delta S^{GT,0}(k)=\frac{\Delta H^{GT,0}(k)-\Delta G^{GT,0}(k)}{T}. \tag{4}$$

These equations are equivalent to those employed previously.[48] In practice, the derivative in Eq. (3) has been calculated by a two-point central difference algorithm. For the sake of example, $\Delta H^{GT,0}(k)$ and $\Delta S^{GT,0}(k)$ contributions at 298 K are shown in Fig. 7.

At $T=0$ K the term $-T\Delta S^{GT,0}(k)$ vanishes and $\Delta H^{GT,0}(k)=V_a^G(k)$. Since $V_a^G(k)$ monotonically decreases from reactants to product (at the PMP4sdtq/b2//MP4sdq/b2[MP2(FULL)/b2] level of calculation), the variational transition state at 0 K coincides with reactants at infinite distance, where $\Delta G^{CVT,0}=\Delta H^{CVT,0}=V_a^{G,CVT}=0$, CVT superscript standing for canonical variational transition state. The entropic contribution becomes more and more important as T increases. Since we are studying an association reaction, $\Delta S^{GT,0}(k)$ becomes more negative in going from reactants to product, and the term $-T\Delta S^{GT,0}(k)$ moves the variational transition state closer and closer to the product as T grows (see Fig. 6), an effect first predicted for association reactions by Rai and Truhlar.[49] As a matter of fact, the variational transition state at a given temperature appears exactly at the point in which the slope of the decreasing $\Delta H^{GT,0}(k)$ curve equals the slope of the increasing $-T\Delta S^{GT,0}(k)$ curve (see Fig. 7). As a consequence of this behavior the enthalpy change associated to the variational transition state becomes more and more negative with increasing temperature.

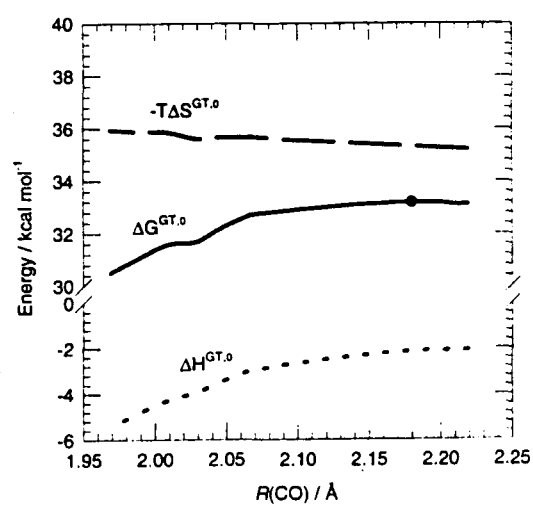

FIG. 7. Gibbs free-energy profile and its enthalpic and entropic contributions at $T=298$ K as a function of the C–O bond distance. The solid dot indicates the position of the generalized transition state on the $\Delta G^{GT,0}$ profile. All the values are taken versus reactants.

At this point it is useful to consider the following relationship between activation energy and the enthalpy change corresponding to the variational transition state

$$E_a=\Delta H^{CVT,0}+2RT, \tag{5}$$

which holds for bimolecular chemical reactions in gas phase (provided that no tunneling effect exists) and is also derived by using the van't Hoff equation.[48,50] Equations (3) and (5) are equivalent when the former is applied to those points that correspond to variational transition states at a given temperature. For the addition of a hydroxyl radical to ethylene (an example of a chemical reaction involving no vibrationally adiabatic energy barrier) the activation energy should be zero at 0 K (recall that $\Delta H^{CVT,0}=0$ at 0 K). At higher temperatures the value of E_a depends on the balance between the terms $\Delta H^{CVT,0}$ and $2RT$ according to Eq. (5). As mentioned above, $\Delta S^{GT,0}$ varies along the distinguished coordinate path $[R(CO)]$ in such a way that becomes more negative as the reaction proceeds to product. This fact causes the variational effect and then moves the variational transition state towards shorter C–O distances with increasing temperature, leading to progressively more negative values for $\Delta H^{CVT,0}$, which becomes large enough in absolute value to overcome the positive $2RT$ term and gives a negative activation energy (that is, a negative temperature dependence of the rate constant). This is the behavior exhibited by the rate constant below 565 K in Fig. 5. When the variational displacement is no longer able to get a transition-state enthalpy change negative enough to overpass the $2RT$ term, the activation energy becomes positive. This is the situation above 565 K in Fig. 5. One of the two RT terms in Eq. (5) comes from the ubiquitous k_BT/h factor of all versions of transition state theory (where k_B is Boltzmann's constant), and the importance of this factor overcoming negative activation energies as the temperature increases has also been noted by Hu and Truhlar.[47]

IV. CONCLUSIONS

In this paper we have theoretically studied the fast addition reaction of a hydroxyl radical to ethylene in gas phase using electronic structure calculations plus canonical varia-

tional transition state theory Although the experimentally reported high-pressure rate constants involve certain uncertainties, it seems clear that a negative temperature dependence of the rate constant has been found in most studies, leading to a negative activation energy of about -1 kcal mol^{-1} Therefore we have focused on reproducing and understanding this behavior The problem arises from the fact that, as known, it is very difficult to accurately describe this kind of barrierless radical reaction, even though high-level ab initio methods are used In effect, for the title reaction, after using two different strategies to build up the reaction path and several methods to solve the Schrodinger equation, we have found that the PMP4sdtq/6-311+G(d,p)//MP4sdq/6-311+G(d,p)[MP2(FULL)/6-311+G(d,p)] level of calculation provides a barrierless adiabatic potential-energy profile as a function of the C–O bond length At this level, negative theoretical activation energies are obtained below 565 K, with a particular value of -0.92 kcal mol^{-1} at 298 K, in very good agreement with experimental measurements This negative dependence of the rate constant for this barrierless addition reaction is due to the variational effect caused by the entropic term, which pushes the variational transition state towards shorter separation of reactants as temperature increases, in this way leading to progressively more negative values of the enthalpy associated with the transition state Furthermore, our theoretical calculations predict that activation energy may become positive at higher temperatures as a consequence of the delicate balance among the different factors that determine the rate constant values

Finally, it has to be emphasized that the present reaction is just an example of a wide range of fast radical chemical reactions in the gas phase, whose accurate kinetic study appears to be very difficult from both the experimental and the theoretical points of view The results presented here are encouraging for the ability of variational transition state theory to be able to contribute to an improved understanding of these reactions.

ACKNOWLEDGMENTS

We thank Professor D. G. Truhlar for supplying us the POLYRATE package and for useful comments on this work Financial support from DGICYT (project No PB94-1030) and DGES (project No. PB95-0637) and the use of the computational facilities of the "Centre de Computació i de Comunicacions de Catalunya" are also gratefully acknowledged

[1] M Wong and L Radom, J Phys Chem **99** 8582 (1995)
[2] C Sosa and H B Schlegel, J Am Chem Soc **109** 4193 (1987)
[3] B S Jursic, J Chem Soc Perkin Trans **2** 637 (1997)
[4] N R Greiner J Chem Phys **53** 1284 (1970)
[5] I W M Smith and R Zellner J Chem Soc Faraday Trans (2) **69** 1617 (1973)
[6] D D Davis, S Fischer R Schiff R T Watson and W Bollinger J Chem Phys **63** 1070 (1975)
[7] A C Lloyd K R Darnall A M Winer and J N Pitts J Phys Chem **80** 789 (1976)
[8] R Overend and G J Paraskevopoulos J Chem Phys **67** 674 (1977)
[9] R Atkinson R A Perry, and J N Pitts J Phys Chem **66** 1197 (1977)
[10] F P Tully, Chem Phys Lett **96**, 148 (1983)
[11] R Zellner and K J Lorenz J Phys Chem **88** 984 (1984)
[12] E D Morris D H Stedman and H J Niki J Am Chem Soc **93** 3570 (1971)
[13] J N Bradley W Hack K Hoyermann and H G G Wagner J Chem Soc Faraday Trans 1 **69** 1889 (1973)
[14] A V Pastrana and R W Carr J Phys Chem **79** 765 (1975)
[15] C Howard J Chem Phys **65** 4771 (1976)
F Stuhl VI International Symposium on Free Radicals Berchtesgaden Konigssee 1973 Preprint No 34 (unpublished)
[16] E W G Diau and Y P Lee J Chem Phys **96** 377 (1992)
[17] D L Singleton and R J Cvetovic J Am Chem Soc **98** 6812 (1976)
[18] M Mozurkewich and S W Benson J Phys Chem **88** 6429 (1984)
[19] C Sosa and H B Schlegel J Am Chem Soc **109** 7007 (1987)
[20] W L Hase H B Schlegel V Balbyshev and M Page J Phys Chem **100** 5354 (1996)
[22] M J Frisch G W Trucks H B Schlegel P M W Gill B G Johnson M A Robb J R Cheeseman T A Keith G A Petersson J A Montgomery K Raghavachari M A Al Laham V G Zakrzewski J V Ortiz J B Foresman J Cioslowski B B Stefanov A Nanayakkara M Challacombe C Y Peng P Y Ayala W Chen M W Wong J L Andres E S Replogle R Gomperts R L Martin D J Fox J S Binkley D J Defrees J Baker J P Stewart M Head Gordon C Gonzalez and J A Pople GAUSSIAN 94 Gaussian Inc Pittsburgh PA 1995
[23] J C Corchado J Espinosa Garcia W-P Hu I Rossi and D G Truhlar J Phys Chem **99** 687 (1995)
[24] C Møller and M S Plesset Phys Rev **46** 618 (1934)
[25] K Fukui Pure Appl Chem **54** 1825 (1982) D G Truhlar and A J Kuppermann J Am Chem Soc **93** 1840 (1971)
[26] C Gonzalez and H B Schlegel J Phys Chem **94** 5523 (1990)
[27] W H Miller N C Handy and J E Adams J Chem Phys **72** 99 (1980)
[28] H B Schlegel J Chem Phys **84** 4530 (1986) C Sosa and H B Schlegel Int J Quantum Chem **29** 1001 (1986)
[29] J A Pople and M Head Gordon J Chem Phys **82** 284 (1985) **87** 5968 (1987)
[30] J Villa and D G Truhlar Theor Chem Acc (to be published)
[31] M J Rothman L L Lohr Jr C S Ewing and J R van Wazer in *Potential Energy Surfaces and Dynamics Calculations* edited by D G Truhlar (Plenum New York 1981) p 653 R Steckler and D G Truhlar J Chem Phys **93** 6570 (1990) D Heidrich in *The Reaction Path in Chemistry* edited by D Heidrich (Kluwer Dordrecht 1995) p 1
[32] D G Truhlar A D Isaacson and B C Garrett in *Theory of Chemical Reaction Dynamics* edited by M Baer (CRC Boca Raton FL 1985) Vol IV S C Tucker and D G Truhlar in *New Theoretical Concepts for Understanding Organic Reactions* edited by J Bertran and I G Csizmadia (Kluwer Dordrecht 1989)
[33] *JANAF Thermochemical Tables* 3rd ed edited by M W Chase C A Davies J R Downey D J Frurip R A McDonald and A N Syverud (National Bureau of Standards Washington DC 1985) Vol 14
[34] J Villa A Gonzalez-Lafont J M Lluch and J Bertran Mol Phys **89** 633 (1996)
[35] R Steckler Y- Y Chuang E L Coitiño W- P Hu Y- P Liu G C Lynch K A Nguyen C F Jackels M Z Gu I Rossi P Fast S Clayton V S Melissas, B C Garrett, A D Isaacson and D G Truhlar POLYRATE Version 7 0 University of Minnesota Minneapolis 1996
[36] J Cizek J Chem Phys **45** 4256 (1966) K Raghavachari G W Trucks J A Pople and M Head-Gordon Chem Phys Lett **157** 479 (1989)
[37] P J Stephens F J Devlin C F Chabalowski and M J Frisch J Phys Chem **98** 11623 (1994)
[38] W Hehre L Radom P Schlever and J Pople in *Ab Initio Molecular Orbital Theory* (Wiley New York 1986) A P Scott and L Radom J Phys Chem **100** 16502 (1996)
[39] G S Hammond J Am Chem Soc **77** 334 (1955)
[40] J C Corchado F J Olivares del Valle and J Espinosa-Garcia J Phys Chem **97** 9129 (1994)
[41] J Espinosa Garcia and J C Corchado J Chem Phys **101** 1333 (1994)
[42] J Espinosa Garcia and J C Corchado J Chem Phys **101** 8700 (1994)
[43] J Espinosa Garcia S Tolosa and J C Corchado J Phys Chem **98** 2337 (1994)
[44] J A Kerr and M J Personage in *Evaluated Kinetic Data on Gas Phase Addition Reactions* (Buttherworths England 1972)
[45] J L Holmes F P Lossing and P M Mayer J Am Chem Soc **113** 9723 (1991)

[46]E. Rabani, D M Charutz, and R D Levine, J Phys Chem **95**, 10551 (1991)
[47]W.-P Hu and D G Truhlar, J. Am Chem Soc **117**, 10726 (1995)
[48]D G Truhlar and B C Garrett, J Am Chem Soc **111**, 1232 (1989)
[49]S N Rai and D G Truhlar, J Chem Phys **79**, 6046 (1983)
[50]M M Kreevoy and D G Truhlar, in *Investigation of Rates and Mechanisms of Reactions*, 4th ed edited by C F Bernasconi (Wiley, New York, 1986) Part I, p 13

6. CONCLUSIONS

En aquest darrer capítol presentem un sumari de les conclusions a les quals s'ha arribat a rel de la realització d'aquest treball. Altre cop hem dividit el capítol en un apartat metodològic i un apartat més aplicat.

Conclusions metodològiques:

I. Aquest treball mostra com la interpolació de les freqüències al llarg de la coordenada de reacció, en un estudi dinàmic segunit la teoria variacional de l'estat de transició, ha de ser duta a terme diabàticament en el cas que existeixin creuaments importants dels modes normals.

II. La corba de potencial adiabàtica (perfil d'energia potencial més la correcció de punt zero al llarg del camí de reacció) no es veu alterada per l'ús de la interpolació adiabàtica o diabàtica de les freqüències, al contrari del que succeeix amb el perfil d'entropia i totes les magnituds derivades d'aquest.

III. Les diferents superfícies de divisió que al llarg de la coordenada de reacció conformen els estats de transició generalitzats en la VTST, seran òptimes si són ortogonals al gradient del camí de mínima energia de la reacció (MEP).

IV. Una forma senzilla de construir les superfícies de divisió al llarg de qualsevol coordenada de reacció (no necessàriament el MEP, sino que és possible utilitzar qualsevol coordenada geomètrica) és orientar-les de manera que minimitzin el fluxe de trajectòries que les travessen. Aquesta minimització del fluxe es tradueix en la maximització del valor del potencial adiabàtic en funció de l'esmentada orientació en un punt donat del camí.

V. La construcció de camins de mínima energia amb valors de δs elevats porta a poca convergència en aquests camins. Això pot provocar l'aparició d'importants fluctuacions en les freqüències generalitzades al llarg del camí, que donguin origen a valors erronis de les constants de velocitat. La reorientació de la superfície de divisió pot fer desaparèixer aquestes fluctuacions.

VI. L'efecte de la reorientació de les superfícies de divisió sobre el càlcul de l'efecte túnel és encara més important. Això és degut a que alguns dels mètodes semiclàssics emprats per

aquest càlcul utilitzen, a més de la corba de potencial adiabàtica, els valors de les components del vector corbatura al llarg del camí, que així mateix es calculen a partir de la variació al llarg de la coordenada de reacció dels vectors propis associats als modes normals de vibració.

VII. La correcta avaluació de la barrera i l'energia de reacció en processos d'addició d'un radical lliure a un doble enllaç es presenta com un problema difícil de resoldre per als mètodes quàntics establerts. Un nou mètode desenvolupat en aquest treball, anomenat Escalatge Variable de la Correlació Externa (VSEC), ha demostrat la seva validesa en la consecució de valors energètics realistes en sistemes on aquests càlculs són complexes.

VIII. El mètode VSEC presenta l'avantatge de no pressuposar cap forma predeterminada del perfil d'energia de la reacció, permetent d'aquesta manera càlculs dels coeficients de transmissió per efecte túnel més realistes.

IX. En l'avaluació del perfil energètic de la reacció d'associació $C_2H_4 + OH \rightarrow C_2H_4OH$ el càlcul del IRC a nivell MP2 ha demostrat ser insuficient per reproduir els resultats experimentals, havent hagut d'emprar el mètode de correlació MP4 al llarg d'una coordenada de reacció definida per la coordenada geomètrica $R_{C\text{-}O}$ per obtenir resultats de qualitat.

Conclusions químiques:

X. Els efectes variacionals i l'efecte túnel poden ser importants en reaccions de transferència de cations metil quan existeix una separació de càrrega.

XI. En una reacció de transferència protònica on només existeixi una barrera significativa d'energia lliure al llarg del camí, l'empírica Regla de la Mitjana Geomètrica (RGM) és útil per a la determinació del grau d'acoblament entre el moviment del protó i el del dissolvent, en el cas que l'efecte túnel sigui menyspreable. Si la regla s'acompleix, és un bon indicatiu que (1) el grau d'acoblament protó-dissolvent és nul en la regió de l'estat de transició i que (2) l'efecte túnel no és important en el sistema.

XII. En una reacció de transferència protònica on existeixi més d'una barrera d'energia lliure

al llarg del camí, pot existir un trencament de la RGM no degut a cap de les dues causes indicades més amunt, sino a l'efecte conjunt d'aquestes dues barreres en la constant de velocitat.

XIII. En la reacció butanona + $OH^-(H_2O)_n$, on n = 0, 1, 2 existeixen dues barreres d'energia lliure ben diferenciades, la primera per a l'associació dels dos reactius (interacció ió-dipol) i la segona per la transferència protònica. La barrera dominant del procés és la d'associació en el cas n = 0 i, contràriament, la de la transferència protònica en el cas n = 2. En el cas n = 1 la barrera d'energia lliure per l'associació és la més elevada a temperatures baixes, essent-ho la de la transferència a temperatures elevades.

XIV. L'estudi de l'estructura i els modes normals dels diferents estats de transició per a la transferència en la reacció butanona + $OH^-(H_2O)_n$, indica l'absència d'acoblament en l'estat de transició entre els moviment del protó i el del dissolvent.

XV. Assumint una variació monòtona de l'efecte isotòpic del solvent de reactius a productes, l'efecte cinètic isotòpic del dissolvent, per comparació amb l'efecte isotòpic d'equilibri també del dissolvent, indica que el grau de desolvatació en l'estat de transició de la reacció per al sistema butanona + $OH^-(H_2O)_2$ a 298 K és del 44%. Això és en bon acord amb el resultat experimental, 50%.

XVI. La utilització conjunta del mètode VSEC, la teoria variacional de l'estat de transició i el càlcul del factor de transmissió per efecte túnel multidimensional ha permès reproduir els valors experimentals i entendre els factors dels quals depenen.

XVII. En la reacció d'associació $C_2H_4 + H \rightarrow C_2H_5$ la posició de la superfície de divisió que determina l'estat de transició variacional depèn de la temperatura. En el rang de variaciód'aquesta, el valor del potencial adiabàtic varia lleugerament (0.4 kcal/mol) però les dues freqüències de plegament C-C-H (la variació de les quals és la màxima responsable d'aquest desplaçament) s'incrementen en un 25-40%.

XVIII. L'estimació de l'efecte túnel en la reacció d'associació $C_2H_4 + H \rightarrow C_2H_5$ mitjançant el mètode ZCT (que no inclou l'efecte de la corbatura en el camí de reacció) va ser

introduïda en els nostres càlculs, mostrant la seva importància en la reproducció dels resultats experimentals.

XIX. En la reacció d'associació $C_2H_4 + OH \rightarrow {}_2C_4H\,OH$, s'ha aconseguit reproduir la dependència negativa de les constants de velocitat amb la temperatura (a 298 K: experimental ≈ -1 kcal/mol; teòric ≈ -0.92 kcal/mol)

XX. L'origen dels valors negatius de l'energia d'activació en aquesta reacció ha estat explicat en el marc de la VTST. Aquest és degut a l'efecte variacional causat pel terme entròpic, que empeny l'estat de transició variacional cap a valors de $R_{C\text{-}O}$ més petits a mesura que la temperatura creix, portant d'aquesta manera a valors cada cop més negatius de l'entalpia associada amb l'estat de transició.

XXI. A temperatures superiors a 565 K, els nostres resultats preveuen que l'energia d'activació per a la reacció $C_2H_4 + OH \rightarrow C_2H_4OH$ esdevindrà positiva donat el delicat balanç entre els diferents factors que determinen la constant de velocitat.

Llista de figures

Bibliografia

[1] Truhlar, D. G.; Gordon, M. S.*Science* **1990**, *249*, 491.

[2] Truhlar, D. G.; Steckler, R.; Gordon, M. S. *Chem. Rev.* **1987**, *87*, 217.

[3] Maseras, F.; Morokuma, K. *J. Comput. Chem.* **1995**, *16*, 1170.

[4] Eurenius, K. P.; *Int. J. Quantum Chem.* **1996**, *60*, 1189.

[5] Warshel, A. *Computer Modeling of Chemical Reactions in Enzymes and Solutions*, John Wiley & Sons, New York, 1991.

[6] Bala, P.; Grochowski, P.; Lesyng, B.; McCammon, J. A. *J. Phys. Chem.* **1996**, *100*, 2535.

[7] McQuarrie, D. A. *Statistical Mechanics*; HarperCollins, New York, 1976.

[8] Hirst, D. M. *A Computational Approach to Chemistry*; Blackwell, Oxford, 1990.

[9] Rodberg, L. S.; Thaler, R. M. *Introduction to the Quantum Theory of Scattering*; Academic Press, New York, 1967.

[10] Gray, S. K.; Miller, W. H.; Yamaguchi, Y.; Schaefer, H. F., III *J. Chem. Phys.* **1980**, *73*, 2733.

[11] Gray, S. K.; Miller, W. H.; Yamaguchi, Y.; Schaefer, H. F., III *J. Am. Chem. Soc.* **1981**, *103*, 1900.

[12] Tachibana, A.; Okazaki, I.; Koizumi, M.; Hori, K.; Yomabe, T. *J. Am. Chem. Soc.* **1985**, *107*, 1190.

[13] Colwell, S. M.; Handy, N. C. *J. Chem. Phys.* **1985**, *82*, 128.

[14] Colwell, S. M. *Theor. Chim. Acta* **1988**, *74*, 123.

[15] Liu, Y. -P.; Lynch, G. C.; Truong, T. N.; Lu, D. -H.; Truhlar, D. G.; Garrett, B. C. *J. Am. Chem. Soc.* **1993**, *115*, 2408.

[16] Baldridge, K. K.; Gordon, M. S.; Steckler, R.; Truhlar, D. G. *J. Phys. Chem.* **1989**, *93*, 5107.

[17] Garrett, B. C.; Koszykowski, M. L.; Melius, C. F.; Page, M. *J. Phys. Chem.* **1990**, *94*, 7096.

[18] Truong, T. N.; McCammon, J. A. *J. Am. Chem. Soc.* **1991**, *113*, 7504.

[19] Liu, Y. -P.; Lu, D. -H.; González-Lafont, A.; Truhlar, D. G.; Garrett, B. C. *J. Am. Chem. Soc.* **1993**, *115*, 7806.

[20] Isaacson, A. D.; Wang, L.; Scheiner, S. *J. Phys. Chem.* **1993**, *97*, 1765.

[21] Truong, T. N.; Evans, T. J. *J. Phys. Chem.* **1994**, *98*, 9558.

[22] Truong, T. N. *J. Chem. Phys.* **1994**, *100*, 8014.

[23] Truhlar, D. G. *The Reaction Path in Chemistry: Current Approaches and Perspectives*; Heidrich, D. Ed.; Kluwer, Dordrecht, 1994.

[24] Eyring, H. *J. Chem. Phys.* **1935**, *3*, 107.

[25] Laidler, K. J.; King, M. C. *J. Phys. Chem.* **1983**, *87*, 2657.

[26] Truhlar, D. G.; Garrett, B. C.; Klippenstein, S. J. *J. Phys. Chem.* **1996**, *100*, 12771.

[27] Wigner, E. *Trans. Faraday Soc.* **1938**, *34*, 29.

[28] Connors, K. A. *Chemical Kinetics*, VCH Publishers, Inc, 1990.

[29] Truhlar, D. G.; Isaacson, A. D.; Garrett, B. C. In *Theory of Chemical Reaction Dynamics*; Baer, M., Ed.; CRC Press: Boca Raton, FL, 1985.

[30] Kreevoy, M. M.; Truhlar, D. G. In *Investigation of Rates and Mechanism of Reactions*; Bernasconi, C. F., Ed.; Wiley: New York, 1986.

[31] Gilbert, R. G.; Smith, S. C. *Theory of Unimolecular and Recombination Reactions*; Blackwell: Oxford, 1990.

[32] Corben, H. C.; Stehle, P. *Classical Mechanics*; John Wiley & Sons, New York, 1960.

[33] Glasstone, S.; Laidler, K. J.; Eyring, H. *Theory of Rate Processes*; McGraw-Hill: New York, 1941.

[34] Eliason, M. A.; Hirschfelder, J. O. *J. Chem. Phys.* **1959**, *30*, 1426.

[35] Truhlar, D. G.; Hase, W. L.; Hynes, J. T. *J. Phys. Chem.* **1983**, *87*, 2664, 5523(E).

[36] Wigner, E. *J. Chem. Phys.* **1937**, *5*, 720.

[37] Wigner, E. *J. Chem. Phys.* **1937**, *5*, 720.

[38] Horiuti, J. *Bull. Chem. Soc. Jpn.* **1938**, *13*, 210.

[39] Keck, J. C. *Adv. Chem. Phys.* **1967**, *13*, 85.

[40] Truhlar, D. G.; Garrett, B. C. *Annu. Rev. Phys. Chem.* **1984**, *35*, 159.

[41] Miller, W. H. *J. Chem. Phys.* **1976**, *65*, 2216.

[42] Garrett, B. C.; Truhlar, D. G. *J. Chem. Phys.* **1982**, *76*, 1853.

[43] Hirschfelder, J. O.; Wigner, E. *J. Chem. Phys.* **1939**, *7*, 616.

[44] Hu, W. -P.; Truhlar, D. G. *J. Am. Chem. Soc.* **1996**, *118*, 860.

[45] Rosentock, H. M.; Wallenstein, M. B.; Wahrhaftig, A. L.; Eyring, H. *Proc. Natl. Acad. Sci. U. S. A.* **1952**, *38*, 667.

[46] Tucker, S. C.; Truhlar, D. G. In *New Theoretical Concepts for Understanding Organic Reactions*; Bertrán, J., Czismadia, I., Eds.; Kluwer: Dordrecht, 1989.

[47] Villà, J.; Truhlar, D. G. *Theor. Chem. Acc.* **1997**, *97*, 317.

[48] Miller, W. H.; Handy, N. C.; Adams, J. E. *J. Chem. Phys.* **1980**, *72*, 99.

[49] Espinosa-García, J.; Corchado, J. C. *J. Chem. Phys.* **1994**, *101*, 1333.

[50] Espinosa-García, J.; Corchado, J. C. *J. Chem. Phys.* **1994**, *101*, 8700.

[51] Truhlar, D. G.; Kuppermann, A. *J. Am. Chem. Soc.* **1971**, *93*, 1840.

[52] Fukui, K.; Kato, S.; Fujimoto, H. *J. Am. Chem. Soc.* **1975**, *97*, 1.

[53] Casamassina, T. E.; Huskey, W. P. *J. Am. Chem. Soc.* **1993**, *115*, 14.

[54] (a) Klinman, J. P. *Enzyme mechanisms from Isotope Effects*; Cook, P. F., Ed.; CRC Press: Boca Raton, FL, 1991; Chapter 4. (b) Amin, M.; Price, R. C.; Saunders, W. H., Jr. *J. Am. Chem. Soc.* **1988**, *110*, 4085.

[55] Nguyen, M. T.; Creve, S.; Vanquickernborne, L. G. *J. Phys. Chem.* **1996**, *100*, 18422.

[56] Hase, W. L.; Schlegel, H. B.; Balbyshev, V.; Page, M. *J. Phys. Chem.* **1996**, *100*, 5354.

[57] Jursic, B. S. *J. Chem. Soc., Perkin Trans. 2* **1997**, 637.

[58] Mayer, P. M.; Parkinson, C. J.; Smith, D. M.; Radom, L. *J. Chem. Phys.*, **1998**, *108*, 0000.

[59] Mok, D. K. W.; Neumann, R.; Handy, N. C. *J. Phys. Chem.* **1996**, *100*, 6225.

[60] Gordon, M. S.; Truhlar, D. G. *J. Am. Chem. Soc.* **1986**, *108*, 5412.

[61] Melissas, V. S.; Truhlar, D. G. *J. Chem. Phys.* **1993**, *99*, 3542.

[62] segona cita melisssas

[63] Greiner, N. R. *J. Chem. Phys.* **1970**, *53*, 1284.

[64] Atkinson, R.; Perry, R. A.; Pitts, J. N. *J. Chem. Phys.* **1977**, *66*, 1197.

[65] Tully, F. P. *Chem. Phys. Lett.* **1983**, *96*, 148.

[66] Zellner, R.; Lorenz, K. J. *J. Phys. Chem.* **1984**, *88*, 984.

[67] Steinfeld, J. I.; Francisco, J. S.; Hase, W. L. *Chemical Kinetics and Dynamics*; Prentice Hall, Englewood Cliffs, New Jersey: 1989.

[68] Pitzer, K. S. *Thermodynamics*; 3rd. Ed. McGraw-Hill: New York, 1995.

[69] Shrödinger, E. *Statistical Thermodynamics*; Cambridge University Press: Cambridge, 1973.

[70] Díaz-Peña, M. *Termodinàmica Estadística*; Alhambra: Madrid, 1979.

[71] Truhlar, D. G.; Schenter, G. K.; Garrett, B. C. *J. Chem. Phys.* **1993**, *98*, 5756.

[72] Truhlar, D. G.; Liu, Y. -P.; Schenter, G. K; Garrett, B. C. *J. Phys. Chem.* **1994**, *98*, 8396.

[73] Wardlaw, D. M.; Marcus, R. A. *J. Phys. Chem.* **1986**, *90*, 5383.

[74] Klippenstein, S. J.; Marcus, R. A. *J. Chem. Phys.* **1987**, *87*, 3410.

[75] Klippenstein, S. J.; Marcus, R. A. *J. Phys. Chem.* **1988**, *92*, 3105.

[76] Klippenstein, S. J.; Marcus, R. A. *J. Phys. Chem.* **1988**, *92*, 5412.

[77] Klippenstein, S. J. *J. Phys. Chem.* **1994**, *98*, 11459.

[78] Gonzàlez-Lafont, A.; Lluch, J. M.; Bertrán, J. *Solvent Effects and Chemical Reactivity*; O. Tapia i J. Bertrán, ed.; Kluwer: Amsterdam, 1996.

[79] Levine, I. N. *Quantum Chemistry*; Allyn & Bacon, Boston, 1974.

[80] Schrödinger, E. *Ann. Physik* **1926**, *79*, 361.

[81] Born, M.; Oppenheimer, J. R. *Ann. Physik*, **1927**, *84*, 457.

[82] Postma, J. M.; Silvester, L. F.; Rock, P. A. *J. Phys. Chem.* **1988**, *92*, 1308.

[83] Szabo, A.; Ostlund, N. S. *Modern Quantum Chemistry*; Macmillan, New York, 1982.

[84] Truhlar, D. G. (Ed.) *Potential Energy Surfaces and Dynamics Calculations*; Plenum Press, New York, 1981.

[85] Anderson, J. B. *J. Chem. Phys.* **1973**, *58*, 4684.

[86] Eliason, M. A.; Hirschfelder, J. O. *J. Chem. Phys.* **1959**, *30*, 1426.

[87] Lu, D. -h.; Zhao, M.; Truhlar, D. G. *J. Comput. Chem.* **1991**, *12*, 376.

[88] Schlegel, H. B. *Ab Initio Methods in Quantum Chemistry-I*, Lawley Ed. John Wiley & Sons; New York, 1987.

[89] Cerjan, C. J.; Miller, W. H. *J. Chem. Phys.* **1981**, *75*, 2800.

[90] Schlegel, H. B. *J. Comput. Chem.* **1982**, *3*, 214.

[91] Bell, S.; Crighton, J. *J. Chem. Phys.* **1984**, *80*, 2464.

[92] McDouall, J. J. W.; Robb, M. A.; Bernardi, F. *Chem. Phys. Lett.* **1986**, *129*, 595.

[93] Baker, J. *J. Comput. Chem.* **1986**, *7*, 385.

[94] Bernardi, F.; McDouall, J. J. W.; Robb, M. A. *J. Comput. Chem.* **1987**, *8*, 296.

[95] Head, J. D.; Weiner, B.; Zerner, M. C. *Int. J. Quantum Chem.* **1988**, *33*, 177.

[96] Madura, J. A.; Pettit, B. M.; McCammon, J. A. *Chem. Phys.* **1989**, *129*, 185.

[97] Peng Z.; Merz, K. M., Jr. *J. Am. Chem. Soc.* **1993**, *115*, 9640.

[98] Empedocles, P. *Theor. Chim. Acta* **1969**, *13*, 139.

[99] Kong, Y. S.; Jhon, M. S. *Theor. Chim. Acta* **1986**, *70*, 123.

[100] Gonzalez, C.; Schlegel, H. B. *J. Chem. Phys.* **1991**, *95*, 5853.

[101] Page, M.; McIver, J. W., Jr. *J. Chem. Phys.* **1988**, *88*, 922.

[102] Natanson, G. A.; Garrett, B. C.; Truong, T. N.; Joseph, T.; Truhlar, D. G. *J. Chem. Phys.* **1991**, *94*, 7875.

[103] Schmidt, M. W.; Gordon, M. S.; Dupuis, M. *J. Am. Chem. Soc.* **1985**, *107*, 2585.

[104] Garrett, B. C.; Redmon, M. J.; Steckler, R.; Truhlar, D. G.; Baldridge, K. K.; Bartol, D.; Schmidt, M. W.; Gordon, M. S. *J. Phys. Chem.* **1988**, *92*, 1476.

[105] Melissas, V. S.; Truhlar, D. G.; Garrett, B. C. *J. Chem. Phys.* **1992**, *96*, 5758.

[106] Garrett, B. C.; Truhlar, D. G. *J. Phys. Chem.* **1991**, *95*, 10374.

[107] Burden, R. L.; Douglas Faires, J. *Numerical analysis*; PWS-KENT: Boston, 1988.

[108] Stoer, J.; Bulirsch, R. *Introduction to Numerical Analysis*; Springer-Verlag: New York, 1993.

[109] Gonzalez, C.; Schlegel, H. B. *J. Phys. Chem.* **1990**, *94*, 5523.

[110] Wilson, E. B.; Decius, G. C.; Croos, P. C. *Molecular Vibrations*; McGraw-Hill: London, 1955.

[111] Villà, J.; González-Lafont, A.; Lluch, J. M.; Bertrán, J. *Mol. Phys.* **1996**, *89*, 633.

[112] Villà, J.; González-Lafont, A.; Lluch, J. M. *J. Phys. Chem.* **1996**, *100*, 19389.

[113] Villà, J.; González-Lafont, A.; Lluch, J. M.; Corchado, J. C.; Espinosa-García, J. *J. Chem. Phys.* **1997**, *107*, 7266..

[114] Villà, J; Gonzàlez-Lafont, A.; Lluch, J. M.; Truhlar, D. G. *J. Am. Chem. Soc.* enviat..

[115] Garrett, B. C.; Truhlar, D. G. *J. Chem. Phys.* **1979**, *70*, 1593.

[116] Hu, W. -P.; Truhlar, D. G. *J. Am. Chem. Soc.* **1995**, *117*, 10726.

[117] Wardlaw, D. M.; Marcus, R. A. *Adv. Chem. Phys.* Part I, **1988**, *70*, 231.

[118] Marcus, R. A. *J. Chem. Phys.* **1966**, *45*, 4493.

[119] Marcus, R. A. *J. Chem. Phys.* **1966**, *45*, 4500.

[120] Marcus, R. A. *J. Chem. Phys.* **1967**, *46*, 959.

[121] Marcus, R. A. *J. Chem. Phys.* **1968**, *49*, 2610.

[122] Garrett, B. C.; Truhlar, D. G.; Grev, R. S.; Magnuson, A. W. *J. Phys. Chem.* **1980**, *84*, 1730.

[123] Marcus, R. A.; Coltrin, M. E. *J. Chem. Phys.* **1977**, *67*, 2609.

[124] Skodje, R. T.; Truhalr, D. G.; Garrett, B. C. *J. Phys. Chem.* **1981**, *85*, 3019.

[125] Truhlar, D. G.; Isaacson, A. D.; Skodje, R. T.; Garrett, B. C. *J. Phys. Chem.* **1982**, 86, 2252.; **1983**, *87*, 4554.

[126] Skodje, R. T.; Truhlar, D. G.; Garrett, B. C. *J. Chem. Phys.* **1983**, *77*, 5955.

[127] Garrett, B. C.; Joseph, T.; Truong, T. N.; Truhlar, D. G. *Chem. Phys.* **1989**, *136*, 271.

[128] Eckart, C. *Phys. Rev.* **1930**, *35*, 1303.

[129] Truong, T. N.; Truhlar, D. G. *J. Chem. Phys.* **1990**, *93*, 1761.

[130] Gonzalez-Lafont, A.; Truong, T. N.; Truhlar, D. G. *J. Chem. Phys.* **1991**, *95*, 8875.

[131] Hu, W. -P.; Liu, Y. -P.; Truhlar, D. G. *J. Chem. Faraday Trans.* **1994**, *90*, 1715.

[132] Corchado, J. C.; Espinosa-García, J.; Hu, W. -P.; Rossi, I.; Truhlar, D. G. *J. Phys. Chem.* **1995**, *99*, 687.

[133] Chuang, Y. -Y.; Truhlar, D. G. *J. Phys. Chem. A* **1997**, *101*, 3808.

[134] Natanson, G. A. *Mol. Phys.* **1982**, *46*, 481.

[135] Jackels, C. F.; Gu, Z.; Truhlar, D. G. *J. Chem. Phys.* **1995**, *102*, 3188.

[136] Chuang, Y. -Y.; Truhlar, D. G. *J. Chem. Phys.* **1997**, *107*, 83.

[137] Miller, W. H. *J. Chem. Phys.* **1974**, *61*, 1823.

[138] Truhlar, D. G. *J. Comput. Chem.* **1991**, *12*, 266.

[139] Hu, W. -P.; Rossi, I.; Corchado, J. C.; Truhlar, D. G. *J. Phys. Chem. A* **1997**, *101*, 6911.

[140] González-Lafont, A.; Villà, J.; Lluch, J. M.; Bertrán, J.; Steckler, R.; Truhlar, D. G. *J. Chem. Phys.* enviat.

[141] Rosenman, E.; McKee, M. L. *J. Am. Chem. Soc.* **1997**, *119*, 9033.

[142] Ryzhov, V.; Klippenstein, S. J.; Dunbar, R. C. *J. Am. Chem. Soc.* **1996**, *118*, 5462.

[143] Fast, P. L.; Truhlar, D. G. en preparació

[144] Barbara, P. F.; Walker, G. C.; Smith, T. P. *Science*, **1992**, *71*, 1876.

[145] Hynes, J. T. *Annu. Rev. Phys. Chem.* **1985**, *36*, 573.

[146] Alvarez, F. J.; Schowen, R. L. *Isotopes in Organic Chemistry*; Buncel, E., Lee, C. C., Eds.; Elsevier: Amsterdam, 1987.

[147] Melander, L.; Saunders, W. H., Jr. *Reaction Rates of Isotopic Molecules*, 2nd ed.; Wiley: New York, 1980.

[148] Quinn, D. M.; Sutton, L. D.; Klinman, J. P. *Enzyme Mechanisms from Isotope Effects*; Cook, P. F., Ed.; CRC Press: Boca Raton, FL, 1991.

[149] Glad, S. S.; Jensen, F. *J. Am. Chem. Soc.* **1997**, *119*, 227.

[150] Celli, F.; Weddle, G.; Ridge, D. P. *J. Chem. Phys.* **1980**, *73*, 801.

[151] Sosa, C.; Schlegel, H. B. *J. Am. Chem. Soc.* **1987**, *109*, 4193.

[152] Sosa, C.; Schlegel, H. B. *J. Am. Chem. Soc.* **1987**, *109*, 7007.

[153] Mebel, A. M.; Diau, E. W. G.; Lin, M. C.; Morokuma, K. *J. Phys. Chem.* **1996**, *100*, 7517.

[154] Singleton, D. L.; Cvetovič, R. J. *J. Am. Chem. Soc.* **1976**, *98*, 6812.

[155] Mozurkewich, M.; Benson, S. W. *J. Phys. Chem.* **1984**, *88*, 6429.

[156] Rai, S. N.; Truhlar, D. G. *J. Chem. Phys.* **1983**, *79*, 6046.

[157] Jensen, F. *Chem. Phys. Lett.* **1990**, *169*, 519.

[158] Mebel, A. M.; Morokuma, K.; Lin, M. C. *J. Chem. Phys.* **1994**, *101*, 3916.

[159] Brown, F. B.; Truhlar, D. G. *Chem. Phys. Lett.* **1985**, *117*, 307.

[160] Feng, Y.; Niiranen, J. T.; Bencsura, Á.; Knyazev, V. D.; Gutman, D.; Tsang, W. *J. Phys. Chem.* **1993**, *97*, 871.

[161] Sekušak, S.; Liedl, K.; Rode, B. M.; Sabljić, A. *J. Phys. Chem. A* **1997**, *101*, 4245.

[162] Tucker, S. C.; Truhlar, D. G. *J. Am. Chem. Soc.* **1990**, *112*, 3347.

[163] DeTuri, V. F.; Hintz, P. A.; Ervin, K. M. *J. Phys. Chem. A* **1997**, *101*, 5969.